INVESTIGATING THE RELIABILITY OF ULTRASOUND PHASED ARRAY
METHOD AND CONVENTIONAL ULTRASONIC TESTING FOR
DETECTION OF DEFECTS IN AUSTENITIC STAINLESS STEELS

A THESIS SUBMITTED TO
THE GRADUATE SCHOOL OF NATURAL AND APPLIED SCIENCES
OF
MIDDLE EAST TECHNICAL UNIVERSITY

BY

BAHADIR AKGÜN

IN PARTIAL FULFILLMENT OF THE REQUIREMENTS
FOR
THE DEGREE OF MASTER OF SCIENCE
IN
METALLURGICAL AND MATERIALS ENGINEERING

AUGUST 2015

Approval of the thesis:

INVESTIGATING THE RELIABILITY OF ULTRASOUND PHASED ARRAY METHOD AND CONVENTIONAL ULTRASONIC TESTING FOR DETECTION OF DEFECTS IN AUSTENITIC STAINLESS STEELS

Submitted by **BAHADIR AKGÜN** in partial fulfillment of the requirements for the degree of **Master of Science in Metallurgical and Materials Engineering Department, Middle East Technical University** by,

Prof. Dr. Gülbin Dural Ünver   _____
Dean, Graduate School of **Natural and Applied Sciences**

Prof. Dr. C. Hakan Gür   _____
Head of Department, **Metallurgical and Materials Engineering**

Prof. Dr. C. Hakan Gür   _____
Supervisor, **Metallurgical and Materials Eng. Dept., METU**

Examining Committee Members:

……………………………………………   ……………………

……………………………………………   ……………………

……………………………………………   ……………………

……………………………………………   ……………………

……………………………………………   ……………………

Date: 07.08.2015

I hereby declare that all information in this document has been obtained and presented in accordance with academic rules and ethical conduct. I also declare that, as required by these rules and conduct, I have fully cited and referenced all material and results that are not original to this work.

Name, Last name: Bahadır AKGÜN

Signature:

ABSTRACT

INVESTIGATING THE RELIABILITY OF ULTRASOUND PHASED ARRAY METHOD AND CONVENTIONAL ULTRASONIC TESTING FOR DETECTION OF DEFECTS IN AUSTENITIC STAINLESS STEELS

AKGÜN, Bahadır

M.S., Department of Metallurgical and Materials Engineering

Supervisor: Prof. Dr. C. Hakan GÜR

August 2015, 111 pages

In recent years Phased Array (PA) method has become an alternative to the conventional ultrasonic method for critical tests in aerospace, oil, gas and nuclear industries. There is a challenge for inspection of austenitic stainless steels due to high attenuation, skewing and scattering of sound beam. The aim of this thesis is to investigate and to compare the flaw detection abilities of conventional ultrasonic and PA systems using the probability of detection (PoD) approach for testing of austenitic stainless steel blocks and weldments having both artificial and natural defects. Grain size, micro hardness, attenuation measurements, radioscopic and macroscopic inspections were also performed. Three types of test blocks were prepared from AISI 304 steel. First specimen is the block having Ø2 mm side drilled holes at different depths; second specimen has side drilled holes with varying diameters between 0.5 to 5 mm at the same depth; and the third specimen is the welded plate having both artificial and natural defects. Although PA method has automated calibration, beam focusing and steering abilities, the PoD analyses did not show remarkable advantage of PA for detecting artificial flaws, except those in the surface near zone. On the welded specimen, however, the PA inspection is clearly more successful than conventional method based on counts of detected flaw possibilities as well as positioning and sizing of the defects. While the automated PA system has superior

detection and positioning abilities over the manual PA system, the manual PA system has superiority of faster scanning and swiveling of the probe which also brings the risk of human factor.

ÖZ

ÖSTENİTİK PASLANMAZ ÇELİKLERDE FAZ DİZİSİ VE GELENEKSEL ULTRASONİK TEST METOTLARININ HATA TESPİT KABİLİYETLERİNİN KARŞILAŞTIRILMASI

AKGÜN, Bahadır

Yüksek Lisans, Metalurji ve Malzeme Mühendisliği Bölümü

Tez Yöneticisi: Prof. Dr. C. Hakan GÜR

Ağustos 2015, 111 sayfa

Son yıllarda Faz Dizi (PA) yöntemi havacılık, petrol, gaz ve nükleer sektörlerinde kritik testler için geleneksel ultrasonik (UT) yönteme alternatif bir metot haline gelmiştir. Östenitik paslanmaz çeliklerde ses zayıflamasının yüksek olması, ses demetinin saçılması ve sapmasından dolayı östenitk paslanmaz çeliklerin ultrasonik yöntemlerle muayenesi oldukça zordur. Bu tezin amacı, yapay hatalara sahip östenitik paslanmaz çelik bloklar ile yapay ve doğal hataları barındıran kaynaklı plakada hata tespit bulma olasılığı (PoD) yaklaşımını kullanarak geleneksel UT ve faz dizi PA sistemlerinin hata tespit etme yeteneklerini karşılaştırmaktır. Ayrıca tane boyutu, mikro sertlik, ses zayıflaması ölçümleri, radyoskopik ve makroskopik muayeneler gerçekleştirilmiştir. 304 paslanmaz çelik olan üç tip test numunesi hazırlanmıştır. İlk numune farklı derinliklerde Ø2 mm çapta delikler olan bloktur; ikinci numune delikleri 5 mm ile 0,5 arasında değişen çaplarda aynı derinlikte olan bloktur ve üçüncü numune yapay ve kaynak hatalarını bulunduran kaynaklı plakadır. PA metodu otomatik kalibrasyon, ses demeti odaklama ve ses demetini farklı zamanlarda ateşleyerek kontrol edebilme özelliklerine rağmen, yapay hatalara sahip test bloklarında gerçekleştirilen hata tespit analizlerinde (PoD) yüzeye en yakın hatayı bulmak dışında büyük bir farklılık ortaya çıkarmamıştır. Fakat kaynaklı plakada yapılan muayenelerde faz dizisi (PA) metodu hata tespit sayısı, hataları konumlandırma ve boyutlandırma yönlerinden geleneksel UT yönteminden daha başarılıdır. Otomatik PA sistemi üstün

algılama ve konumlandırma yetenekleri yönünden manuel PA sisteminden daha başarılı olmasına rağmen, manuel PA sistemi daha hızlı tarama ve prob dönüşü üstünlüğüne sahiptir fakat bu durum insan faktörü riskini de beraberinde getirmektedir.

Anahtar Sözcükler: Ultrasonik Test; Faz Dizisi; Hata Tespit Olasılığı (PoD).

TABLE OF CONTENTS

x

LIST OF FIGURES

xvi

LIST OF TABLES

CHAPTER 1

1   INTRODUCTION

1.1   GENERAL

Nondestructive Testing (NDT) or Nondestructive Evaluation (NDE) is a very broad and interdisciplinary field that plays a crucial role in structural components and systems to perform their function in a reliable and cost effective fashion. It is the technique of inspecting and evaluating materials, parts without causing damage.

Since its first use, many industries have already been familiar with some NDT technologies from medical to industrial usage. NDT provides valuable opportunities to all industries, hence, the evolution of techniques grows rapidly as shown below.

Conventional NDT Methods	**Most Popular Advanced NDT Methods**
• Visual testing	• Long range ultrasonic testing
• Ultrasonic Testing	• Time of flight diffraction
• Radiographic Testing	• Phased array ultrasonic testing
• Eddy Current Testing	• Digital radiography
• Magnetic Particle Testing	• Acoustic Emission Testing
• Dye – Penetrant Testing	• Alternating current field measurement

1.2   ULTRASONIC TESTING

1.2.1   Introduction to Ultrasonic

Ultrasound is defined as the sound of higher frequencies than 20 kHz. It is reported that while frequency range of human voice fall within 300 Hz to 4 kHz, the hearable sounds are in a wide range of frequencies, 20 Hz to 20 kHz.
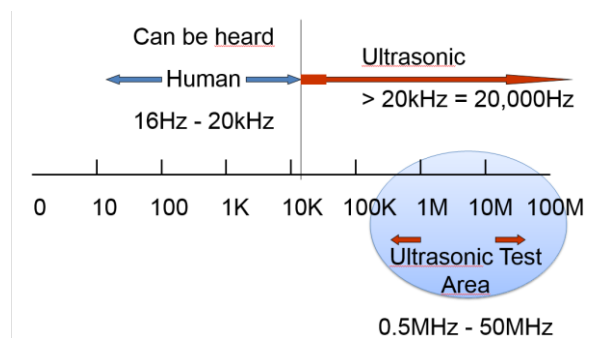
Figure 1.1 The frequency range [1]

Ultrasound propagates in a medium such as gas, liquid or solid, but it does not propagate in a vacuum. Propagation rate depends on medium where the efficiency and speed of sound propagation increases with the order of gas (lowest), liquid and solid (highest). The speed of sound in the air and the water are 340 m/s and 1500 m/s respectively [1].

1.2.2   Conventional Ultrasonic Inspection – Advantages and Disadvantages

Conventional ultrasonic inspection is commonly used for flaw detection in materials. Ultrasonic inspection method utilizes the transmission of high-frequency sound waves in a material to detect a discontinuity or to locate changes in material properties.

Ultrasonic inspection is a very useful and versatile NDT method. Some of the advantages and disadvantages of ultrasonic inspection are given in Table 1.1.

Table 1.1 Advantages and disadvantages of ultrasonic testing [2]

Advantages of Ultrasonic Testing

- Extensive experience on conventional UT Inspections
- The testing and acceptance criteria are well established
- The setup of conventional equipment is easy
- Costs for the equipment and operators relatively low
- Non-hazardous operations

Disadvantages of Ultrasonic Testing

- The scanning of weld is time consuming.
- Evaluation of results must be assessed by well experienced operators
- A later data analysis is not possible due to missing data recording
- The defect positioning is determined manually
- Reference standards shall be used both for calibration and characterizing

1.2.3 Physics of Ultrasound

Sound waves occurred from mechanical vibrations propagates in a medium like liquid, solid or gas. Sound waves pass through in this medium at a certain sound velocity, frequency and wavelength. When the sound waves hit to a boundary of a different medium, they are reflected and transmitted.

Sound wave is described by Velocity, frequency and wavelength of a sound energy. The relationship between them is as follows:

$$\lambda = \frac{c}{f}$$ (Eq. 1.1)

λ : Wavelength, c : Velocity, f : Frequency

V $_{Steel}$: 5960 m/s   V $_{Water}$: 1470 m/s   V $_{Air}$: 330 m/s
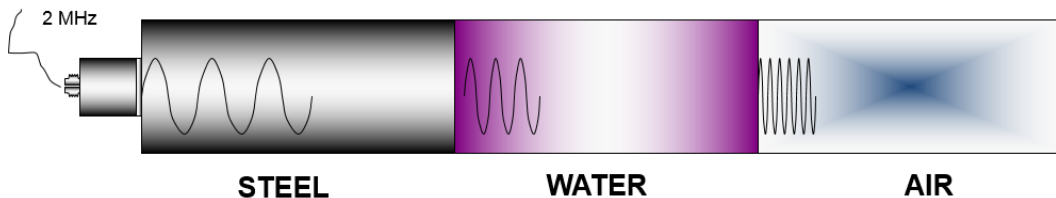
Figure 1.2 Sound velocities in various mediums [4]

In a certain medium, velocity of sound wave is constant and depends on properties of medium such as density and elastic modulus. The wavelength is directly proportional to the velocity of the wave and inversely proportional to the frequency of the wave. As shown in Equation 1.1, when the frequency is changed, velocity of ultrasound does not change but the wavelength is replaced to another value.
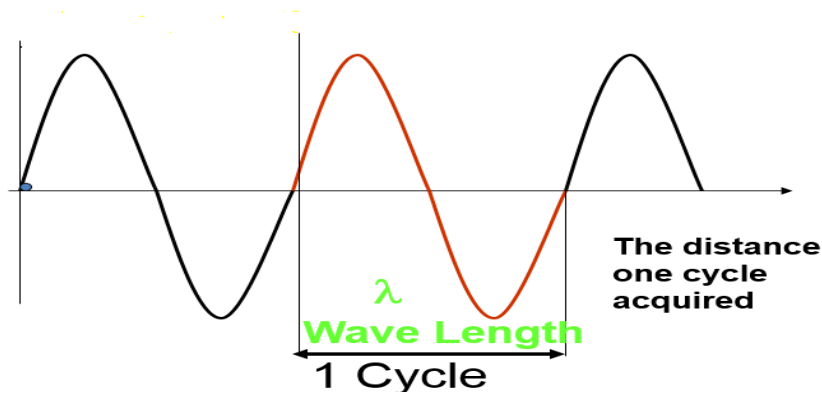
Figure 1.3 Wavelength display [4]

Table 1.2 Compressional and shear velocities in various materials [4]

Material	Compressional velocity (m/s)	Shear velocity (m/s)
Aluminum	6320	3130
Steel (1020)	5890	3240
Cast iron	4800	2400
Stainless Steel	5740	3100
Copper	4660	2330
Titanium	6070	3310

1.2.4   Major Variables in Ultrasonic Inspection

The major variables in ultrasonic inspection are the properties of ultrasonic waves and the properties of the material being tested. In order to obtain accurate results, the ultrasonic equipment must be in compliance with these variables.

Frequency is the number of occurrences of a repeating event per unit time.

Sensitivity is the capability of ultrasonic equipment to identify small discontinuities. The chance to detect small discontinuities is mostly increased by high frequencies (short wavelengths).

Resolution is the capability of the ultrasonic equipment to identify simultaneously whether is a discontinuity exist in material's front surface and lateral position. Resolution increases with frequency band-with and decreases with pulse length.

Penetration is the distance where the sound wave can go through. It is decreased by the increasing of frequency. The penetration decreases in case of inspection of coarse grain structure due to scattering from grain boundaries.

Beam spread is the divergence of an ultrasonic beam. As frequency decreases, ultrasonic beam spread deviates from ideality. Accordingly this phenomena, it is almost encountered every bandwidth of frequencies. Parameters of transducers such as diameter, frequency, sensitivity, resolution and depth focusing affect beam spread [3].

The pulse length, type and voltage applied to the crystal, properties of the crystal, backing material, transducer diameter and the receiver circuit of the equipment will also affect the ability to locate defects.

1.2.5 Wave Propagation

In solids, there are four fundamental modes of sound waves that can be generated by oscillating of the particles. The main modes are longitudinal waves, shear waves, surface waves and plate waves in thin materials. The most extensively used types in ultrasonic testing are longitudinal and shear waves in which the particle movement is responsible for these types of propagation illustrated in Figure 1.4 [4].
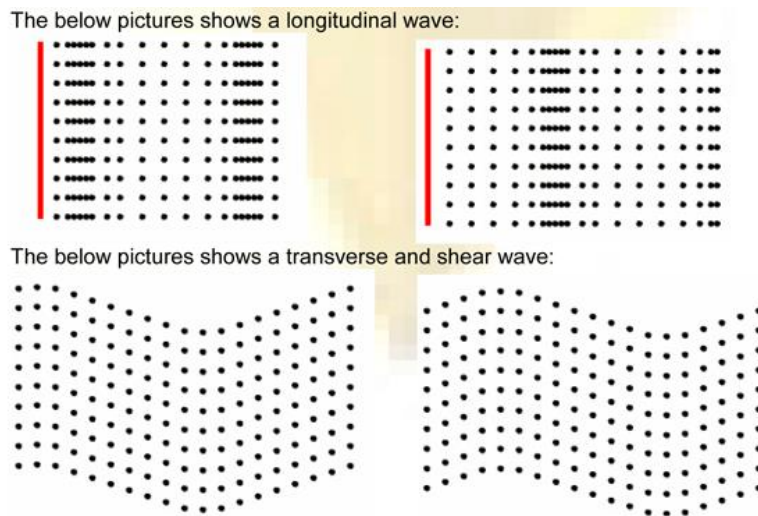
Figure 1.4 Longitudinal and transverse waves [4]

Since longitudinal waves (pressure or compressional waves) are moved by compressional and dilatational forces, these forces lead to energy fluctuations in the atomic structure. Therefore, longitudinal waves can be created in solids as well as liquids.

In the transverse or shear waves, the particles oscillate at a right angle or transverse to the direction of propagation. Shear waves require an acoustically solid material for effective propagation, as a result, are not effectively propagated in mediums such as liquids or gases. Shear waves are relatively weak compared to longitudinal waves.

1.2.6 Mode Conversion and Snell's Law

Shear wave is generated by the oscillating particles transverse to the direction of propagation. Shear waves are only active in solid material since atomic package or molecules are tightly packed in solids. Actually, shear waves are achieved from longitudinal wave energy when the sound wave bump into a plane, some of the energy continue to their journey as a longitudinal wave while some of this energy is transforming to transverse waves as shown in the Figure 1.5.

6
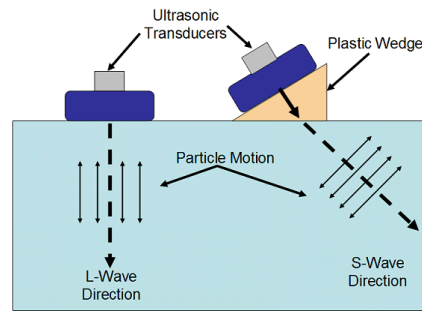
Figure 1.5 L-Wave and S-Wave schematic display [5]

Since the mediums have various acoustic impedance, refraction occurs at interface (Figure 1.6). When the difference in sound velocities between the two mediums increase, the refraction of sound wave enlarges.
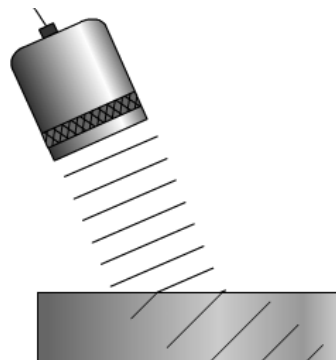
Figure 1.6 Refraction of waves [6]

Snell's Law defines the relationship between the angles and the velocities of the waves. Snell's law relates the ratio of material velocities V_1 and V_2 to the ratio of the sine's of incident (Q1) and refracted (Q2) angles, as described in the Equation 1.2 [6].
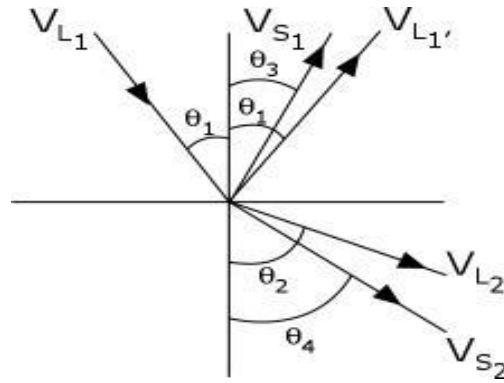
Figure 1.7 Snell's Law correlation of velocity and refracted angle

$$\frac{\sin\theta 1}{V_{L1}} = \frac{\sin\theta 2}{V_{L2}} = \frac{\sin\theta 3}{V_{S1}} = \frac{\sin\theta 4}{V_{S2}} \qquad \text{(Eq. 1.2)}$$

Where:

V_{L1} is the longitudinal wave velocity in material 1.

V_{L2} is the longitudinal wave velocity in material 2.

V_{S1} is the shear wave velocity in material 1.

V_{S2} is the shear wave velocity in material 2.

In addition to Snell's law, there is a "Critical Angle" subject that should be taken into consideration as well. The critical angle is the point of longitudinal wave refracted as 90°. This angle is referred to first critical angle which can be derived from Snell's law by putting angle of 90° for the refracted incidence.

Shear wave forms when the incident angle is equal or greater than the first critical angle. In order to prevent any confusion due to the presence of two wave mode in the system, the longitudinal waves have to be eliminated.

When refraction angle of the shear waves becomes 90°, at this point second critical angle develops upon surface as a shear wave or shear creep wave. Starting from second critical angle, surface waves will take place at the surface.

There is another type of ultrasonic wave, called surface waves (Rayleigh waves), which mostly occurs in the flat or curved surface of relatively thick solid parts. In order

to propagate, they need to move on an interface between the strong elastic forces of a solid and weakly elastic forces compound of gas molecules.

Surface waves can be used in inspection of the parts having complex geometries because of their ability to reflected back easily from rounded curves. For instance, some surface waves reflected back from the sharp edge of a metal block travel on the top surface unless they bump into a curved edge which makes it possible to move side edge and the lower edge of the part. As long as all edges of the part is rounded off, surface waves will travel completely around of the part [3].

1.2.7   Attenuation of Sound Waves

In ideal situation, as the sound wave energy is spreading by the distance, sound energy or pressure (signal amplitude) is diminished. However, in reality the sound amplitude is much more weakened by the effects of scattering, absorption and beam skewing. Scattering is the reflection of sound wave deviated from its original direction, whereas the absorption is the transforming of the sound energy into other forms of energy. The total effect of scattering and absorption is referred to attenuation. Furthermore, there is a correlation between attenuation and frequency which is changed directly proportional to the square of sound frequency (Equation 1.3) [8].

$$A = A_0 \, e^{-\alpha z} \qquad\qquad \text{(Eq. 1.3)}$$

A_0: initial amplitude, α: attenuation coefficient (Np/m), z: travelled distance (m)

Np (Neper) is a logarithmic dimensionless quantity and it can be converted to decibels by dividing with 0.1151.   The decibel (dB) is a logarithmic unit that measured a ratio of two signals. Use of dB units allows to ratios of various sizes for easy to work with numbers.

$$\Delta I(dB) = 10 \log \frac{X_2}{X_1} \qquad\qquad \text{(Eq. 1.4)}$$

The change in sound pressure (Table 1.3) or the intensity of sound waves can be gauged with the use of a transducer. Next, the difference in sound pressure is conducted to a voltage signal. The ratio of sound intensity in decibels between sound pressure and intensity is described in Equation 1.5.

$$\Delta I \ (dB) = 10 \log \frac{I_2}{I_1} = 10 \log \frac{P_2^2}{P_1^2} = 20 \ \log \frac{P_2}{P_1} = 20 \log \frac{V_2}{V_1} \qquad \text{(Eq. 1.5)}$$

ΔI: The change in sound intensity between two measurements

V_1 and V_2: The two different transducer output voltages (or readings)

Table 1.3 Change in the sound pressure

Ratio Between Measurement 1 and 2	Equation	dB
1 / 2	dB = 20 log 1/2	-6 dB
1	dB = 20 10 log 1	0 dB
2	dB = 20 10 log 2	6 dB
10	dB = 20 10 log 10	20 dB
100	dB = 20 10 log 100	40 dB

By evaluating the multiple back-wall signals, attenuation can be determined from a typical A-scan display (Figure 1.8).
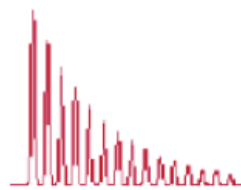
Figure 1.8 Attenuation [9]

Grain size influences the sound attenuation during ultrasonic inspection. The scattering coefficient which is the major aspect of the attenuation can be calculated using Eq.1.6;

$$\alpha_s = C_r \ . \ D^3. \ f^4 \qquad \text{(Eq.1.6)}$$

where C_r is the scattering parameter depending on the wave type and the material anisotropy, D is the mean grain size and f is the frequency.

The Equation 1.6 is also valid for Rayleigh waves in which wavelength is larger than the grain size. Ultrasonic examination is carried out at this range where the scattering coefficient (α_s) is proportional to both frequency and grain size [24].

1.2.8 Acoustic Impedance

Sound energy pass through mediums with the influence of sound pressure. For the reason that molecules or atoms are bond coherently together, wave propagation is occurred due to excess pressure. The acoustic impedance (kg/m^2s) or ($N\ s/m^3$) is a function of density (kg/m^3) and sound velocity (m/s).

The acoustic impedance; $Z = \rho V$ (Eq. 1.7)

Table 1.4 Acoustic impedances (kg/m^2s) of various media

Aluminum	Copper	Steel	Titanium	Water (20°C)	Air (20°C)
17.1×10^6	41.6×10^6	46.1×10^6	28×10^6	1.48×10^6	413

Acoustic impedance (Z) is vital for various circumstances. First, sound wave travels in media having different acoustic impedances which affects the transmission and reflection of sound waves. Second, it is required for constructing the design of ultrasonic transducers and evaluation of absorption of sound in a medium.

1.2.9 Reflection and Transmission Coefficients

The difference in acoustic impedances of the materials or each side of the boundary media leads to reflection of ultrasonic sound waves. The larger impedance mismatch,

the more percentage of energy that will be reflected at the interface or boundary. If the acoustic impedances of the materials are known, the reflection coefficient (the fraction of wave intensity) can be calculated (Eq. 1.8).

$$\left(R = \frac{Z_2 - Z_1}{Z_2 + Z_1} \right)^2$$
(Eq. 1.8)

As seen in Figure 1.9, 12 % of the ultrasound energy produced by the transducer is transmitted into steel while 88 % of the energy is reflected back. As the sound is traveling in the steel, just 10.6 % of sound energy continue to its path while 1.4 % is off track. Finally, just the 1.3 % of initial sound energy comes back to the transducer. Moreover, it should be noted that in such calculation the attenuation of the signal as it passes through the material is not considered. If it is considered, the amount of signal received back by the transducer will be even smaller.
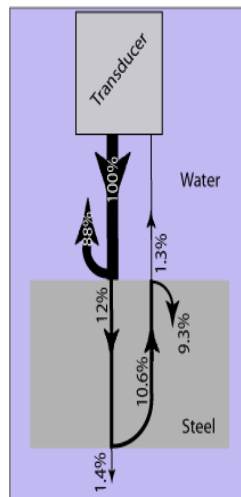
Figure 1.9 Transmission and refraction [4]

1.2.10 Wave Interaction or Interference

In order to understand wave interaction and interference, it is mandatory to understand ultrasonic transducers function and how they are working. Although sound waves propagate as one sound beam from a single point, in reality sound beams are ignited along the surface of ultrasonic transducers. Therefore, all these waves or sound beams

are both interacting and interfering with each other, consequently this event results in generating a sound field.

In Phase
(0° phase difference)
Constructive Interference

90° phase difference

Out of Phase
(180° phase difference)
Destructive Interference
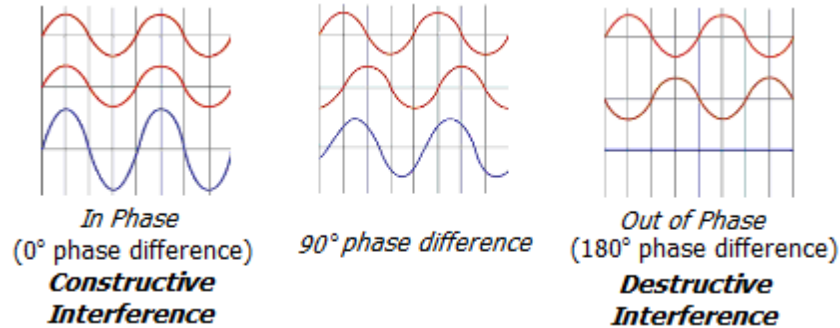
Figure 1.10 Phase interference [10]

In case of identical waves which originate from the exact source while they are in same phase (0° phase difference), they become constructive interference. On the other hand, when they have 180° phase difference so that the peaks of signals are anti-symmetrical, they adversely affect each other and it is referred as destructive interference. When the two waves are partly in phase or out of phase, sum of the wave amplitudes for all points is considered as a resulting phase [10].

1.2.11 Wave Interference

The waves always are examined in 2D plot wave, amplitude versus wave position by now. However, Figure 1.11 represents a stone dropped in a pool of water of the waves radiating from one point. In case of two particles dropped in water, then the waves are interacting each other and the sum of amplitude is considered at every displacement of individual waves [10].

Wave from
one point

Interference of waves
from two points
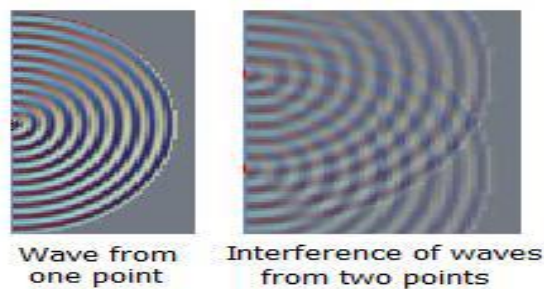
Figure 1.11 Wave interference [10]

1.2.12 Ultrasonic Equipment and Transducers

The fundamental of ultrasonic testing is transforming electrical pulses into mechanical vibrations and collection of data is carried out by returned mechanical vibrations transforming back into electrical energy. Whole process is carried out with the help of transducers consisting of a piece of piezoelectric material (a polarized material having some parts of molecule are positively charged while the other parts are negatively charged). When electric energy is applied to transducer, the polarized molecules in the transducer's material will forced to align themselves as a result of electric field causing the material to change dimensions. Also, an electric field is created by the elements of polarized material permanently-polarized material such as quartz (SiO_2) or barium titanate ($BaTiO_3$) as a consequence of induced mechanical forces. This phenomenon is called piezoelectric effect.

Transducers are categorized into two major groups according to the application. Contact transducers are used for direct inspections in a wide range of applications. Since they are moved by hand, they are composed of variety of materials preventing from sliding. In order to expand the useful life, the replaceable wear plates are wielded as long as coupling materials water, grease, oils and other commercial materials for removing the air in the gap between the material being inspected and contact transducers. Unlike contact transducers, the immersion transducers are not in direct contact with component or material. In order to utilize these type of transducers all connections are water proof and designed to engage in the liquid environment. Moreover, a big advantage of immersion transducers is minimizing the difference impedance matching layer by sending more energy into the water and in return receiving more energy from the material being inspected [4].

1.2.13 The Characteristics of Piezoelectric Transducers

The piezoelectric transducers are made up one transmit mode which is converting electrical signals into mechanical vibrations, the other is receive mode converting mechanical vibrations into electrical signals.

A contact transducer is illustrated in Figure 1.12. In order to create energy as much as possible in the transducer, first a matching layer is placed between the active element and in front of the transducer. The size or thickness of matching layer must be 1/4 of the desired wavelength for the optimal matching layer. Therefore, the reflected waves are same phase within the matching layer as they go out layer. While acoustic impedance value of matching layer must be between the active element and steel, for the immersion transducers acoustic impedance matching layer must be suitable for the active element and water.
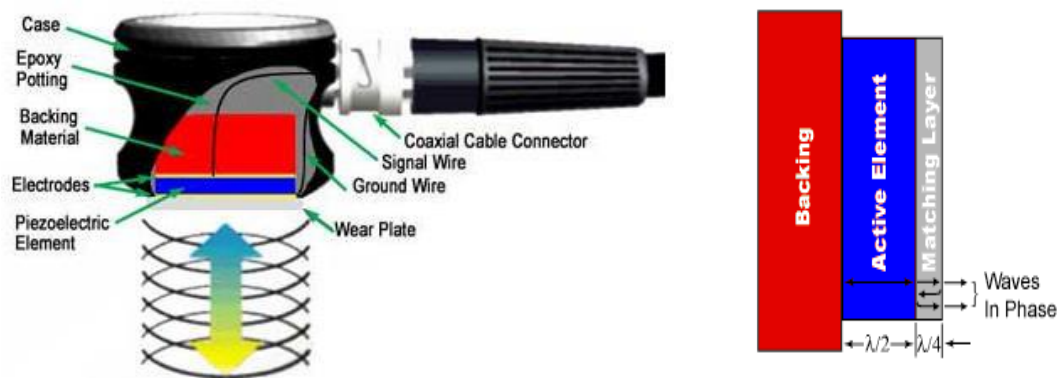
Figure 1.12 The piezoelectric transducers [4]

The backing material supporting the crystal with an impedance similar will produce most effective damping. Hence, the backing material gives to transducer a wider bandwidth producing higher sensitivity as well as higher resolution. While the difference in impedance between the active material and the backing material escalates, penetration of sound waves increases. However, sensitivity is diminished.

The frequency and band width is usually linked with a transducer having a central frequency and depending heavily on the backing material. The more broad range band

width frequency is the more resolution and high damping power, as the less damping power means that narrower frequency range, less resolution and greater penetration.

1.2.14 Radiated Fields of Ultrasonic Transducers

Wave interference affects directly the ultrasound intensity in terms of the beam because ultrasound propagates from many points along the transducer. Therefore, extensive wave fluctuations are occurred by the prompting of wave interference near the source where this zone is referred to "near field". In the near field zone the detection of defects and evaluation of signals are difficult due to excessive acoustic fluctuations (Figure 1.13).

A more uniform phase of ultrasonic beam spread is obtained beyond the near field where this field is called "far field". The relationship between far field and near field zone is correlated with a distance N, and sometimes referred to as the natural focus of a transducers. Thus, the best detection ability is reached for the flaws at this distance [9].
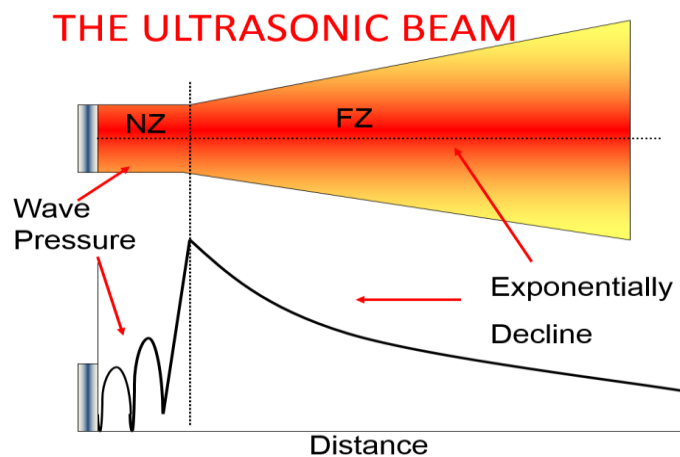
Figure 1.13 Variations of acoustic sound pressure with distance for circular crystal [9]

The near field distance can be found as for a round transducer:

$$N = \frac{D^2 f}{4V} \qquad \text{(Eq. 1.9)}$$

where;

θ: Beam divergence angle from centerline to the point where signal is at half strength

V: Sound velocity in the material

D: Diameter of the transducer

f: Frequency of the transducer

1.2.15 Beam Divergence and Beam Spread

The beam spread is a measure of the whole angle, whereas beam divergence is a measure of the half angle from one side of the sound beam to the central axis of the beam in the far field as described in Figure 1.14.
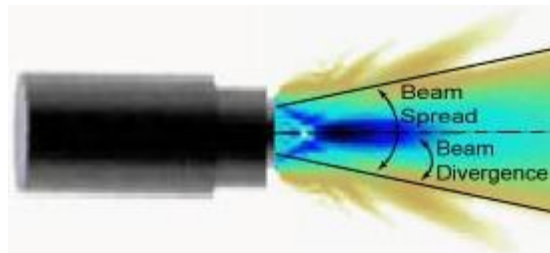
Figure 1.14 Beam spread [4]

The frequency and diameter of the transducer alter directly the beam spread. In case of straight beam probes where the centerline sound pressure is optimal, the sound pressure decreases by one half (-6 dB) from this optimal value away from the centerline [4].

1.2.16 Ultrasonic Measurement Methods

Portable ultrasonic measurement systems including transducers and an oscilloscope are utilized for flaw detection and thickness measurement in all kind of materials, i.e., metals, plastics, ceramics and composites.

1.2.16.1 The Transmission Method

The transmission method, in which one probe is the transmitter and the other one is the receiver, demands access from both sides of the items inspected (Figure 1.15).
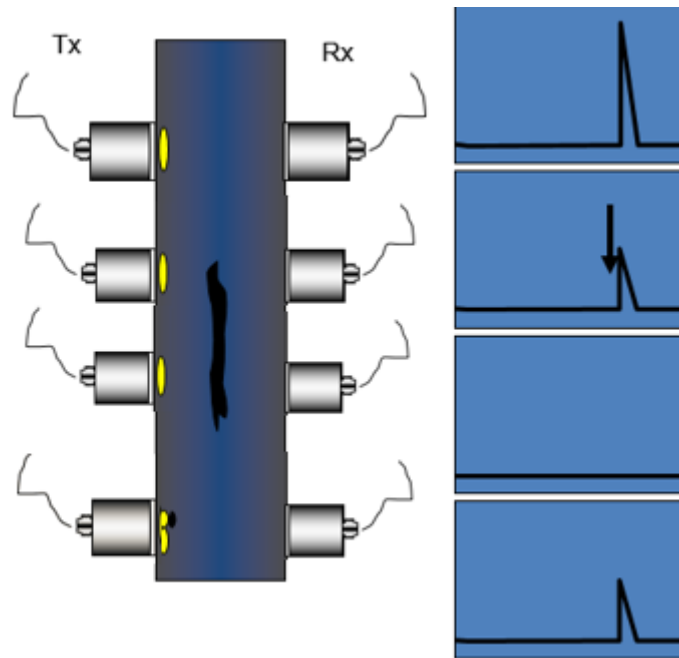
Figure 1.15 Transmission method [9]

There are some losses in the sound pressure due to contact of the probes with surface. Thus, the change in the amplititude of peaks can misguide the operator to a signal of defect. Second, an exact face to face position must be maintained during inspection otherwise the transmission method is failed [9].

1.2.16.2 The Pulse – Echo Method

In the pulse – echo system the reflected sound pressure is measured with one probe acting as transmitter and receiver. The time between pulse sent and received back from the back wall or an obstacle is directly proportional to the sound distance. The instant

time of sound wave transmitted from the probe is referred to zero scale of the display or outburst echo "S" while the reflected signal from back wall is demonstrated as "R" signal.
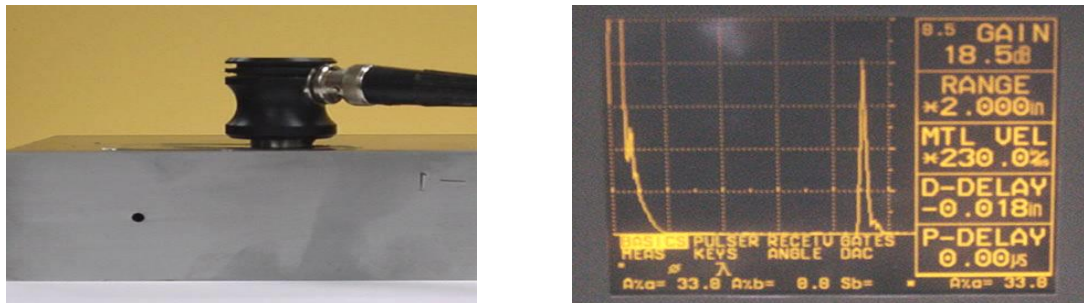
Figure 1.16 Signal presentation of the back wall

In case of no defect on the way of sound wave, there will be only pulse echo (S) and back wall echo (R) on the screen. Supposing that the calibration of ultrasonic measurement system is right, the distance between S and R corresponds to actual thickness of measured item (Figure 1.16).
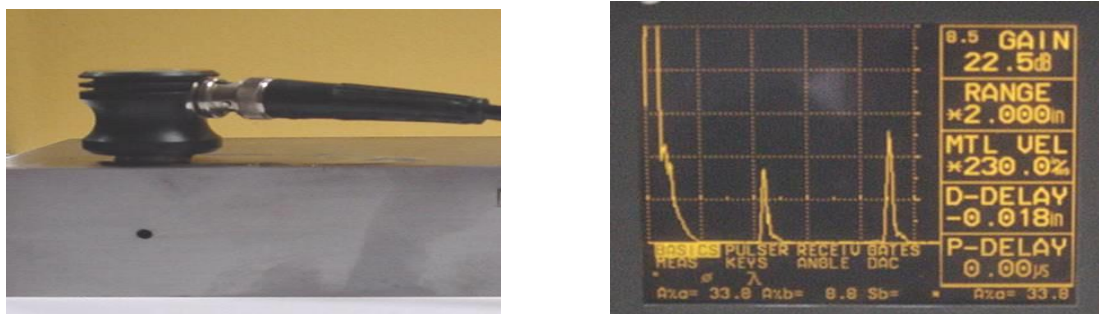
Figure 1.17 Signal presentation of the back wall and a defect

As seen in Figure 1.17, there will be another echo between the back wall signal (R) and pulse echo (S), if there is a defect intercepted with sound wave. The defect position with respect to the probe can be calculated from the echoes on the screen, the amplitude of the back-wall echo will decrease [9].

19

1.2.17 Data Presentation of Ultrasonic Testing

Data presentation can be done in a number of different formats. There are three common types of data presentation, A-Scan, B-Scan and C-Scan presentations. Each scan mode provides to the inspector different advantage, in terms of detecting, positioning and evaluating. Advanced systems have the capability of displaying data simultaneously in all three presentation formats.

A – Scan Presentation

The amount of received ultrasonic energy (vertical axis) versus the energy as a function of a time (horizontal axis) are displayed on the A-Scan presentation. Moreover, in the A-scan presentation a discontinuity can be detected by comparing the signal amplitude retrieved from a known reflector and unknown reflector. The position of the signal on the horizontal time axis gives information about depth or the position of the discontinuity.
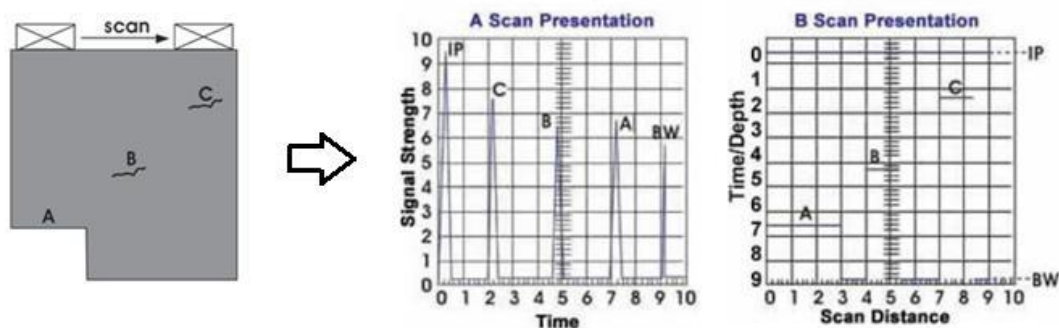
Figure 1.18 The back wall and B, C defect signal presentation [10]

In Figure 1.18, first echo is represented by initial pulse starting time at zero in the A-Scan presentation. As the transducer is moved along the surface of item inspected, four other signals are appeared depending on the scan direction at different times. The A surface leads to A signal along with initial pulse (IP). As the transducer is moving right, the B discontinuity leads to B signal, distinctive from A signal, in terms of positions B signal closer than A signal.

1.3 PHASED ARRAY SYSTEM

Phased Array technique is superior to conventional ultrasonic method regarding high automated inspection speeds, full documentation with data storage for auditing, and better detection capabilities in volume inspections.

Phased Array method can be used in manual or encoded form. A typical Phased Array device is demonstrated on Figure 1.19, along with multiple works demonstrated showing simultaneously scanning with encoders A-Scan, S-scan and C-Scan [11].

Figure 1.19 A commercial Phased Array instrument [11]

1.3.1 Basic Principles of Phased Array

Basic principles of Phased Array system are match up with ultrasonic waves which are mechanical vibrations induced in a medium or test piece.

A number of elements exist in a single probe, and they are ignited at different times. Delaying ignition times is controlled by a sophisticated software. This phenomena leads to adjusting focal depth or focal distance, steering angle, controlling beam width. Moreover, choosing the essential probe apertures or grouping elements and displaying of the data in a more efficient way take place in Phased array method.

A single transducer is used in conventional ultrasonic testing, while the Phased Array system utilizes up to 256 elements (Figure 1.20). Therefore, multi structure of the Phased Array probes is the major factor for increasing detection abilities.
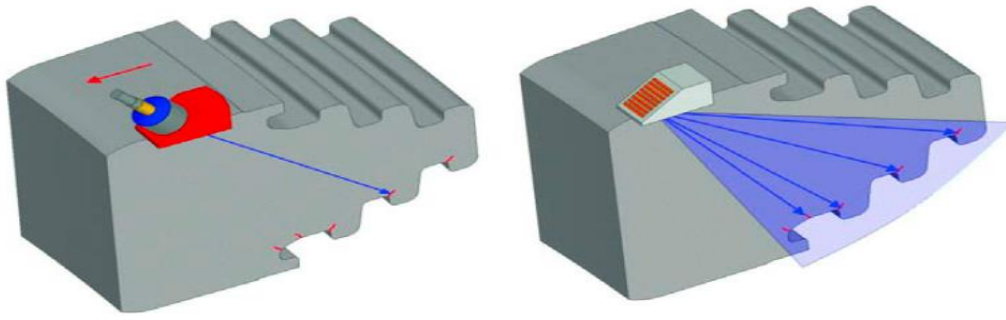
Figure 1.20 (On the left) a single transducer's element, (on the right) a multi PA transducers [12]

The specialty of the Phased Array system is control of amplitude and delayed by computer processor. The piezoelectric elements excited electrically lead to create beams with defined parameters such as correct angle, focal depth or beam width.

In order to create longitudinal and shear waves at the same time, the ignition of active elements must be slightly diversified and coordinated times. In the reception phase every element sends their pulses or signals at different time of flight values, however, the values are adjusted time based on by software the whole event called focal law. At last all signals are transferred to the acquisition mode by converting to just one signal like ultrasonic system. Therefore, multi elements signals transmitted by acquisition instrument activate to create a sound beam along with a specific angle and focus depth [12].
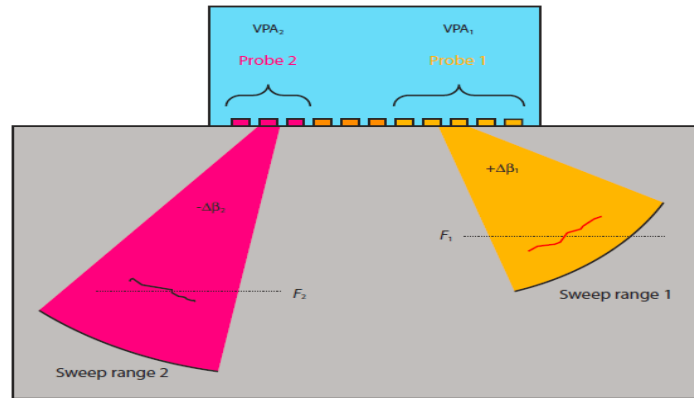
Figure 1.21 Grouping of elements in the Phased Array probe [12]

1.3.2 Phased Array Probe Characteristics

The ordinary Phased Array probe has a number of ultrasonic transducer elements organized to accelerate the inspection speed and to enlarge the inspection area as well. Every single element represents an ordinary conventional ultrasonic probes; however, they are much smaller. These elements electronically controlled to form an electronic beam which makes possible multiple areas inspection simultaneously.

Contemporary Phased array probes for industrial applications are focused around piezocomposite materials, which are consist of many tiny, thin rods of piezoelectric ceramic implanted in a polymer matrix. Although their manufacturing process is more difficult than the process of piezo ceramic probes, composite probes give sound energy from 10 dB to 30 dB over the ordinary probes [13].

1.3.3 Software Control and Phased Pulsing of Phased Array

While creating a beam, many variables involve in process such as acquisition unit, Phased array instrument, transducers elements and natural flaws (Figure 1.22). As acquisition unit is controlling on traffic of information flow, Phased array unit regulates transmitting delays of pulses and summing total reflected back echo signals

23

up to transferring unit. A-scan, B-scan, C-scan or S-Scan displays are compromised on the Phased array instrument.
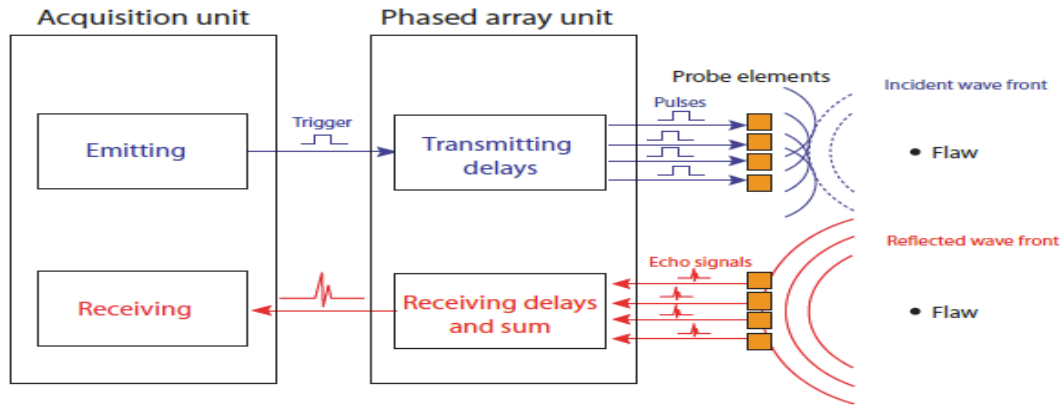
Figure 1.22 Beam forming, time delay for pulsing, receiving multiple elements [15]

The Phased array instrument software adjusts particular delay times for creating a desired beam shape. Mostly the software part is referred as focal law calculator including transducer and wedge properties, part geometry, and material characteristics (Figure 1.23).
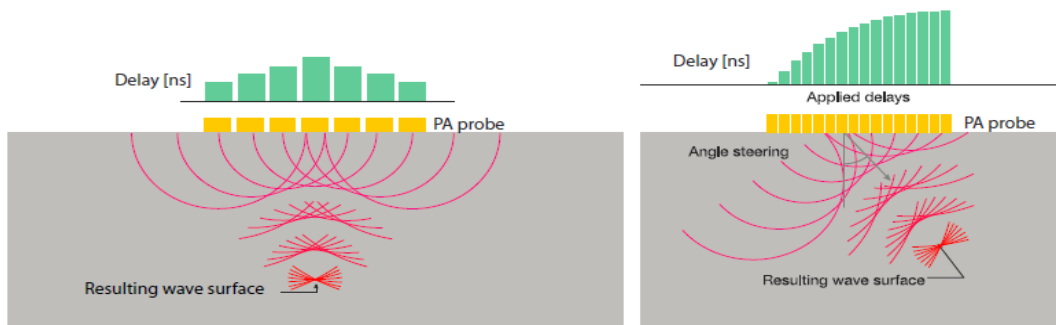
Figure 1.23 Beam focusing first normal longitudinal sound beam second shear wave generation [15]

Phased array inspections can be adapted in almost any implementations where conventional ultrasonic methods have been used. However, boosting waves or cancellation wave effects can be used particularly in the favor of beam shaping and

24

steering in Phased array technique. Also, ignition of a single or a group elements is carried out in different delays leading to occur a wave front as shown on the Figure 1.24 - time delays on firing (Figure 1.24) - is special for Phased Array [15].
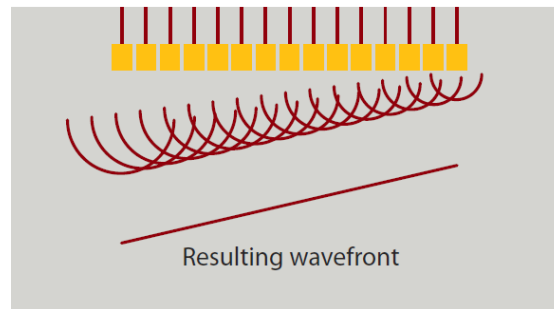
Figure 1.24 Time delays on firing of Phased Array elements [15]

1.3.4   Beam Steering and Shaping

The change in pitch size and elements lie with in the same manner changing of single ultrasonic beam. This event can be altered into a new form in the favor of detection capabilities. The beam direction, refracted angle and focusing abilities manipulated or adapted into a new form by changing firing times electronically. The significant factors about beam steering and shaping are given in Table 1.5.

Figure 1.25 shows the number of elements fired or effective grouping elements comparing to conventional ultrasonic transducer in terms of creating sound beams.
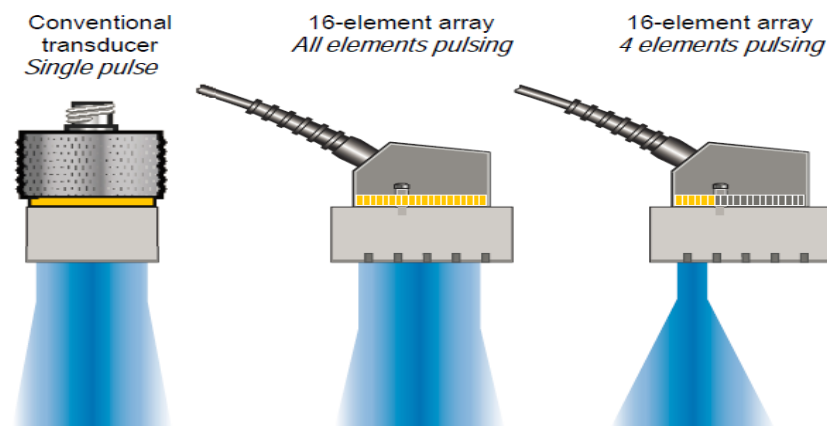
Figure 1.25 Conventional UT and PA probes [15]

Table 1.5 The Correlation between beam steering and pitch size - elements

Decreasing pitch size and elements	Beam steering capability increases
Escalating pitch size and frequency	Formation of unwanted grating lobs
Increasing element width	Creates side lobs as in conventional UT Reducing beam steering
Increasing active aperture with small pitch sized elements	Increasing focus factor or sharpness of the beam

1.3.5 Beam Focusing with Phased Array Probes

In Phased Array inspection, most prevailing scanning method is linear scanning with rectangular elements, where the sound beam is oriented to focus. According to Table 1.5, increasing aperture size leads to escalation in the sharpness of focused beam. As seen in the Figure 1.26, the red areas represent high sound pressure and blue areas correspond low pressure levels of sound waves respectively [11].
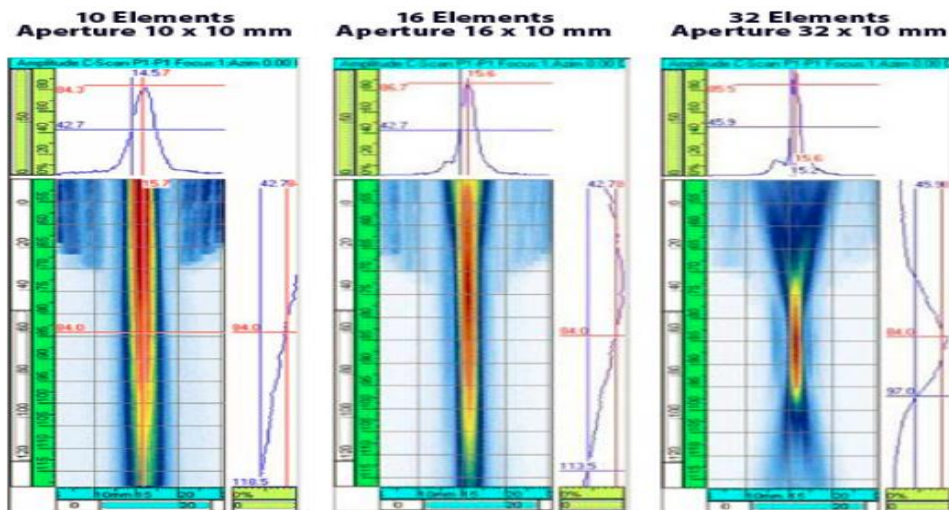
Figure 1.26 Beam focusing for different number of elements and apertures [11]

1.3.6 Application of Phased Array System

A-Scan Presentation

The classical display of conventional ultrasonic and Phased Array system is the A-Scan, representing echo signal and time so that the x-axis corresponds to time while y-axis is corresponding to amplitudes. As appears in the Figure 1.27 the green marks represents echoes or amplitudes, the red bar is the gate for analyzing data for the A-scan [13].

B-Scan Presentation

Rather than a single amplitude of data gathered from gate, the B-Scan is a transformed form of A-Scan by digitizing at all transducer positions. The transformed data of A-Scan successfully are transferred to generate a cross sectional area of the image. With respect to form a B-Scan image every digitized signal waveform must be rendered and make sure that the colors corresponding to appropriate depths of images [13].

C-Scan Presentation

C-Scan represents the top view of the material which is inspected with the help of an encoder C-scan data, as in the x-axis corresponds to distance passed by encoder and y-axis corresponds to defect size. C-Scan is often called as "One line Scan" [13].
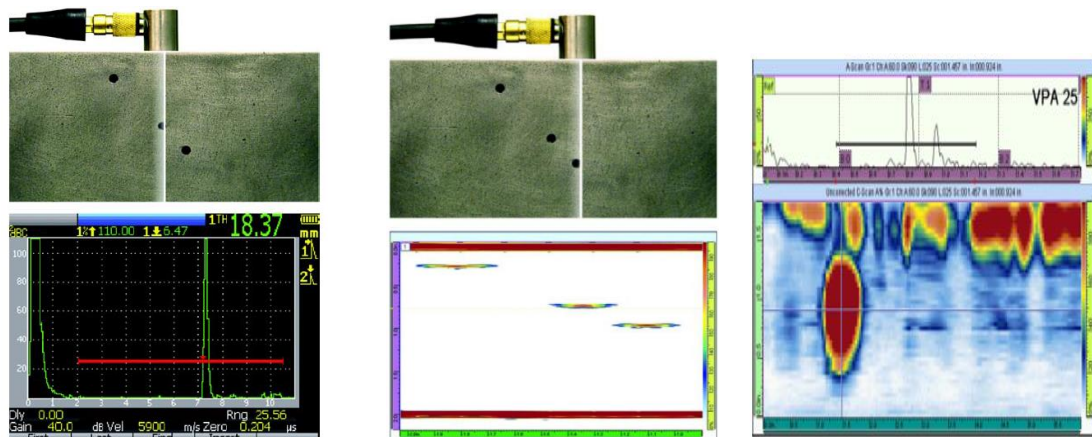
Figure 1.27 Phased Array A-scan, B-scan and C-scan respectively [13]

S-Scan Sectorial Scan Presentation

While S-scan is special for Phased Array system, A-Scan, B-Scan and C-Scan uses fixed angles and ordering aperture. S-scan also uses fixed apertures however, the angles can be changed which is called steering. Most prevailing S-scan type makes possible beam sweeping from 30° to 70° generating sectorial scan (Figure 1.28).
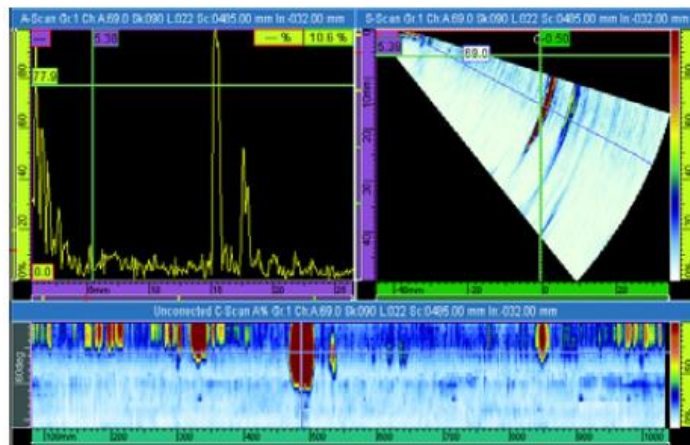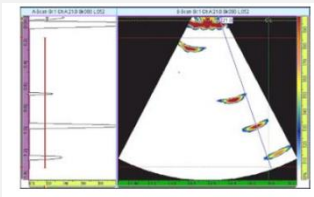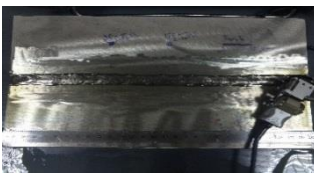
Figure 1.28 Multiple image display [13]

In the real inspections, S-scan have huge advantage comparing to other scanning types in terms of constructing dynamic scan which creates an effect of moving probe. Therefore, dynamically scanned method gives a distinctive advantage to detect defects particularly disoriented flaws detection [13].

Table 1.6 The essential variables of the Phased Array technique [14]

Probe	Number of Elements
	Element width (height)
	Element Length and Element Pitch
	Nominal Frequency and Gap
Wedge	**Material**
	Wedge Material velocity
	Incident Angle
	Height of Ref. Element over test piece
Instrument	**Model**
	Pulse Voltage and Shape
	Pulse Duration
	Receiver Frequency settings
	Processing settings
Beam – Setups	**Scan Type (A-Scan, B-Scan, C-Scan, S-Scan)**
	Number Of Elements in Focal Law
	Start Element
	Step Increment (angle or elements)
Test mechanics	**Immersion Or Contact**
	Scan Type (Manual, Mechanized, Automated)
	Scanning Pattern
Materials	**Test piece material and velocities**
	Couplant
	Geometry (Thickness and Shape)
	Scan Surface
Reference	Reference blocks and targets

The main advantages of PA system are given below:

- Inspection speeds in linear or sectorial scanning are faster than conventional ultrasonic testing. Phased Array saves inspection time and operator costs.
- Multifunctional property of Phased Array provides ability to inspect different components or parts in a wide range of distinctive patterns.
- Complex inspections such as nozzle welds or pipe welds are relatively easy through programing properties like multiple angles, modes and zone discrimination of Phased Array.
- Flexible Phased Array inspections give opportunity to inspect specifically small components like jet turbines and discs where narrow region aggravates the inspection.
- Mechanical reliability increases in the Phased Array method since the electronics used instead of mechanical systems such as rastering transducers lead to wear and tear.
- Increase in the signal-to-noise ratio (SNR) with specific angular resolution induce to focus depth ability which improves the detection performance [15].

1.4   Probability of Detection (PoD) Analysis

Materials are degraded by environmental effects in a specific time period so that a number of discontinuity occurs such as cracks, segregation or corrosion. Besides natural effects, there is another situation recently has risen which is budget cuts induced by governments or authorities. This situation has been affecting engineering world in a different way naming extended operational life of assets.

Numerous variables affect the material life under different circumstances. These factors can be measured by a quantitative statistically method called as Probability of Detection (PoD) which is very useful to evaluate of a non-destructive method. As PoD is applied to NDT methods and is developed in this field, the importance of NDT procedures and how it is altered by materials, human factors or processing parameters has been well understood recently in all industrial areas. PoD gives a distinctive

advantage to engineers about evaluating of NDT methods in terms of reliability [16] (Figure 1.29).
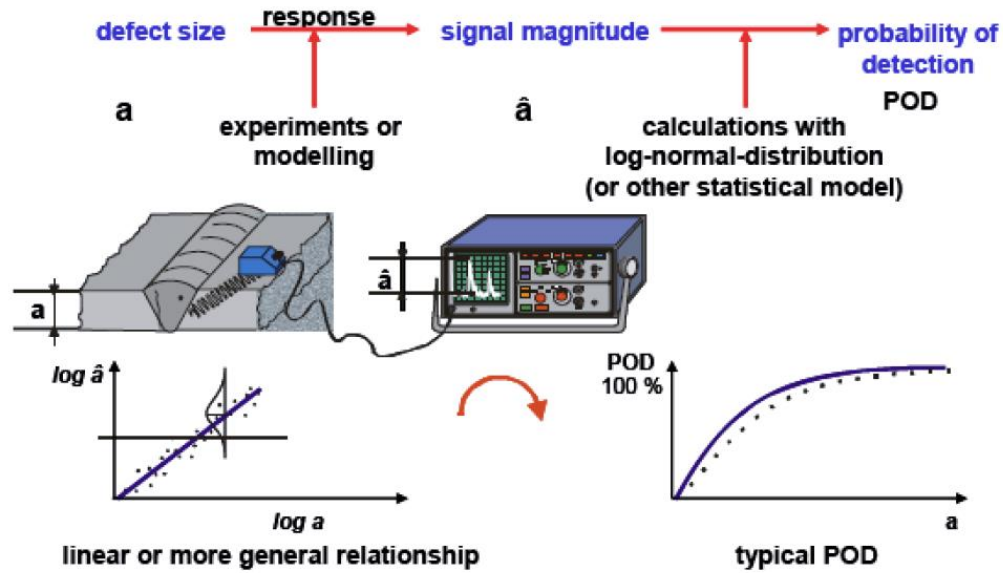
Figure 1.29 A typical PoD process presentation [16]

Nondestructive testing is a priority for constructing and commissioning a pipeline, nuclear power plant or any specific industrial projects. For instance, nuclear industry requires strict inspection rules, they have additional required tests sufficient flaws must be detected according to nondestructive procedures before procedures implemented on. Another choice to prove a NDT method is the statistical approach based on the probability of detection. The researches on PoD in various fields (medical sciences, material science, physics and especially NDT) has risen sharply as seen in the Figure 1.30 [17].
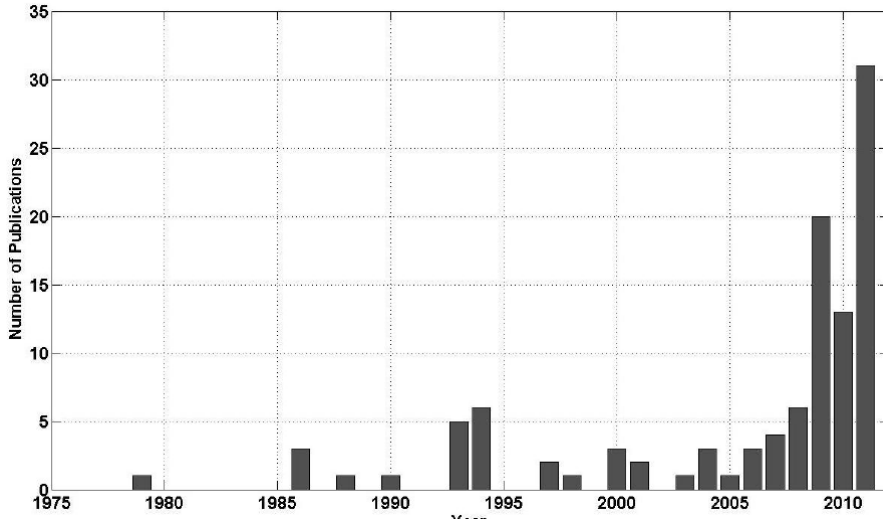
Figure 1.30 The publications dealing with PoD in the field of NDT [17]

Probability of detection is divided into two groups. First is hit/miss data, second one is signal response data. Both of them are based on whether a flaw is detected or not.

It is estimated that every single crack size have its own detection probability *(p)* and its probability density function of detection is referred as $f_a(p)\,d_p$ [16]. The sum of the detection probabilities including randomly selected ones from all data being detected in the scope of p, that is:

$$PoD\ (a) = \int_0^1 p \times f_a(p) \times d_p \qquad \text{(Eq. 1.10)}$$

The core of probability of detection in the field of NDE is attributed to an indication related with crack size *a*. This indication versus crack size can be distinctive for every method. For instance, in ultrasonic or eddy current it is peak voltage, for fluorescent penetrant method it can be brightness value. Recorded data is gathered and determined whether it is a positive value or not. The positive value of â falls into over the decision threshold of â $_{\text{decision}}$ (Figure 1.31).
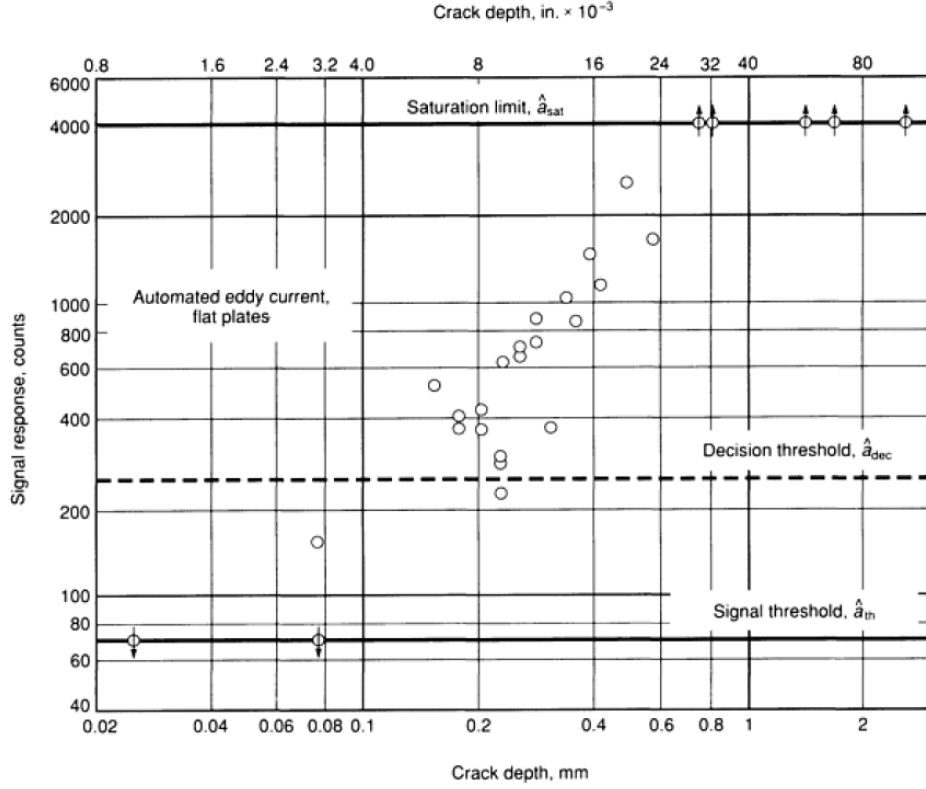
Figure 1.31 Signal Response versus Crack Depth [18]

The values for crack depth versus signal response in eddy current inspections of 28 cracks are listed in Figure 1.32. These results are derived from three different probes, under the threshold there are no recorded values. The decision threshold is fixed at 250 counts. The values above 250 were recorded and represented in Figure 1.31.

$$PoD\ (a) = \int_{\hat{a}_{dec}}^{\infty} g_a(\hat{a}) \times d\hat{a} \qquad \text{(Eq. 1.11)}$$

The PoD (a) function is created with the relation between *a* (size) and *â* (amplitude). Where $g_a(\hat{a})$ represents the probability density of the *â* values for fixed crack size *a* [18].

The essential parameters, affecting probability of detection can be numerous in accordance with the related field and relevant variables. The essential variables are listed below [19];

33

- ✓ Size and orientation of flaw,
- ✓ Flaw surface texture,
- ✓ Beam characteristics,
- ✓ Position of the flaw with respect to the sound path,
- ✓ Potential that the flaw was off-axis,
- ✓ Anisotropic characteristics of the materials,
- ✓ Coupling variation due to test surface roughness,
- ✓ Local variations of the conditions,
- ✓ Weld cap and weld root geometry,
- ✓ Mismatch conditions, etc.

1.5 Ultrasonic Inspection of Austenitic Stainless Steels

Austenitic materials are one of the basic metal groups having corrosion resistance at all levels. They have not only high strength and creep resistance at elevated temperatures, but also having ductility at low temperatures. Therefore, austenitic materials are used in various applications where particularly from pipework and primary circuit of a fast reactor to cryogenic tanks and food sector [20].

Among other stainless steels the most prevailing and applying kind is the austenitic stainless steel. Since austenitic stainless steels are weldable, formable and having excellent corrosion resistance, they are specialized for from jet turbines to red hot furnace parts. Although they are nonmagnetic and hard to inspect ultrasonically, they can be handled with more advanced techniques. Because the austenitic stainless steel's nature is comprised of coarse grains, strongly textured columnar structure and anisotropic behavior, they require special inspection techniques such as Phased Array systems due to their beam sweeping and focusing abilities.

The conventional ultrasonic testing has being applied in various sectors for decades. When the part has a complex geometry or anisotropic properties, lots of experience or many trials are existed in conventional ultrasonic testing as well as experienced operators. Since it is a widespread method, the test procedure and acceptance criteria

are acknowledged by all authorities. The system set up, training and auxiliary equipment are relatively simple and it is possible to detect oriented defects particularly in difficult conditions by moving the probe.

Ultrasonic inspection of austenitic stainless steel is however hard to accomplish getting proper results due to high attenuation, scattering and beam skewing. Changes in sound speed and beams refraction cause false alarms about size and positioning of defects. Although conventional ultrasonic testing is capable of detecting artificial defects in austenitic microstructure, it is not easy to detect natural defects because anisotropic nature of austenitic stainless steel causes beam divergence and skewing as well as scattering. One single element used in conventional ultrasonic technique is the major limitation for inspection of anisotropic materials inspection. In ultrasonic testing, the inspection is carried out using one transducer element or solely sound beam which is refracted to another angles. On the other hand, even Phased array sound beams refracted, they can cover scanning area because of their capability of firing multiple elements, steering and sweeping traits (Figure 1.32). Regarding refracted angles Phased array method is much better than conventional ultrasonic testing [30].
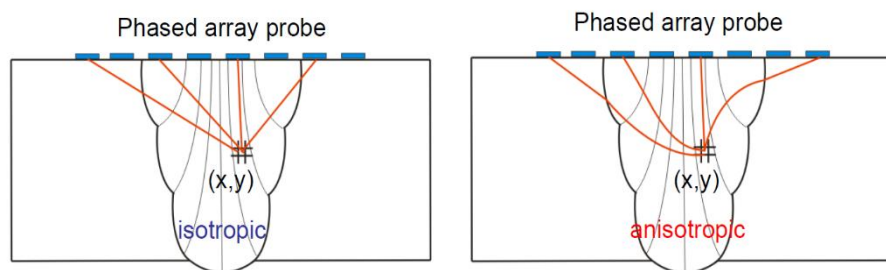
Figure 1.32 Isotropic and anisotropic phenomena in phased array method [30]

Anisotropic media is considered as homogeneous anisotropic media if anisotropic behavior of the media does not vary locally. One good example is fiber reinforced composite. In carbon fiber material, sound propagation changes its direction depending on fiber orientation and acoustic properties of media. When they are known, the change in sound velocity for any direction can be determined easily.

Problems in ultrasonic inspection of inhomogeneous austenitic welds are as follows;

- Elastic properties of the austenitic weld material are changed depending on direction. The wave vector and velocity of sound wave or energy flow directions are no longer equal due to beam skewing phenomenon.

- Since the dimensions of the columnar grains in the austenitic weld are large as compared to the ultrasonic wavelengths, ultrasound is affected by the anisotropy of the grains.

- The wave vector depends on directions.

- Inhomogeneous orientation of the crystal (Fig. 1.33).
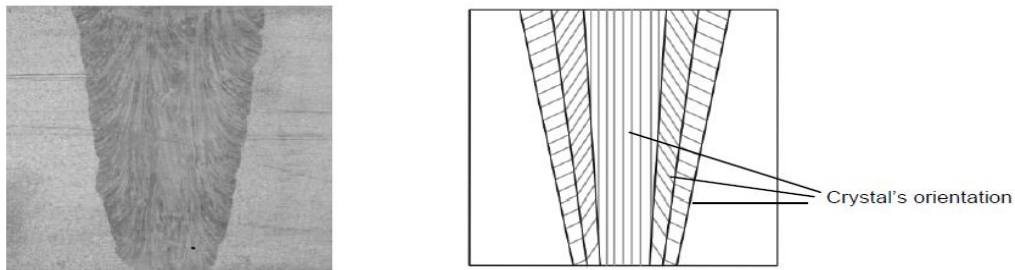
Figure 1.33 Macro graphic view (a), domain model (b) [30]

- Remarkable effects of beam divergence, beam separation and beam spreading exist.

- Scattering of ultrasound at the grain boundaries leads to the high attenuation of the ultrasound beam. For that reason low frequency transducers are used.

- High noise level leads to difficulty in interpretation of the ultrasonic signals.

- Complicated reflection and transmission behaviors of ultrasound in austenitic welds exist due to incidence at the interface between two adjacent anisotropic columnar grains resulting three reflected and three transmitted waves in contrast to the isotropic ferritic steels, in which two transverse waves are

degenerated and coupling exists only between longitudinal and shear vertical
waves. (Figure 1.34 – 1.35).

- Defect response in homogeneous isotropic material is easily calculated by the
  basic geometric principles whereas in austenitic welds geometric laws are no
  longer valid due to inhomogeneous anisotropic columnar grain structure
  leading to complicated defect response.
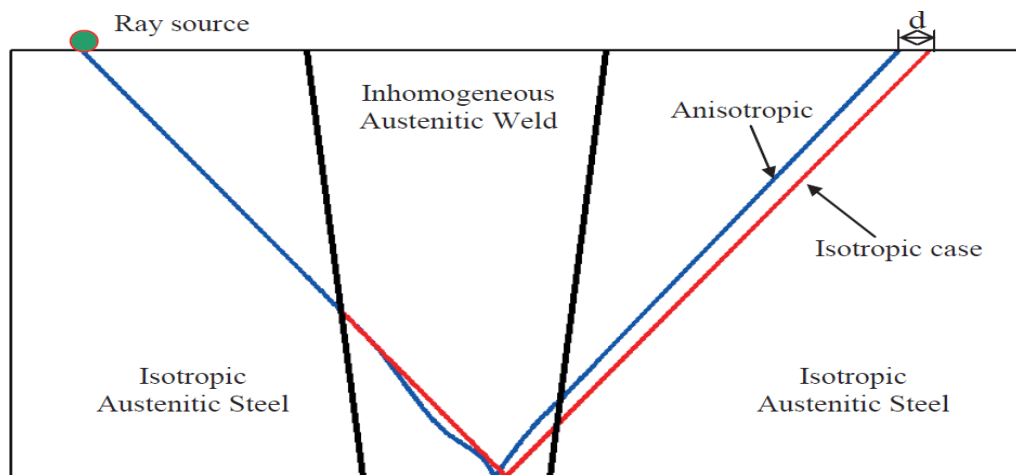
Figure 1.34 Illustration of anisotropic reflection and transmission behavior of the
ultrasonic wave in testing of austenitic weld. 'd' represents the deviation between the
locations of the reflected signals for isotropic and anisotropic cases [33]
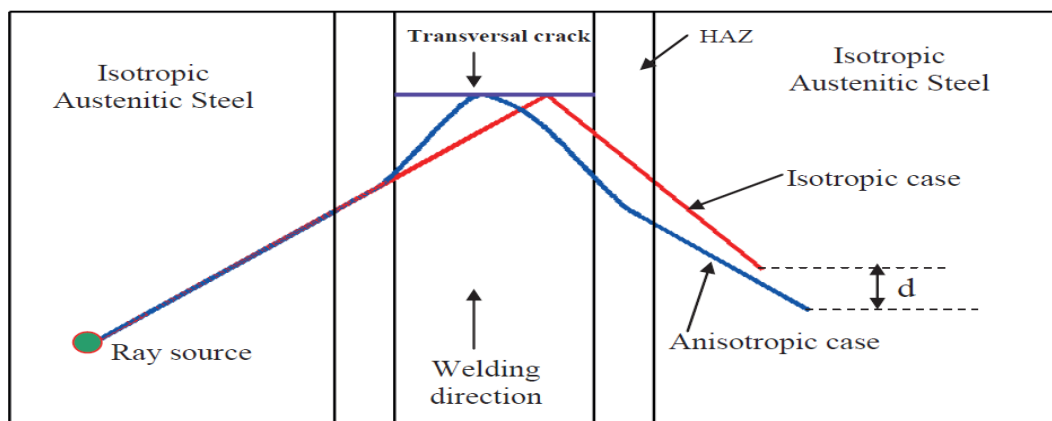
Figure 1.35 Illustration of the interaction of an ultrasonic ray with transversal crack in
isotropic and anisotropic weld materials. 'd' represents the deviation between the
locations of reflected signal [33]

1.5.1 Symmetry of the Austenitic Weld Material

Investigations by X-ray diffraction and electron diffraction techniques showed that transversely isotropic (orthotropic) behavior exist in cast stainless steels. This means that the columnar grains are randomly orientated about their long axes [20]. Therefore, austenitic weld material can be assumed as transversely isotropic.
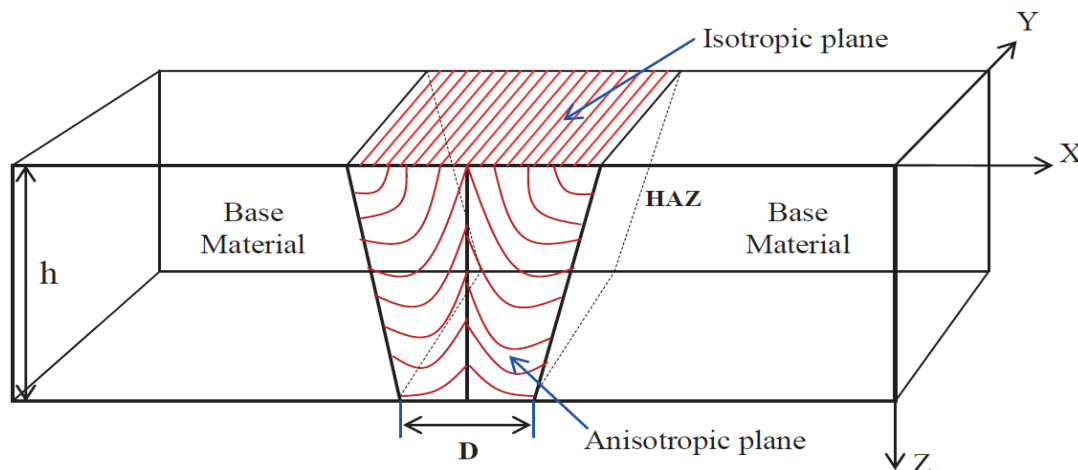
Figure 1.36 Illustration of the transverse isotropic symmetry in austenitic welds material [33]

On the plane perpendicular to the weld run direction (i.e. the XZ plane in Figure 1.36) the columnar grain structure results in direction dependent elastic properties. Macroscopically, the austenitic weld material has to be evaluated as transverse isotropic because of the anisotropic columnar grain structure [34].

1.5.2 Phase Velocity

In the transverse isotropic structure, generally, three wave modes will exist in which one with quasi longitudinal wave character (qP), one with quasi shear wave character (qSV) and one pure shear wave (SH). The selection of proper phase velocity magnitudes for the two shear wave modes is obtained by imposing the boundary condition for shear horizontal waves.

The austenitic welds exhibit commonly columnar grain orientation in 3D. The 3D columnar grain orientation of the austenitic weld material is illustrated by rotating the coordinate system over the crystallographic axes (Figure 1.37). If the incident wave

38

propagates in the XZ-plane and the columnar grain orientation in the plane perpendicular to the incident plane (i.e. layback angle) is zero, then the issue of evaluating wave propagation properties reduces to two dimensions. As a consequence, the coupling occurs only between quasi longitudinal and quasi shear vertical waves. However, the shear horizontal wave decouples with quasi longitudinal and quasi shear vertical waves.
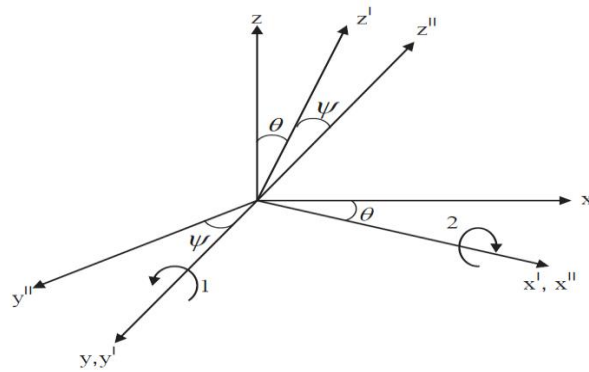
Figure 1.37 Coordinate system used to represent the three dimensional crystal orientation of the transversal isotropic austenitic weld material. Θ represents the columnar grain orientation and Ψ represents the layback orientation [33]
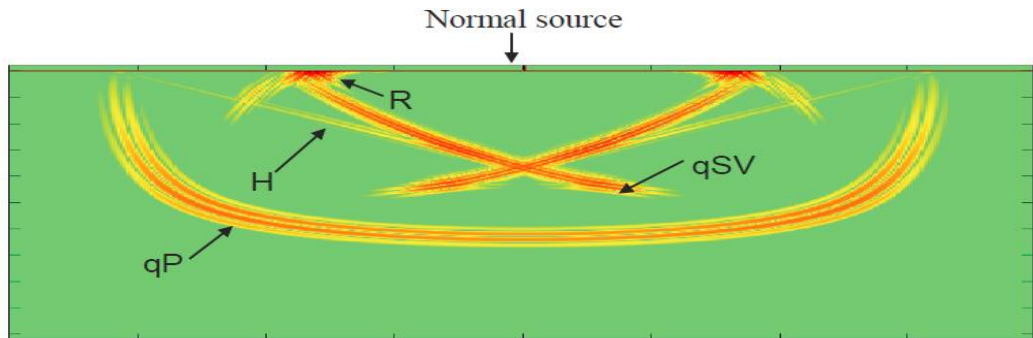
Figure 1.38 The columnar grain orientation in the austenitic steel is 90º. R: Raleigh wave, H: Head wave, qSV: quasi shear vertical wave, qP: quasi longitudinal wave [33]
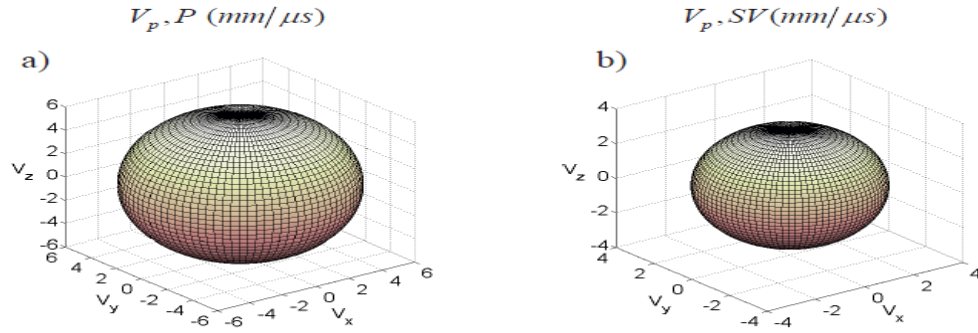
Figure 1.39 Acoustic wave phase velocity surfaces in the isotropic steel material: a) longitudinal wave and b) shear vertical wave [33]

In case of isotropic material, the phase velocity surfaces for the three wave modes are spherical, in other words normal, because the velocity magnitudes of longitudinal and shear waves are independent directionally (Figure 1.39).

The phase velocity magnitudes for the three wave modes particularly qP, qSV and SH waves in an austenitic steel material exhibiting 0° columnar grain orientation and 0° layback orientation is illustrated in Figure 1.40. It is clearly seen that the phase velocity surfaces for three wave modes are non-spherical, since the phase velocity direction does not symbolize the actual energy direction except along the acoustical axes. The results of phase velocity surfaces for the three wave modes in an austenitic steel exhibiting 45° columnar grain orientation and 20° layback orientation are demonstrated.
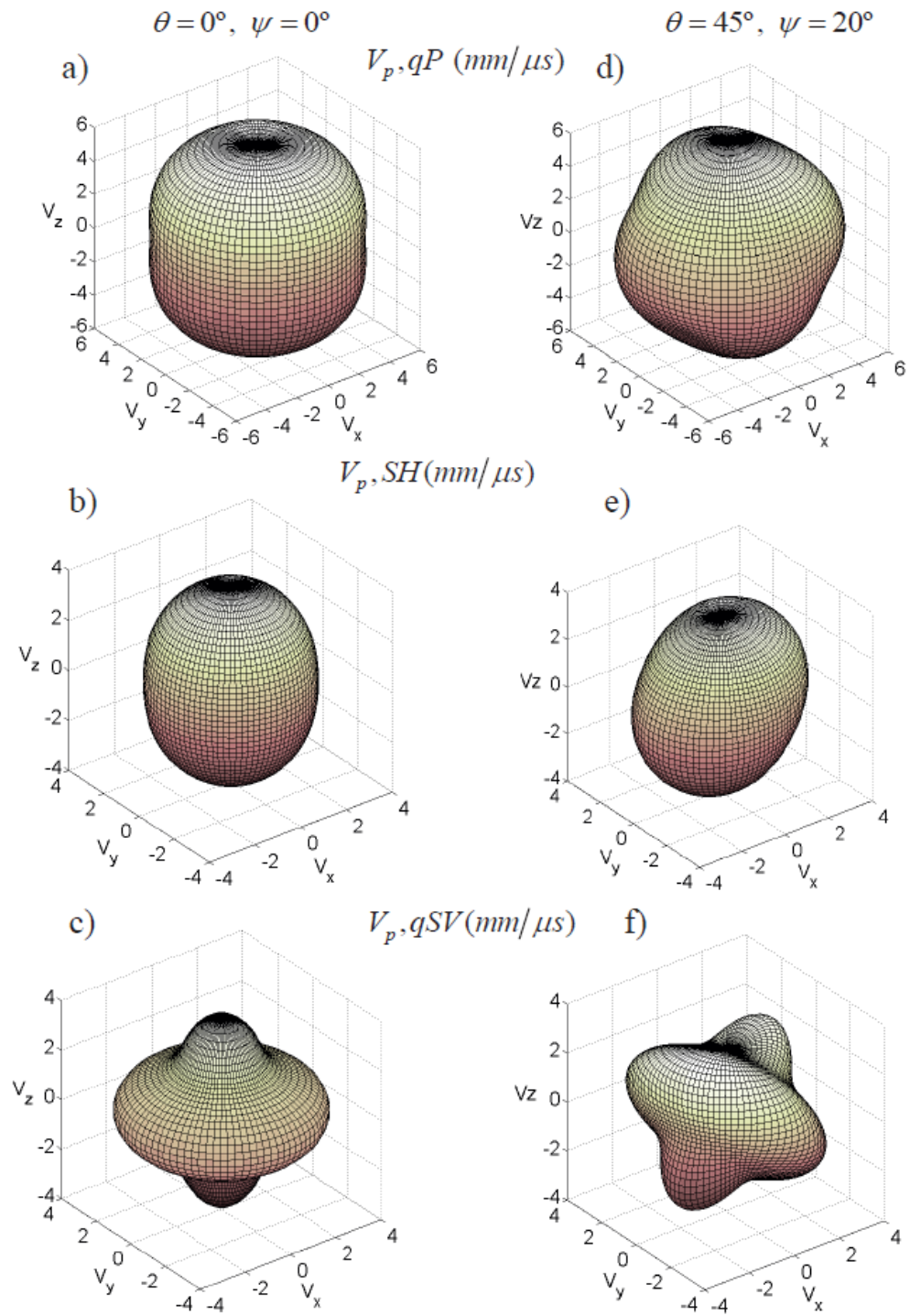
Figure 1.40 Phase velocity surfaces in the transversely isotropic austenitic stainless steel (X6 Cr Ni 1811): a), d) quasi longitudinal waves, b), e) Shear horizontal waves and c), f) quasi shear vertical waves [33]

1.5.3 Polarization Vector

The polarization vectors for the qP, qSV and SH waves are numerically classified for the austenitic steel material. Figure 1.41 demonstrates the polarization vector representation for the longitudinal (P) and shear vertical (SV) waves in the isotropic steel material. The polarization directions of P and SV waves in isotropic steel material are equal to the wave vector directions because their phase velocity components are independent on direction.
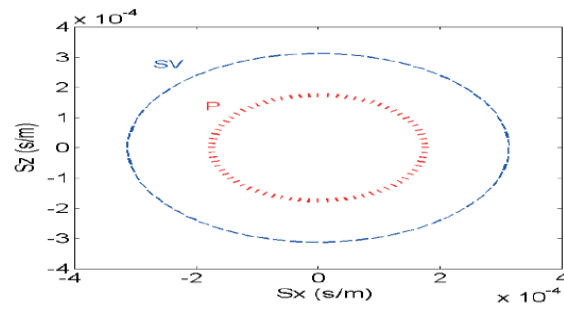
Figure 1.41 Polarization vectors for the longitudinal (P) and shear vertical (SV) waves in the isotropic steel [33]

As shown in Figure 1.42, the polarization vectors for the qP and qSV waves in transverse isotropic austenitic steel exhibiting columnar grain orientations are 0° and 50°. The polarization directions for the qP and qSV waves are deviated from the wave vector direction since their phase velocity components alter depending upon propagation direction.
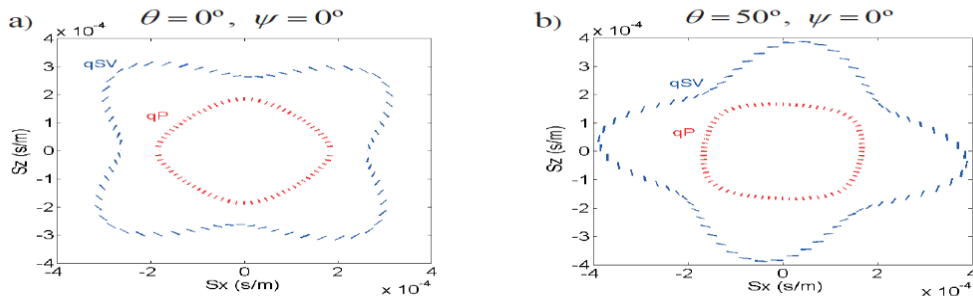
Figure 1.42 Polarization vectors for the quasi longitudinal (qP) and quasi shear vertical (qSV) waves in the austenitic stainless steel (X6 CrNi 1811) with a) 0° and b) 50°columnar grain orientation [33]

42

1.6 Beam Distortion in Anisotropic Media

1.6.1 Beam Divergence

While a sound beam propagates in an anisotropic medium, it is exposed to certain beam divergence which is described as fractional change in the phase velocity direction and finding the associated change in energy velocity direction [33]. Beam divergence is expressed as follows

$$BD = \frac{\Delta\theta_g}{\Delta\theta_p} \qquad\qquad (Eq.\ 1.12)$$

where θ_g, θ_p are the directions of group velocity and phase velocity respectively.

1.6.2 Beam Skewing

The phase velocity and group velocity directions do not converge in anisotropic media. Because the phase velocity vector is perpendicular to the wave front and the group velocity vector is parallel to the direction of energy flux. Hence, the group velocity vector is not perpendicular to the wave front. The deviation between phase and energy velocity direction is defined as beam skewing.

Compression waves are less influenced by the beam skewing phenomenon than the vertically polarized (S_v) shear waves. However, horizontally polarized (S_h) shear waves are even less affected than compression waves, but they are difficult to generate without special equipment. Kupperman and Reimann [35] have visualized ultrasonic compression and shear wave beams after they have passed through austenitic weld specimens and the distortions to the beam shape caused by skewing have been observed. Most of the distortions could be explained by assuming that the weld metal was transversely isotropic.

Beam skewing is expressed as follows;

$$\beta = \cos^{-1} \frac{Vp.Vg}{|Vp.Vg|} \qquad \text{(Eq. 1.13)}$$

Where V_p, V_g are phase velocity magnitude and energy velocity magnitude respectively.

Austenitic welds and castings display beam skewing in all directions apart from the plane at right angles to the long axis of the columnar grains, Figure 1.43, shows the calculated beam skewing effect in transversely isotropic austenitic weld metal for compression waves and both shear waves [20].
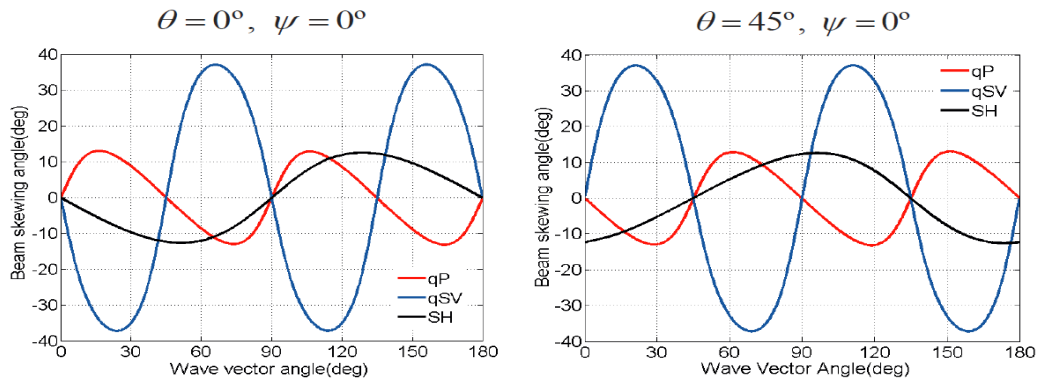
Figure 1.43 Variation of beam skewing angle with incident wave vector angle for the three wave modes in the columnar grained austenitic steel material. Ө represents the columnar grain orientation and Ψ represents the layback orientation [33]

1.6.3 Beam Spreading Factor

Beam spreading factor is defined as the fractional change in the phase velocity magnitude and finding the associated change in the energy velocity magnitude. Beam spreading factor is expressed as

$$BS = \left| \frac{\Delta Vg}{\Delta Vp} \right| \qquad \text{(Eq. 1.14)}$$

In the isotropic ferritic steel media, beam spreading factor is zero since the energy velocity magnitude is equivalent to the phase velocity magnitude. The beam spreading factor changes regarding the phase velocity direction. Higher beam spreading factor

leads to higher energy scatter reducing the energy density as well. Figure 1.44 illustrates the variation of beam spreading factor for qP, qSV and SH waves in transverse isotropic austenitic steel material with phase velocity direction. Also, the presence of layback orientation in austenitic weld materials scales down the beam spreading factor. For the ultrasonic inspection of austenitic welds, it is more significant to prefer the range of incidence angles where beam spreading factor is close to zero [33].
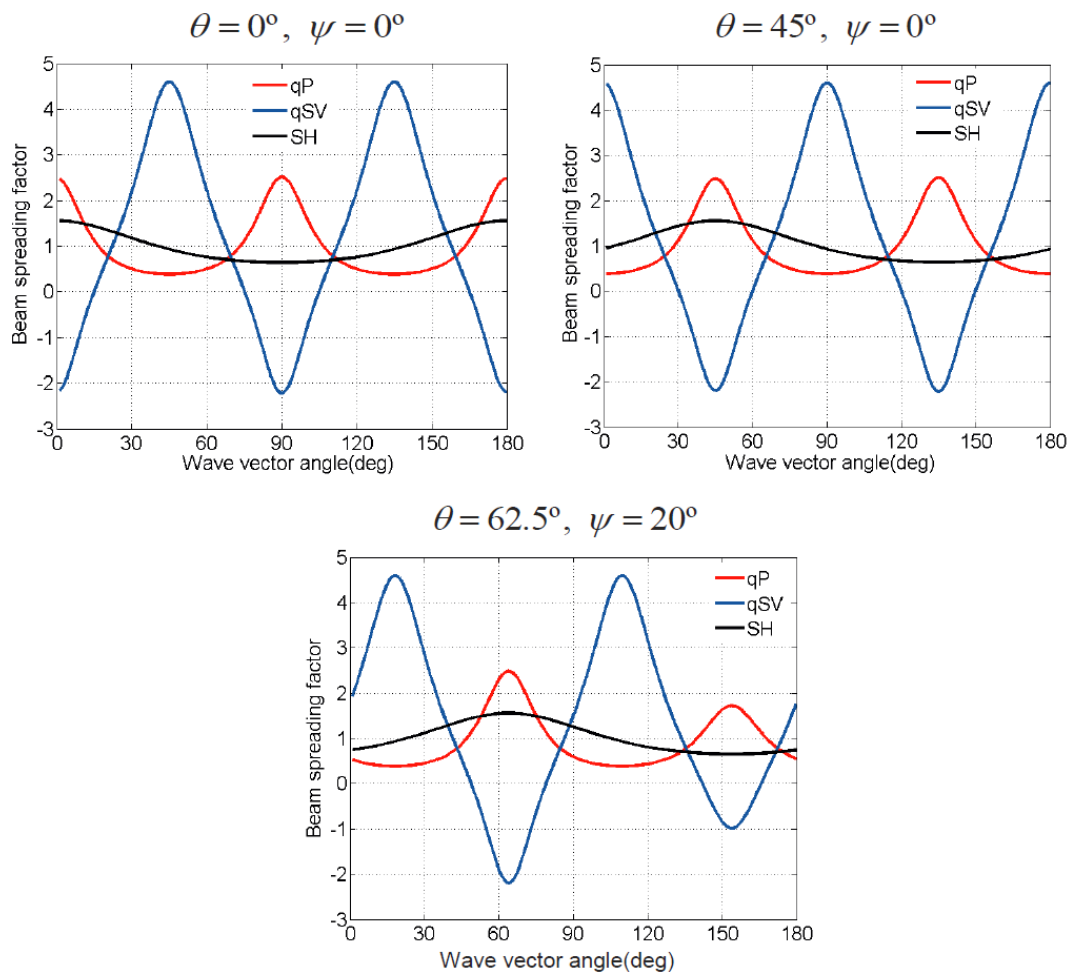
Figure 1.44 Variation of beam spreading factor with incidence wave vector angle for the three wave modes in the columnar grained austenitic steel material [33]

1.6.4 The effects of inhomogeneous austenitic weld metal on sound propagation

The transmitted ultrasound energy sound paths for the three wave modes are affected by the inhomogeneity of the austenitic weld material. It is obvious from Figure 1.45(b), that the shear vertical wave (SV) ray paths exhibits rapid fluctuations in the ray direction as they transmit through the weld material. The strong focusing and bending effects are observed for shear vertical waves. These strong focusing traits for the shear vertical waves are occurred due to complex slowness surface of these particular waves. On the contrary to SV waves, the longitudinal (P) and shear horizontal wave (SH) energy sound paths are less affected by the anisotropy of the austenitic weld material.
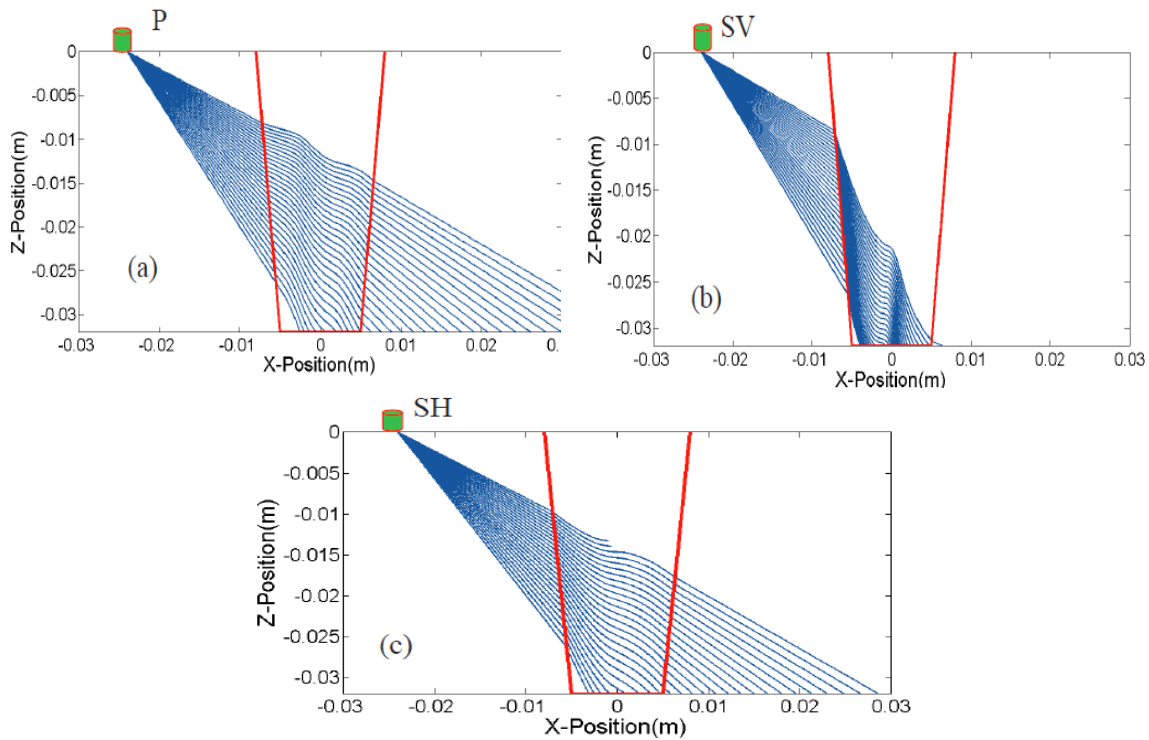
Figure 1.45 A 45º ultrasonic beam propagation in the inhomogeneous austenitic weld (a) Longitudinal waves (P), (b) shear vertical waves (SV) and (c) shear horizontal waves (SH) [33]

1.7 Modelling the grain orientation

Before welding procedure has implemented on, there is a need of description of the weld anisotropy to improve the capability of simulating real weld testing. One way of obtaining the resulting grain orientation is to develop a solidification model, however, the solidification of multilayer weld raises many unsolved modelling questions as it involves heat and fluid flow modelling in addition to solute redistribution models. To overcome these difficulties there are some developed models to predict the resulting grain orientations without using a complete solidification model [36].
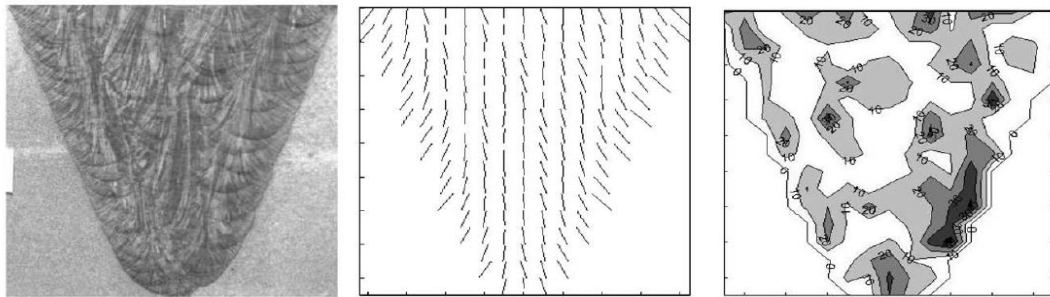
Figure 1.46 Weld macrographs; modelled orientations as vectors; contour plots of differences between modelling and orientation by contour lines (0–10–20–30°) [36]

The modelling of grain orientation is performed by using both micrographic observations supplemented by Electron Back Scattered Diffraction (EBSD) and X-ray analyses and knowledge of crystalline growth mechanisms and also correlated by information contained in the welding literature with macrographs of welds.

The epitaxial growth, temperature gradient and the selective growth which is the result of the competition between the grains result in grain growth physical phenomena. From these three physical phenomena the grain orientation model will calculate the angle α_n (initial direction of grains), α_g (the direction of the temperature gradient). By including welding parameters into calculation, modelled orientations as vectors; contour plots of differences between modelling and orientation by contour lines (0–10–20–30°) Figure 1.46 [36].

The models are commonly two dimensional and based on to the laws that govern the initiation of crystalline growth, the evolution of the solidification front, and the consideration of the grain crystallographic orientation. The properties of the parent metal also have direct impact on the texture of the welded joint, especially the average size of the grains. Depending on composition differences and on crystalline structure differences, there can be an epitaxial growth or a heterogeneous nucleation. Figure 1.46 shows that macrograph of a weld, modeling of grain orientations and contour lines of these grains.

A better understanding of the weld elastic properties that are connected to the grain orientation provide that a better defined coordinate system related to the material symmetry. Consequently, there is a good correlation with the beam deviation derived from anisotropy determination of macro graphic analyses (Figure 1.47).
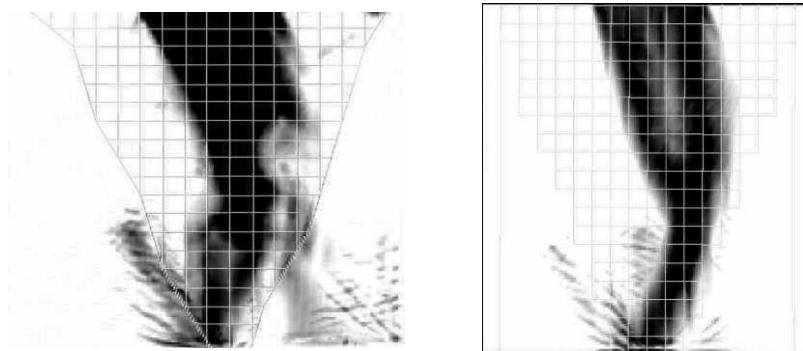
Figure 1.47 (On the left) Beam deviation and splitting in a weld with a transducer, (on the right) example of simulated propagation using a grain orientation model to describe material anisotropy [36]

The results of the grain orientation model provide a new validation method for welding notebooks. Interpretation of data from ultrasonic inspection or the information needed for ultrasonic testing about anisotropy will thus be more accurate.

1.7.1 Solidification Modes

The solidification phase directly influences on grain orientation which affects significantly anisotropy. The solidification mode varies from planar to cellular and from cellular to dendritic as the cooling rates increases. Figure 1.48 demonstrates schematically the effect of constitutional super cooling on the microstructure within the grains in the weld metal. Heterogeneous nucleation aided by constitutional super cooling promotes the formation of equiaxed grains in the weld metal [21].

Temperature gradient and growth rate are the main variables during the solidification. They inversely depend upon each other, i.e., as the temperature gradient escalates growth rate diminishes (Equation 1.15).

$$R = \frac{V\cos\alpha}{\cos\alpha-\beta}$$ (Eq. 1.15)

R represents growth rate, V welding speed, α angle between the welding direction and the normal to the pool boundary and β is the angle between the welding direction and the growth direction of a dendrite at the point <100> in fcc and bcc materials.
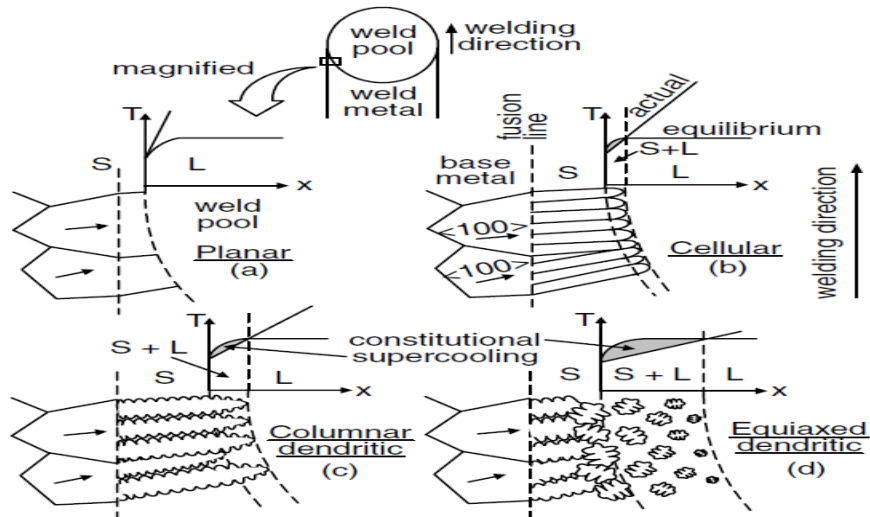
Figure 1.48 (a) planar; (b) cellular; (c) columnar dendritic; (d) equiaxed dendritic [21]

The distance between the maximum pool temperature (T_{max}) and the pool boundary (T_L) is much more at the centerline than at the fusion line since the weld pool is

elongated. As a result, the temperature gradient (G) normal to the pool boundary at the centerline, G_{CL}, is less than that at the fusion line (Equation 1.16), G_{FL}. Since $G_{CL} < G_{FL}$ and $R_{CL} \gg R_{FL}$ [21] (Figure 1.49).

$$\left(\frac{G}{R}\right) CL \ll \left(\frac{G}{R}\right) FL \qquad \text{(Eq. 1.16)}$$
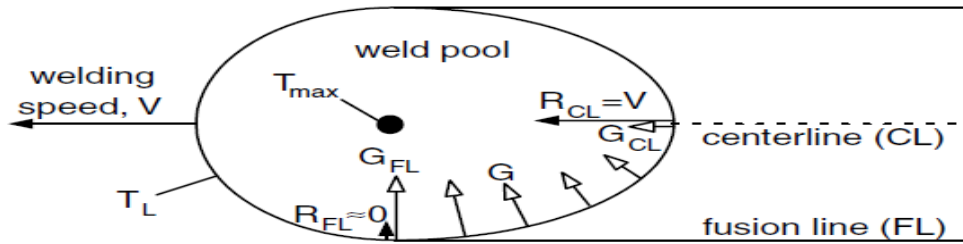
Figure 1.49 Variations in temperature gradient G and growth rate R [21]

The ratio G/R diminishes from the fusion line toward the centerline. Hence, the solidification mode vary from planar to cellular, columnar dendritic, and equiaxed dendritic across the fusion zone (Figure 1.50). Three grains are demonstrated to grow epitaxially from the fusion line. If it grows with the planar mode along the easy-growth direction <100> of the base-metal grain. Close the fusion line, solidification alters to the cellular mode. Further away from the fusion line, solidification transforms to the columnar dendritic mode. Some of the cells evolve into dendrites and their side arms block off the neighboring cells. Near the weld centerline equiaxed dendrites nucleate and grow, blocking off the columnar dendrites.
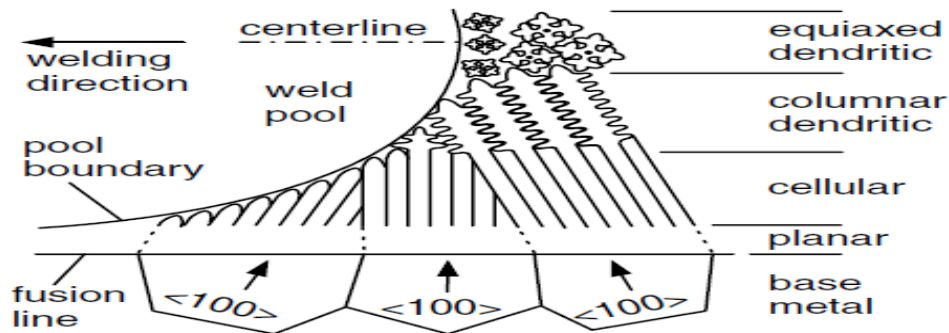
Figure 1.50 Variation in solidification mode across the fusion zone [21]

1.8 Motivation and Aim of the study

Phased Array investigations have significantly increased in recent years particularly on polyethylene pipes or dissimilar welds with anisotropic properties. The transition stage from conventional ultrasonic testing to automated Phased Array system is continuing and approval of Phased array systems has been already started in several critical industries. To accomplish this evolution, there are some issues to prove such as whether Phased Array really a superior method or not over the conventional ultrasonic method in all aspects of inspection.

The aim of this thesis is to compare the flaw detection abilities of conventional ultrasonic and Phased Array systems via the Probability of Detection method for testing of austenitic stainless steel blocks and weldments having artificial and natural flaws. It is also aimed to contribute the literature by investigating the efficiency and reliability of the Phased Array method for testing of austenitic stainless steels.

CHAPTER 2

EXPERIMENTAL PROCEDURE

2.1 Material and Sample Preparation

All specimens were delivered as AISI 304 with a certificate according to EN 10204 (Table 2.1). Next, the predetermined dimensions of plates manufactured with using CNC vertical lathe and artificial defects were created with electrical discharge machine (EDM).

Table 2.1 Chemical composition of AISI 304 steel (Specimen type 3)

	Fe	*Cr*	*Ni*	*Mn*	*Si*	*Mo*	*Cu*	*Others*
%	70.09 ± 0.23	18.75 ± 0.09	8.37 ± 0.12	1.39 ± 0.07	0.533 ± 0.042	0.040 ± 0.02	0.129 ± 0.27	0.10N

First and the second type of the specimens were prepared in the form of blocks and the third type of specimen was prepared from a butt welded plate. Chemical composition of AISI 304 steel was verified by BTX II Compact Benchtop X-ray Diffraction System device (Table 2.1).

2.1.1 Specimen Type 1 (Flaws at Different Depths)

In the specimen type 1, 10 side drilled holes with 2 mm diameter were created at different depths by Electrical Discharge Machining (EDM). Before drilling process, the block dimensions and positions of flaws were drawn by Solid works 2014 SP014 software program (Figure 2.1).
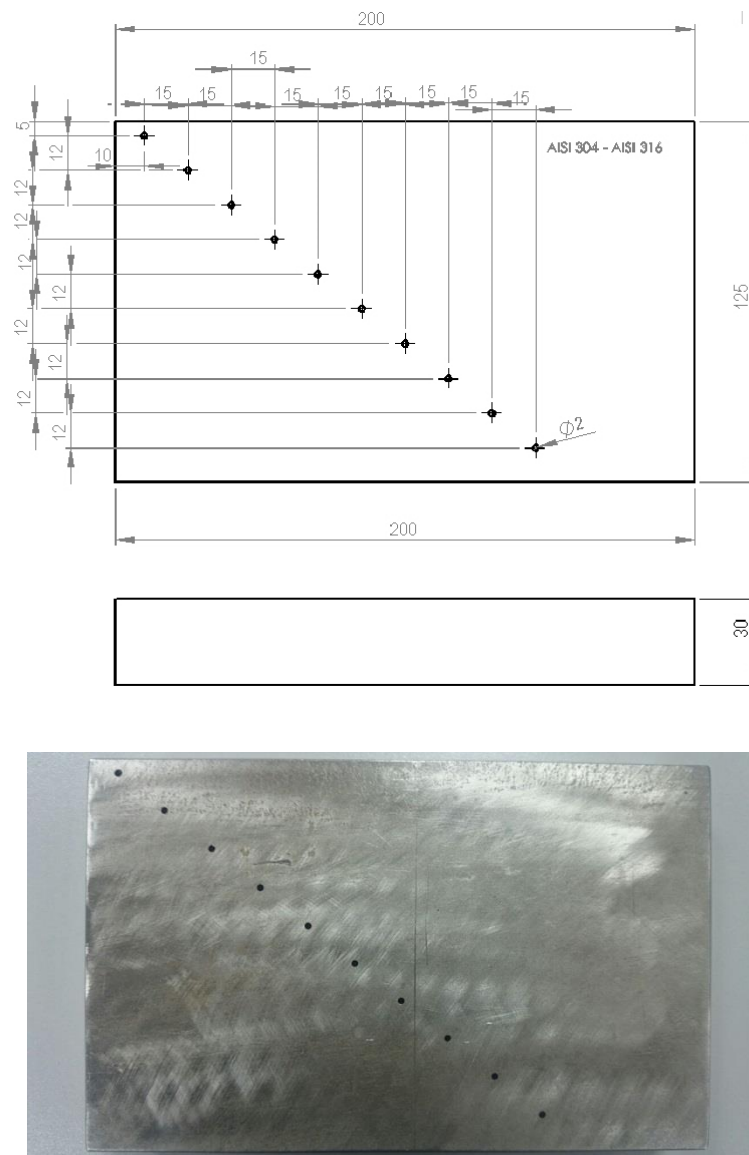
Figure 2.1 Specimen Type 1

2.1.2   Specimen Type 2 (Flaws of Different Sizes at the Same Depth)

11 holes having different diameters from 0.5 to 5 mm were drilled at 40 mm depth by EDM in the specimen type 2 (Figure 2.2).
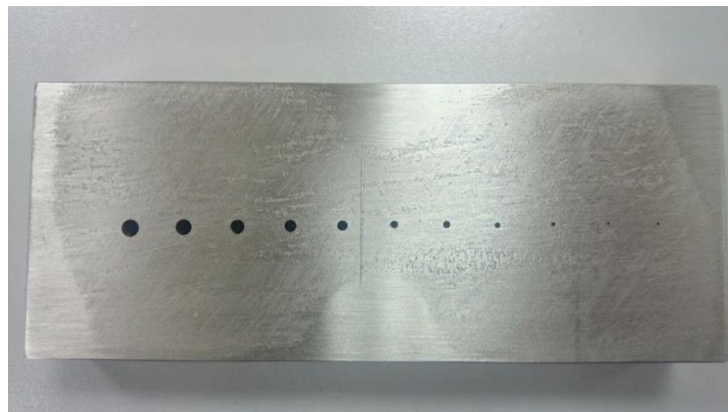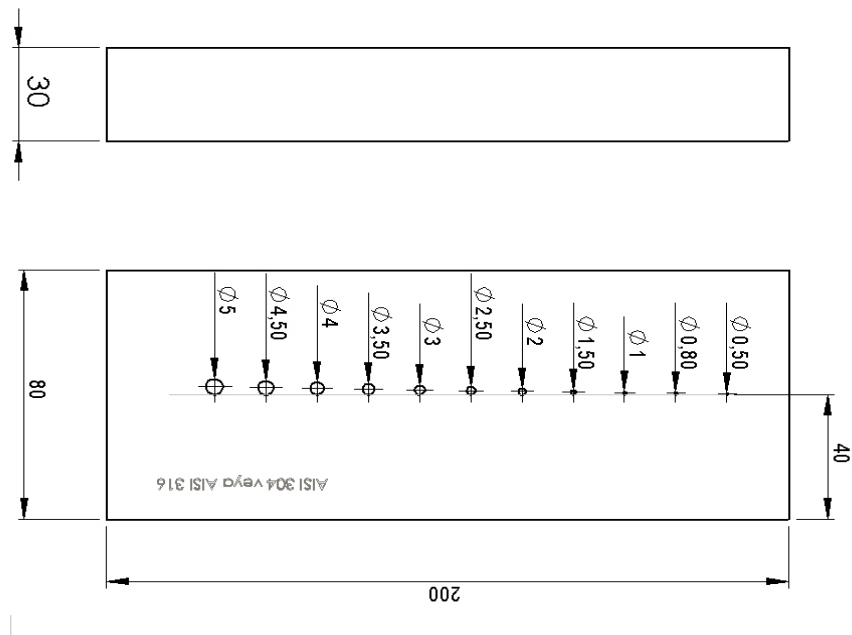
Figure 2.2 Specimen Type 2

2.1.3   Specimen Type 3 (Butt Welded Plate)

AISI 304 plates (300 mm x 150 mm x 10 mm) are butt welded (full penetration from both sides at PA position as multilayer) with the Gas Metal Arc Welding (GMAW).

The Magma Weld brand filler material solid wire (MG2) in the diameter (Φ=1 mm) was used.

Table 2.2 Chemical Composition of GMAW Solid Wire MG2 Weld Metal (Specimen type 3) [39]

%	C	Mn	Si	P	S	Others
	0.07	1.45	0.85	< 0.025	< 0.025	0.10N

Weld parameters were adjusted intentionally wrong in order to create natural flaws in the weldment. The width of weld bead is 16 mm (w=16 mm), angles of top-root bevel is approximately 42° (Figure 2.3).
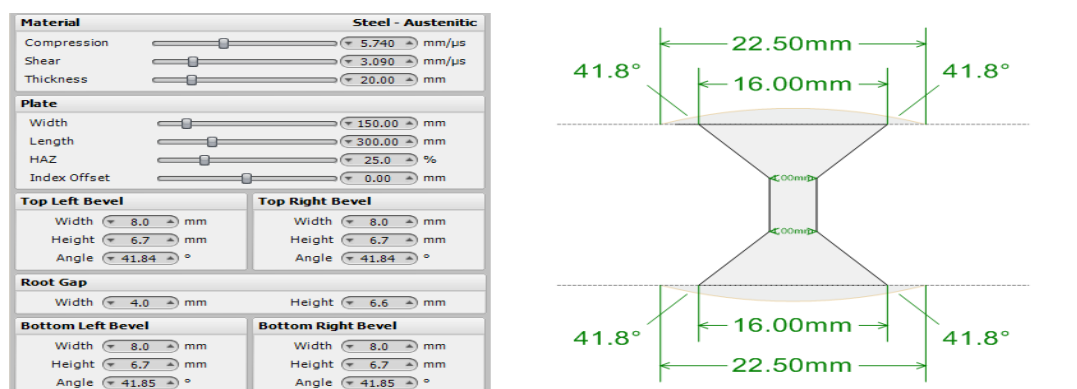
Figure 2.3 Weld bevel preparation with ES beam tool3 software

The specimen type 1 and type 2 are well manufactured blocks with sufficient surface quality. However, the weld splashes on the surface of the butt welded plate were removed by grinding to eliminate any inspection problem.

Surface roughness have a direct impact on ultrasonic inspection because the energy transferring to sample is carried out on the surface. The high loss in the transferring energy due to surface roughness cause weakening the amplitude of the received signal. For that reason the probability of detection of a discontinuity such as cavities, cracks, etc. is diminished. If the surface roughness is lower than the wavelength, the amplitude

56

of signal is declined but the shape and location of amplitude is maintained. On the other hand, if the surface roughness is higher than wavelength, the position of signals will change. It has been pointed out that the couplant viscosity leads directly to losing of the signal amplitude due to viscosity effects, and the inspection on the front face roughness significantly affects to chance of detection [24].

2.2 Investigation of Microstructure

The mean grain size and micro hardness values were measured on the butt welded plate (specimen type 3). First, the specimen was sectioned, and then, the sample surfaces were polished by a series of abrasive papers, down to 2 μm. All stages were applied properly according to ASM Metals Handbook Volume 9 [31].

Following polishing, the specimens were electrolytically etched (60:40 ratio − 70 wt.% HNO_3:H_2O, 10 mA/cm^2) for 4-5 seconds.

For determining the mean grain size, Olympus Stream Motion Image Analysis software was utilized. The number of intercepts were 408 in the base metal zone, the mean intercept length value was found as 13 μm, which corresponds to ASTM Grain Size Number G: 9. 24 was obtained according to ASTM E 1382 [32].

On the other hand, the number of intercepts were 436 in the heat affected zone, the mean intercept length value was found as 12 μm which corresponds to ASTM Grain Size Number G: 9. 44 was obtained according to ASTM E 1382 [32].

Micro hardness measurements were repeated four times in each zone (base metal, HAZ and weld metal). The mean micro hardness values were calculated as 188 ± 3 HV for the parent metal, 192 ± 4 HV for the heat affected zone and 200 ± 1 HV for the weld metal.

2.3 Ultrasonic Inspections (Specimen Type 1 and Type 2)

Both inspections were carried out by 2 MHz transducers straight beam probes. The machine oil was used as a couplant. Data retrieved for PoD analysis were the remaining screen height values received from the artificially created flaws. The

intention by utilizing remaining screen height instead of screen height was providing linear distribution to create an accurate PoD curve in specimen type 1 and type 2.

2.4 Phased Array Inspections (Specimens Type 1 and Type 2)

The 5 MHz transducer having 0.5 mm pitch size, 32 elements was utilized respectively in phased array method and Phased Array equipment (Figure 2.4) for detecting known artificial defects on specimen type 1 (flaws at same sizes in different depths) and specimen type 2 (flaws at different sizes in the same depth).

Figure 2.4 Manual Phased Array Equipment Sonotron Isonic 2010

Phased Array equipment is capable of adjusting the focal depth / focal distance basically focusing to one point or area of all transducer elements (Figure 2.5).
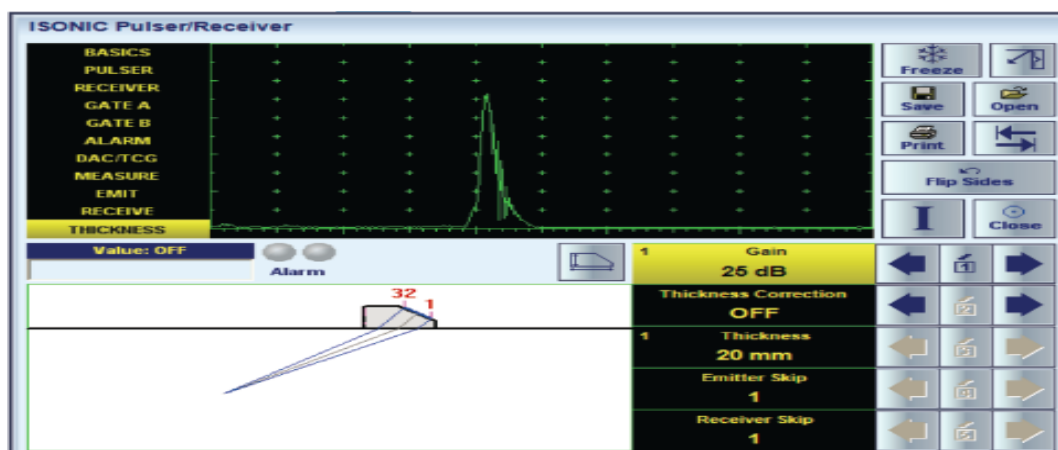
Figure 2.5 Sonotron Isonic 2010 PA Software

2.5 Ultrasonic inspections (Specimen Type 3 – The Butt Welded Plate)
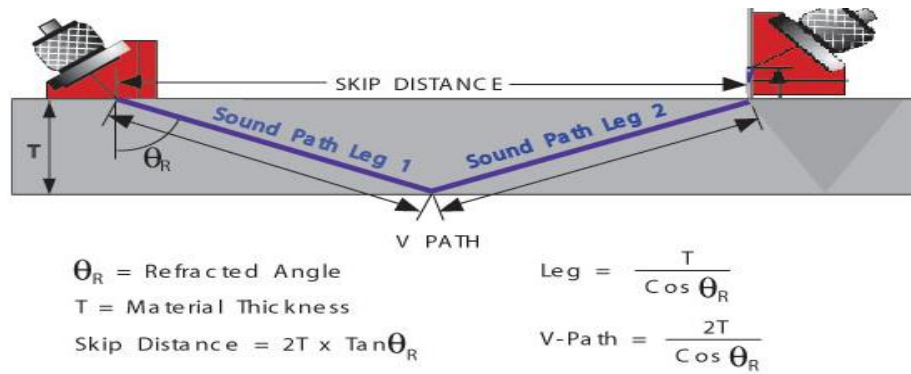
Figure 2.6 Calculation of sound path distance

According to probe refraction angle (70°) and plate thickness (10 mm), half sound path, full sound path and 3/2 sound path were calculated (Figure 2.6 and Table 2.3).

$$\frac{10}{\cos 70} = 29{,}23 \text{ mm } (S_p / 2), \; S_p = 58{,}46 \text{ mm, } 3/2 \; S_p = 87{,}69 \text{ mm}$$

According to calculations,

$\frac{3040}{3250} = \frac{\sin \alpha}{\sin 70}$, the angle of refraction (α) was found as 61.5°. If this angle applied to equation of $\frac{10}{\cos 61} = 20{,}6$ value obtained. But in the device display the measured value approximately was seen as "19 "due to sound attenuation and angle change. When the calculated value and measured value deviation is considered, the real sound velocity was found as 3134 m /s.

Table 2.3 S_p Calculations

	Sound Path	Skip Distance
S_p	20	19
$\frac{3}{2} S_p$	30	28
$2S_p$	40	38
$\frac{5}{2} S_p$	50	47

Finally, the angle was calculated;

$$\tan^{-1} 0{,}94 \cong 43°$$

From the Snell's law

$\dfrac{\sin 43}{\sin 45} = \dfrac{\times}{3250}$, velocity $= 3134$ m /s

The calculation about sound pressure decrease was performed for the austenitic stainless steel test blocks comparing with plain carbon steel K1 block as a reference. The mean attenuation values were calculated by repeating the measurement three times on each specimen. For the velocity and sound pressure drop measurements in the test block, the time of flight between two back-wall echoes was measured using Krautkrammer USM 35 device.

Firstly, 45 ° probe was used for calculations, on the K1 block the first peak is obtained at $\dfrac{25\ mm}{\sin 45} = 35{,}35\ mm$ at 24.5 dB sound pressure, and second peak is 70.7 mm at 27 dB. Therefore, for 35 mm sound distance, sound pressure loss corresponds to 2.5 dB, and it is approximately 70 dB / m.

Secondly, the attenuation calculations were performed by using half skip and full skip method for the butt welded specimen by 45 ° probe (Figure 2.6), the first signal obtained at $\dfrac{10\ mm}{\sin 47} = 13{,}67$ mm at 27 dB, while 1,5 $S_p = 41{,}8$ mm obtained at 31.3 dB. Hence, 4.3 dB approximately sound pressure loss was occurred on the austenitic stainless specimen for the 28 mm sound distance. Consequently, the attenuation rate corresponds to 1.54 dB / cm for the transition from weld metal. On the other hand, in case of the same measurements were performed on the parent metal of butt welded specimen, the attenuation rate corresponds to 1.06 and 1.22 dB / cm at 45 ° and 60 ° test angles respectively.

In the last part, 70° - 4 MHz probe was used for the UT inspection of austenitic stainless steel plate and $\dfrac{3140}{3250} = \dfrac{\sin \alpha}{\sin 70}$ so that $\alpha = 65°$ is found and then sound distance calculation plate thickness $\dfrac{10\ mm}{\cos 65} = 23.6\ mm$, while the sound distances are $S_p = 47.2$

mm and $\frac{3}{2}$ S_p = 70.9 mm as well. When the sound distance is 23.7 mm, the sound pressure loss is approximately equal to 4 dB which is equivalent to 168 dB / m.

Because of the sound pressure losses and attenuation, the signal amplitudes decrease as the distance passed by sound beam increases. Sizing functions allow us to do evaluate the size of a crack or discontinuity, DAC method was used to calculate sizing functions (Figure 2.7). 2 mm diameter side drilled holes of specimen type 1 were used for drawing a proper DAC curve.
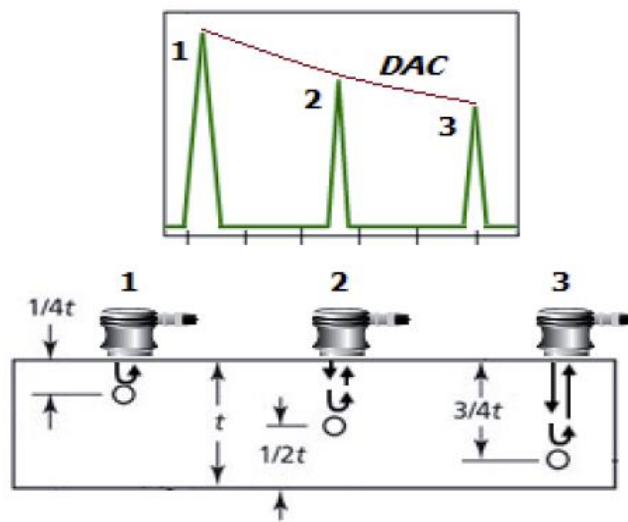
Figure 2.7 DAC curve schematic presentation
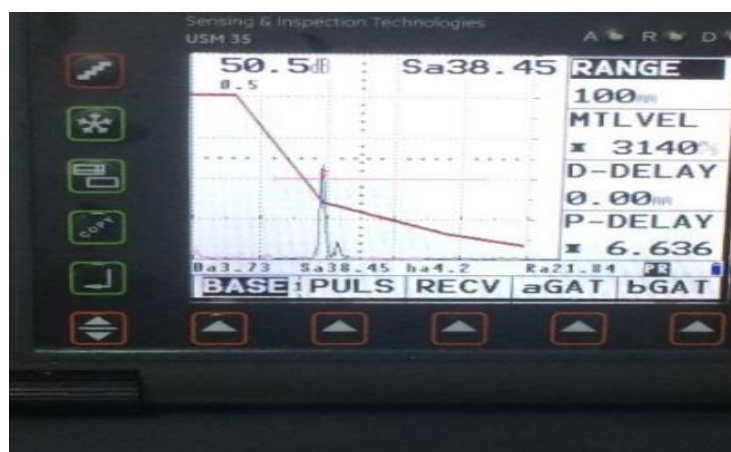
Figure 2.8 Display of 2nd defect signal

2.6 Automated Phased Array Inspections with Encoder (Specimen Type 3 – The Butt Welded Plate)

Automated PA inspections with Encoder were performed by Olympus Omniscan MX Flaw Detector (Figure 2.8 and 2.9)
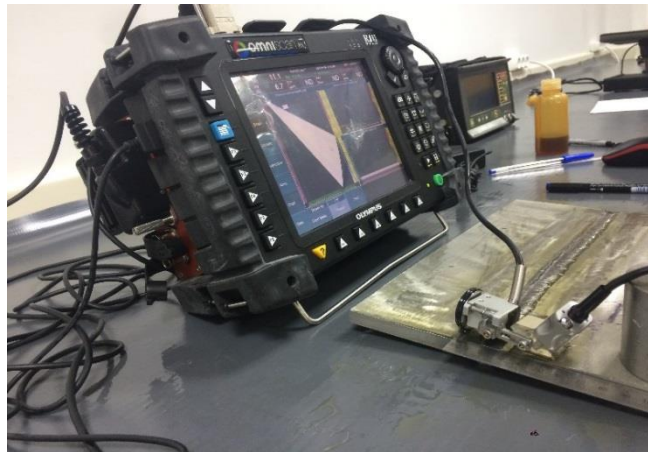
Figure 2.9 Phased Array testing apparatus – Olympus Omniscan MX

Second, probe configuration and position according to weld bevel were carried out with ES Beam Tool3 software piece and weld configuration (Figure 2.14).
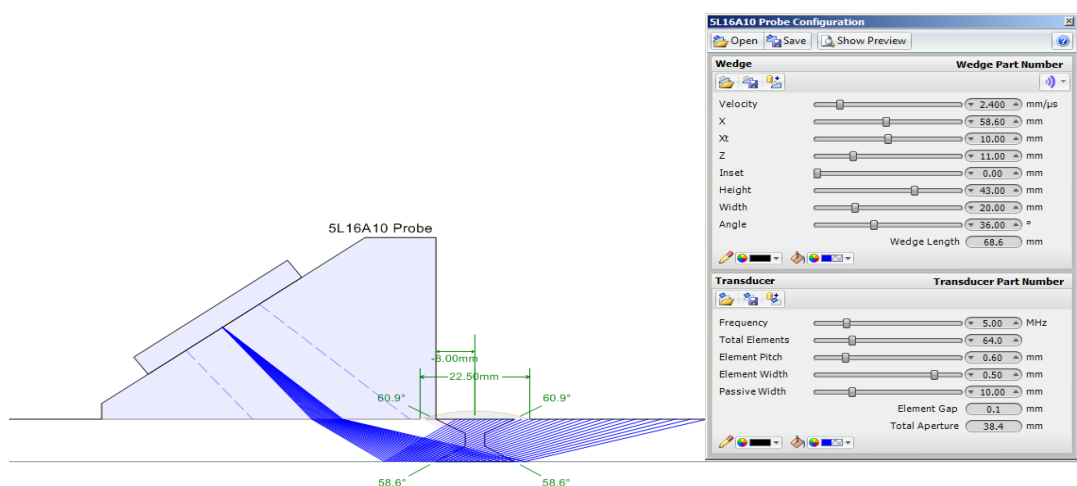
Figure 2.10 ES Beam Tool3 probe configuration

The probe configuration such as frequency, total elements used and particularly position of probe, together with material properties like sound velocity, sectorial beam

set configuration were adjusted (Figure 2.10 – 2.11). The aperture elements, the minimum and maximum angle were adapted to the Omniscan MX software by using the ES Beam Tool3. The intention was to implement exactly the same configuration parameters which are determined to apply them in real inspection. Moreover, the encoder position on the x- axis of the welded plate is a significant factor in terms of detection of flaws.
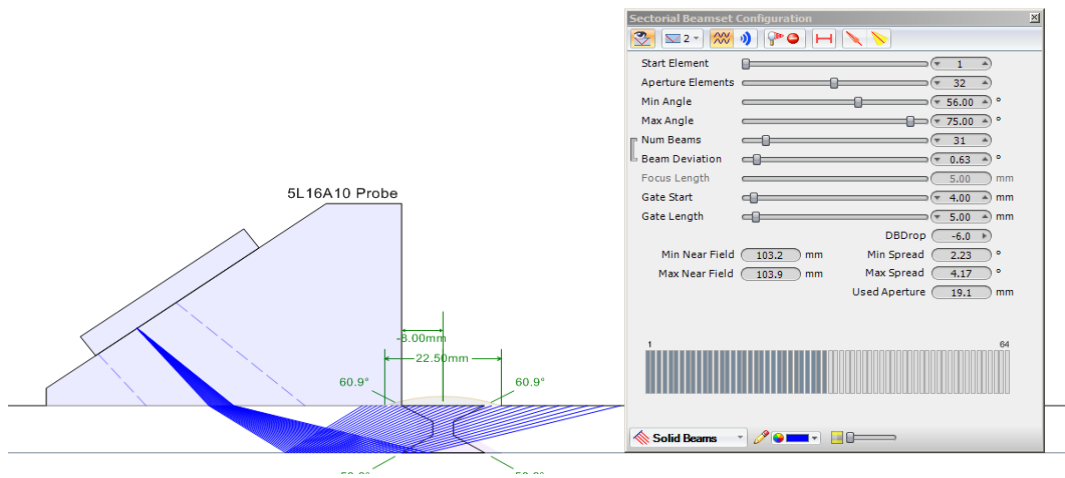
Figure 2.11 Sectorial beam set configuration

Finally, five tests including different parameters in focal depth and the x-axis / - x axis of butt welded palte (specimen type 3) inspections were carried out. The software setup and all parameters are demonstrated in Table 2.4.

Table 2.4 Phased array Omniscan MX software parameters

Probe Characterization					
Probe Model	**Probe Serial #**				
5L16-A10	G1255				
Probe Frequency	**Peak Frequency**	**Wedge Model**	**Wedge Angle**	**Probe Aperture**	
5.00 MHz	N/A	SA10-N55S 5L16-A10	36.1º	9.60 mm	
	Lower Frequency	**Higher Frequency**	**Center Frequency**	**Bandwidth (MHz)**	**Bandwidth (%)**
-6 dB	N/A	N/A	N/A	N/A	N/A
-20 dB	N/A	N/A	N/A	N/A	N/A
Date	**Time**	**Procedure**	**Calibration Block**	**Characterization Gain**	**A%**
N/A	N/A	N/A	N/A	N/A	N/A

Setup					

A:45.0 Sk:090 L:001					
Beam Delay	**Start (Half Path)**	**Range (Half Path)**	**Max. PRF**	**Type**	**Averaging Factor**
10.95 us	-0.25 mm	180.71 mm	5	PA	1
Scale Type	**Scale Factor**	**Video Filter**	**Pretrig.**	**Rectification**	**Band-Pass Filter**
Compression	36	Off	0.00 µs	FW	None (0.54 - 22 MHz)
Voltage	**Gain**	**Mode**	**Wave Type**	**Sound Velocity**	**Pulse Width**
40 (Low)	11.10 dB	PE (Pulse-Echo)	User-Defined	3137.4 m/s	100.00 ns
Scan Offset	**Index Offset**	**Skew**			
0.00 mm	0.00 mm	90.0º			

Gate	Start	Width	Threshold	Synchro
I	110.48 mm	3.65 mm	20.00 %	Pulse
A	0.49 mm	3.92 mm	17.00 %	Pulse
B	73.61 mm	3.65 mm	30.00 %	Pulse

TCG Point Number	Position (Half-Path)	Gain
1	0.00 mm	0.0 dB

2	1.66 mm	9.9 dB
3	7.71 mm	8.2 dB
4	13.62 mm	5.8 dB

Calculator					
Used Element Qty.	**First Element**	**Last Element**	**Resolution**	**Wave Type**	**Material Velocity**
16	1	16	1.0	User-Defined	3137.4 m/s
Start Angle	**Stop Angle**	**Angle Resolution**	**Focal Depth**	**Law Configuration**	
45.0º	70.0º	1.0º	10.00 mm	Sectorial	

Part		
Material	**Geometry**	**Thickness**
STEEL, STNLSS	Plate	10.00 mm

Scan Area					
Scan Start	**Scan Length**	**Scan Resolution**	**Index Start**	**Index Length**	**Index Resolution**
0.00 mm	300.00 mm	12.00 mm	0.00 mm	0.00 mm	1.00 mm
Synchro	**Max. Scan Speed**				
Encoder	60.00 mm/s				

Axis	Encoder	Encoder Type	Encoder Resolution	Polarity
Scan	1	Quadrature	12.07 step/mm	Normal
Index	Off	Off	Off	Off

According to 1st, 2nd and 3rd inspection, repeated detections are marked with the same color in Table 2.5.

Table 2.5 Results of the first trial (10 mm focal depth)

1st Inspection												
Entry #	Scan (mm)	Index (mm)	Group	Channel	A% (%)	DA^ (mm)	PA^ (mm)	SA^ (mm)	A% (%)	DA^ (mm)	ViA^ (mm)	VsA^ (mm)
1 *	12.00	0.50	1	53.0º	73.2	6.06	8.98	23.16	73.2	6.06	8.98	12.00
2 *	0.00	0.50	1	51.0º	77.1	5.65	7.90	22.80	77.1	5.65	7.90	0.00
3 *	300.00	0.50	1	55.0º	2.4	---	---	---	2.4	---	---	---
4 *	180.00	0.50	1	70.0º	27.8	8.62	16.53	25.19	27.8	8.62	16.53	180.00

2nd Inspection												
Entry #	Scan (mm)	Index (mm)	Group	Channel	A% (%)	DA^ (mm)	PA^ (mm)	SA^ (mm)	A% (%)	DA^ (mm)	ViA^ (mm)	VsA^ (mm)
1 *	12.00	0.50	1	53.0º	73.2	6.06	8.98	23.16	73.2	6.06	8.98	12.00
2 *	0.00	0.50	1	51.0º	77.1	5.65	7.90	22.80	77.1	5.65	7.90	0.00
3 *	300.00	0.50	1	55.0º	2.4	---	---	---	2.4	---	---	---
4 *	180.00	0.50	1	70.0º	27.8	8.62	16.53	25.19	27.8	8.62	16.53	180.00
5 *	48.00	0.50	1	67.0º	34.4	7.45	22.03	32.11	34.4	7.45	22.03	48.00
6 *	0.00	0.50	1	57.0º	25.1	7.27	10.67	23.37	25.1	7.27	10.67	0.00

3rd Inspection												
Entry #	Scan (mm)	Index (mm)	Group	Channel	A% (%)	DA^ (mm)	PA^ (mm)	SA^ (mm)	A% (%)	DA^ (mm)	ViA^ (mm)	VsA^ (mm)
1 *	96.00	0.50	1	69.0º	30.9	6.29	9.12	17.55	30.9	6.29	9.12	96.00
2 *	72.00	0.50	1	70.0º	29.0	9.12	17.91	26.66	29.0	9.12	17.91	72.00
3 *	36.00	0.50	1	64.0º	27.8	8.51	15.63	26.21	27.8	8.51	15.63	36.00
4 *	48.00	0.50	1	69.0º	23.1	6.45	9.54	18.01	23.1	6.45	9.54	48.00
5 *	60.00	0.50	1	70.0º	29.0	9.16	22.64	31.70	29.0	9.16	22.64	60.00
6 *	48.00	0.50	1	70.0º	30.5	6.80	11.53	19.87	30.5	6.80	11.53	48.00
7 *	24.00	0.50	1	70.0º	32.9	2.48	-0.34	7.24	32.9	2.48	-0.34	24.00
8 *	24.00	0.50	1	68.0º	48.1	8.30	21.58	31.25	48.1	8.30	21.58	24.00
9 *	36.00	0.50	1	70.0º	29.4	9.18	22.57	31.62	29.4	9.18	22.57	36.00
10 *	84.00	0.50	1	70.0º	27.0	8.93	23.26	32.36	27.0	8.93	23.26	84.00
11 *	24.00	0.50	1	70.0º	44.6	8.71	23.87	33.00	44.6	8.71	23.87	24.00

Since the probe characteristics, material properties and the setup or calibration parameters were not changed, there was no need to display repetition tables. In the second trial, the focal depth was adjusted on 25 mm, the material velocity was changed to 3146.1 m/s, and angle resolution was set to 0.5° instead of 1° in the calculator (Table 2.6). A crucial point of inspection, the probe start and stop angles were set or expanded from 45° to 55° and 70° to 75° with respect to position of the encoder.

Table 2.6 Phased array Omniscan MX software parameters for the Second trial

Calculator					
Used Element Qty.	First Element	Last Element	Resolution	Wave Type	Material Velocity
16	1	16	1.0	User-Defined	3146.1 m/s
Start Angle	Stop Angle	Angle Resolution	Focal Depth	Law Configuration	
55.0º	75.0º	0.5º	25.00 mm	Sectorial	

Setup				
A:55.0 Sk:090 L:001				
Beam Delay	Start (Half Path)	Range (Half Path)	Max. PRF	Type
11.55 us	-2.01 mm	176.18 mm	5	PA
Scale Type	Scale Factor	Video Filter	Pretrig.	Rectification
Compression	35	Off	0.00 µs	FW
Voltage	Gain	Mode	Wave Type	Sound Velocity
40 (Low)	9.60 dB	PE (Pulse-Echo)	User-Defined	3146.1 m/s
Scan Offset	Index Offset	Skew		
0.00 mm	0.00 mm	90.0º		

Table 2.7 Results of the second trial no (25 mm focal depth)

1st Inspection

Entry #	Scan (mm)	Index (mm)	Group	Channel	A% (%)	DA^ (mm)	PA^ (mm)	SA^ (mm)	A% (%)	DA^ (mm)	ViA^ (mm)	VsA^ (mm)
1 *	0.00	0.50	1	62.5º	55.2	7.22	16.41	27.67	55.2	7.22	16.41	0.00
2 *	144.00	0.50	1	57.5º	32.5	6.59	12.19	24.95	32.5	6.59	12.19	144.00
3 *	216.00	0.50	1	75.0º	28.6	7.04	94.32	104.47	28.6	7.04	94.32	216.00
4 *	180.00	0.50	1	75.0º	43.4	7.28	95.20	105.38	43.4	7.28	95.20	180.00
5 *	252.00	0.50	1	75.0º	41.1	7.27	95.17	105.35	41.1	7.27	95.17	252.00
6 *	96.00	0.50	1	75.0º	30.9	6.65	92.86	102.96	30.9	6.65	92.86	96.00

2nd Inspection

Entry #	Scan (mm)	Index (mm)	Group	Channel	A% (%)	DA^ (mm)	PA^ (mm)	SA^ (mm)	A% (%)	DA^ (mm)	ViA^ (mm)	VsA^ (mm)
1 *	84.00	0.50	1	57.0º	54.4	6.23	12.28	25.28	54.4	6.23	12.28	84.00
2 *	204.00	0.50	1	75.0º	66.5	7.09	94.52	104.68	66.5	7.09	94.52	204.00
3 *	48.00	0.50	1	64.5º	57.5	6.96	19.49	30.30	57.5	6.96	19.49	48.00
4 *	24.00	0.50	1	64.5º	68.1	7.54	18.27	28.95	68.1	7.54	18.27	24.00
5 *	84.00	0.50	1	64.5º	52.8	6.91	19.59	30.41	52.8	6.91	19.59	84.00
6 *	252.00	0.50	1	75.0º	49.7	7.84	97.32	107.57	49.7	7.84	97.32	252.00
7 *	72.00	0.50	1	70.0º	28.6	3.83	3.37	11.19	28.6	3.83	3.37	72.00
8 *	24.00	0.50	1	63.5º	58.3	7.92	16.24	27.08	58.3	7.92	16.24	24.00
9 *	252.00	0.50	1	75.0º	45.0	6.30	91.56	101.61	45.0	6.30	91.56	252.00
10 *	72.00	0.50	1	70.5º	29.4	4.33	5.15	12.98	29.4	4.33	5.15	72.00
11 *	96.00	0.50	1	75.0º	42.7	6.73	93.18	103.29	42.7	6.73	93.18	96.00
12 *	240.00	0.50	1	75.0º	34.0	6.40	91.95	102.02	34.0	6.40	91.95	240.00

2.7   Manual Phased Array Inspection on Butt Welded Plate (Specimen Type 3)

In the manual inspections with Phased Array system, the probe is scanned towards and away from the weld line, and the operator follows the screen for any signal detection. Phased Array provides much simpler detection along with S-scan, C-Scan or B-Scan displays rather than simple A-Scan [27].
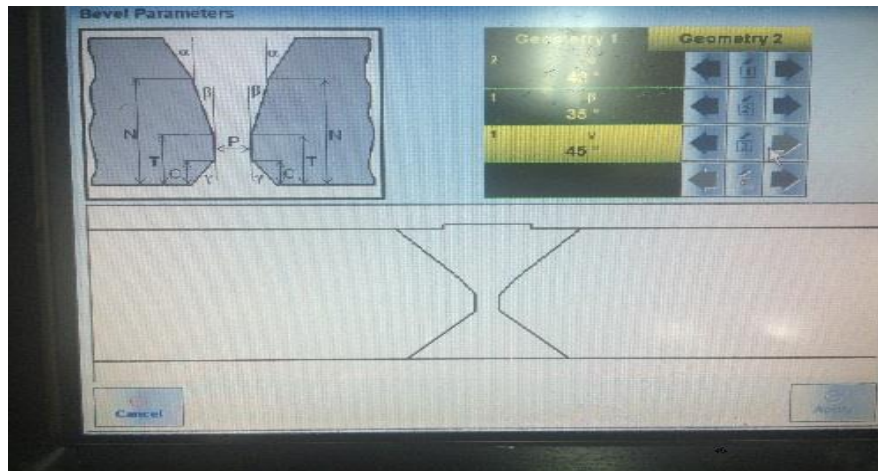
Figure 2.12 Weld bevel image on the screen of Sonotron Isonic 2010

Manual Phased Array inspection was carried out by Sonotron isonic 2010 device and linear array probe with 32 elements (Figure 2.12 – 2.13). Since the inspection is time based data collection, i.e., depends on operator's speed, the position and length of defects are influenced by manually time-based scanning or beam sweeping. Therefore, these results are not acceptable in terms of probability of detection analysis because there is no relationship between defect size and defect amplitude or signal and or any other verification codes such as ASME Code Case 2235.

Nevertheless, Manual Phased Array inspections were performed on butt welded plate in order to prove the dominance of Phased Array over the conventional UT from the point of detecting discontinuities.
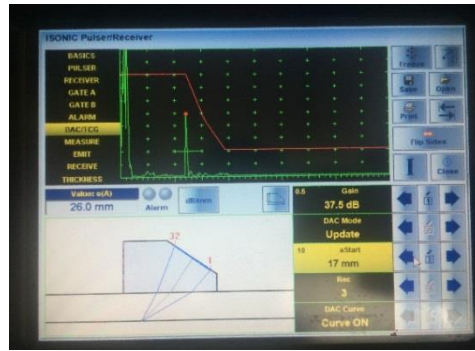
The advantages such as beam steering and

Figure 2.13 Manual Phased Array inspection

sweeping, and adjusting focus distance, give a superiority to Phased Array over conventional ultrasonic testing in terms of detection capabilities.

#	Length	Width	Area Size	Highest Amplitude	Average Amplitude	Start Length	End Length	Start Width
1	3.0 mm	3.0 mm	0.09 cm²	34.1 dB	31.6 dB	3.0 mm	6.0 mm	13.0 mm
2	3.0 mm	2.0 mm	0.06 cm²	32.7 dB	30.7 dB	37.0 mm	40.0 mm	15.0 mm
3	4.0 mm	2.0 mm	0.08 cm²	34.7 dB	32.5 dB	46.0 mm	50.0 mm	16.0 mm
4	4.0 mm	2.0 mm	0.08 cm²	35.4 dB	33.4 dB	55.0 mm	59.0 mm	17.0 mm
5	4.0 mm	2.0 mm	0.08 cm²	31.9 dB	30.3 dB	64.0 mm	68.0 mm	15.0 mm
6	3.0 mm	2.0 mm	0.06 cm²	34.4 dB	34.1 dB	80.0 mm	83.0 mm	13.0 mm
7	3.0 mm	2.0 mm	0.06 cm²	34.7 dB	32.4 dB	89.0 mm	92.0 mm	17.0 mm
8	4.0 mm	3.0 mm	0.12 cm²	38.4 dB	33.8 dB	95.0 mm	99.0 mm	17.0 mm
9	13.0 mm	7.0 mm	0.91 cm²	38.0 dB	32.6 dB	101.0 mm	114.0 mm	12.0 mm
10	4.0 mm	1.0 mm	0.04 cm²	29.3 dB	28.8 dB	119.0 mm	123.0 mm	16.0 mm

Figure 2.14 Defect list captured by Sonotron Isonic 2010

Data demonstrated in Figure 2.14 are inaccurate since the defect sizes are not matching with defect amplitudes due to time based scanning errors. Time-based scanning can be used only to demonstrate detection of a flaw, it does not give properly defect positions or size results.

2.8   Probability of Detection Analysis

The inspection results are transferred to probability of detection analysis software program (mh1823) and then, the rules and procedure steps in the MIL-HDBK-1823A criteria were followed for drawing the Probability of Detection graphs (PoD).

In order to evaluate the reliability of a nondestructive method, there are two realistic and probabilistic approach. Namely, the first one "hit/miss" data is based on whether a flaw detected or not. The second one is used for defect sizes versus signal responses where this approach is appropriate for eddy current or ultrasonic testing methods due to outputs of these methods. Selected feedback about flaw property for ultrasonic and eddy current case is called â data (i.e. "a hit / miss data") or "signal response" data [18].

PoD curves were generated with data obtained from artificial defect sizes versus signal responses on the behalf of conventional ultrasonic and Phased array inspections. In case of manual Phased array inspection on the butt welded plates since the real defect sizes are unknown and time based inspection performed without encoder, the data derived from this type of inspection is not appropriate for generating PoD curves.

All PoD curves were created with the correlation of *"a vs â"* data. The results of inspections were processed by using mh1823 software [26].

CHAPTER 3

RESULTS and DISCUSSION

3.1   Microstructure

The representative micrographs for the specimen type 3 are given in Figure 3.1. The number of intercepts is 408 and the mean intercept length values for the parent metal were found to be 13 µm, which corresponds to ASTM Grain Size Number G: 9. 24 according to ASTM E 1382. On the other hand, in the heat affected zone the number of intercepts is 436 and the mean intercept length values were found to be 12 µm.
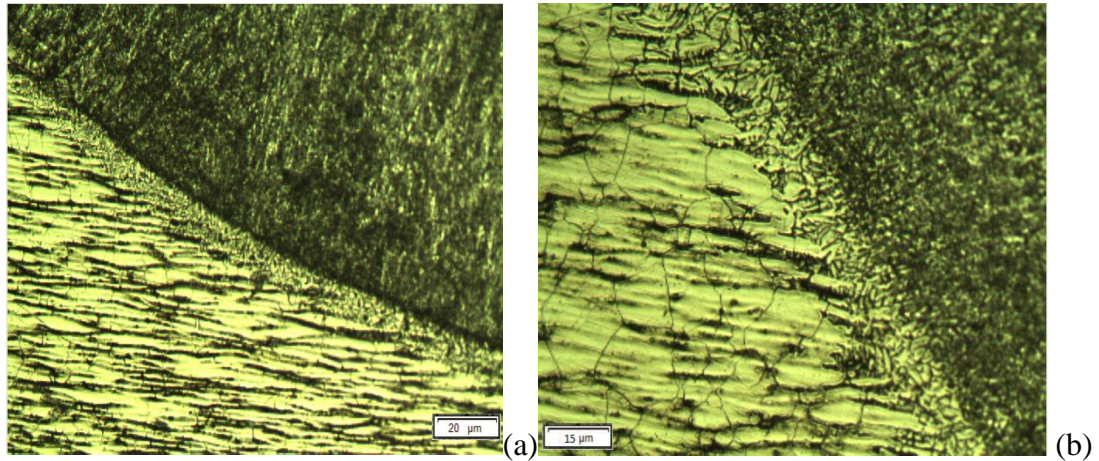
Figure 3.1 Representative micrographs for the specimen type 3 Parent, HAZ and weld metal at (5 x) (a), Fusion line at (20 x) (b)

The average grain size of the parent metal is 13 µm while it is approximately 12 µm in the heat affected zone. These results indicate occurrence of recrystallization in the

heat affected zone. Figure 3.2 shows the mean micro hardness values of the parent metal, heat affected zone and weld metal.
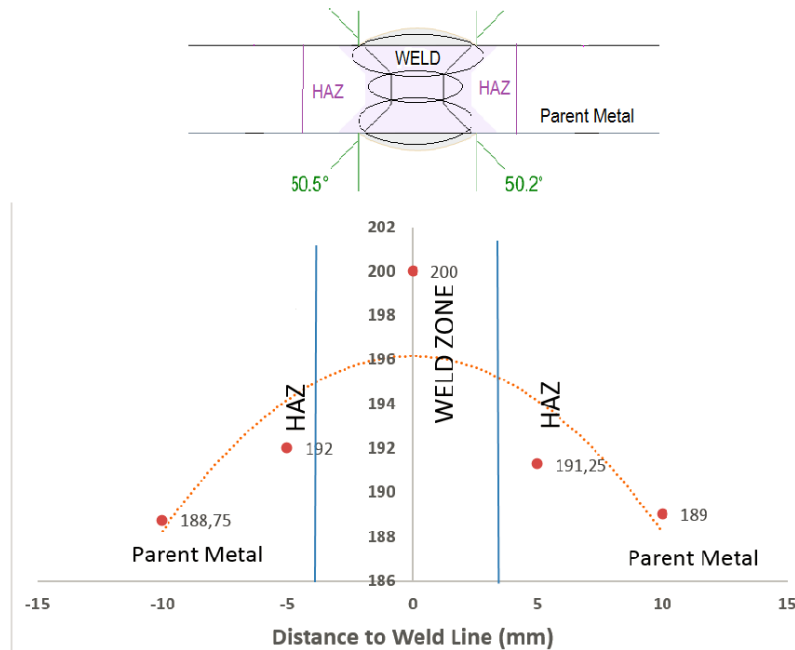
Figure 3.2 Micro hardness values versus distance to weld line

Grain size and micro hardness values are in accordance with literature [25, 32]. An example is given in Table 3.1.

Table 3.1 Grain sizes and mechanical values of the AISI 304 [25]

	Grain size (μm)	Hardness (HV)	Tensile strength (N/mm^2)	0.2% Yield strength (N/mm^2)
AISI 304	2.5	242.5	790	480
	40	163.5	650	240

The only difference between literature data and the results of this study is high hardness of the weld metal. The reason is the selection of the filler material (Table 2.2) intentionally wrong to create inherent discontinuities since the whole study is based on probability of detection of such defects.

It was assumed that the differences in the grain morphology of the cast austenitic stainless steels (equiaxed or columnar) can be detected by longitudinal waves. The estimate is based on the attenuation of equiaxed structure more than attenuation of columnar structure in the study of P. Ramuhalli et al. [28]. While the bandwidth frequency of transducers is being lowered, the difference in attenuation is getting smaller (300 to 800 kHz). It has been already reported that attenuation in columnar grain structure is less than ~ 2 dB/cm, while it is greater than or equal to ~2.5 dB/cm in the equiaxed-grain structure (Table 3.2). Since the beam skew, texture and related degree of anisotropy, also preferred orientations of grains were not involved, it seems that the attenuation in columnar grain structure is less than that in equiaxed structure. Moreover, lower frequencies (longer wavelengths) scattering from the grain boundaries (whether equiaxed or columnar) is low particularly for small ultrasonic path lengths (corresponding to the first back-wall signal). As the sound path distance escalates (corresponding to second, third, and later reflections), scattering from the more grain boundaries in equiaxed structures becomes more significant and results in larger attenuation values.

Table 3.2 Average attenuation in the columnar and equiaxed structure [28]

Frequency	Columnar Microstructure		Equiaxed Microstructure	
	Mean Attenuation (dB/cm)	Standard Deviation (dB/cm)	Mean Attenuation (dB/cm)	Standard Deviation (dB/cm)
500 kHz	1.92	0.17	2.64	0.20
1 MHz	1.74	0.24	2.72	0.21

In general ultrasonic inspection is very hard due to inhomogeneous media in the coarse columnar grains, it is likely difficult to predict ultrasonic capabilities, or to choose reference for the UT inspection. On the other hand, in case of fine structures (equiaxed microstructure) it is more homogeneous acting like transverse isotropic. However, attenuation or background noise can be an issue as important as in coarse columnar grain structures. Therefore, the presence of fine columnar zone does not interfere the detection and the localization of defects. Since a stable echo is preferred to disturbed one, these materials are considered easier to control [38].
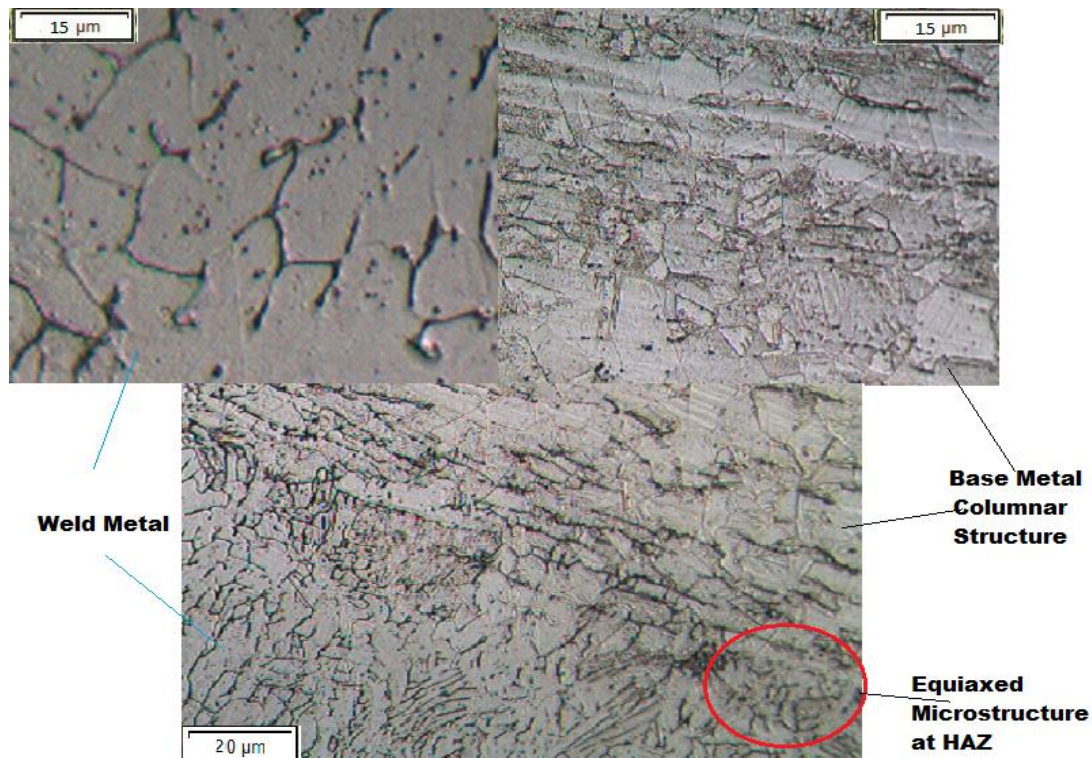
Figure 3.3 Representative axial-radial cross sections of the specimen type 3

Based on the calculations carried out by different frequencies and angles, the mean attenuation values are given in Table 3.3 for different test frequencies by longitudinal waves, and in Table 3.4 for different test angles by shear waves.

Table 3.3 The mean attenuation values in the specimen type 1 and 2 (longitudinal wave)

Test frequency	Longitudinal Wave		
	4 MHz	2 MHz	1 MHz
Sound velocity (m /s)	5752	5766	5617
Mean attenuation (dB / cm)	0.56	0.58	0.78

Attenuation rate in equiaxed structure which was measured by using half skip and full skip method is higher than that in the columnar structure of specimen type 3 butt welded plate (Table 3.4).

76

Table 3.4 The mean attenuation values in the columnar and equiaxed structure of the specimen type 3 butt welded plate (shear wave)

Angles of Test Probes	45°	60 °	45°	60 °
	Columnar		Equiaxed	
Sound velocity (m /s)	3106	3137	3140	3135
Mean Attenuation (dB / cm)	1.06	1.22	1.54	1.50

Ultrasonic propagation is homogeneous close to fusion line because of the equiaxed microstructure (relatively finer grains) of heat affected zone. Although the sound propagation in the columnar structure of austenitic test blocks is commonly harder than that in equiaxed microstructure, attenuation in fine grains can, however, be as significant as in coarse columnar grain structures regarding the chemical composition or the manufacturing conditions of the specimen. The difference in attenuation rate measurement might have arisen because the weld material was chosen intentionally inappropriate for the welding in order to create defects as much as possible. Furthermore, the percentage of ferrite have direct impact on ultrasonic attenuation. According to the study of Ferreira et al. [37], the increase in the percentage of ferrite in the microstructure, resulted in the decrease of the sonic speed, and in sonic attenuation increase. Also, the higher percentages of ferrite (Figure 3.2) lead to the highest average hardness values at AISI 304L of the butt welded plate specimen type 3.

3.2   Results of Ultrasonic and Phased Array Inspections

Table 3.5, 3.7 shows the data retrieved from the flaws at different depths (Specimen Type 1), while Table 3.6, 3.8 shows the data retrieved from the flaws at different sizes at the same depth (Specimen Type 2) by ultrasonic method and Phased Array testing respectively. In addition, Table 3.9 demonstrates the data collected from the flaws in butt welded plate (specimen type 3) by conventional ultrasonic inspection.

Table 3.5 UT data retrieved from the flaws at different depths of (Specimen Type 1)

ID	Sound path (mm)	Remaining screen height (%)	ID	Sound path (mm)	Remaining screen height (%)
1	10,71	1	1	10,49	1
2	22,46	34	2	22,38	44,44
3	34,47	59	3	34,28	62
4	47,1	67	4	46,29	72,6
5	58,52	75	5	58,27	79,6
6	71,16	77	6	70,85	83
7	83,2	81	7	82,2	87,1
8	95,32	83	8	94,24	88,6
9	107,3	85	9	106,13	89
10	119,3	87	10	118,29	93
ID	**Sound path (mm)**	**Remaining screen height (%)**	**ID**	**Sound path (mm)**	**Remaining screen height (%)**
1	10,06	1	1	10,34	1
2	22,57	34	2	22,4	46
3	34,89	59	3	34,6	61
4	47,0	67	4	45,7	72
5	58,3	73	5	58,6	78,8
6	70,9	76	6	70,9	82
7	83,4	81	7	82,6	86,9
8	95,22	83	8	94,2	89,3
9	107,1	86	9	106,6	89,4
10	118,8	88	10	118,4	92,5

Table 3.6 UT data retrieved from the flaws at different sizes at the same depth (Specimen Type 2)

ID	Screen height (%)	Amplitude (dB)	ID	Screen height (%)	Amplitude (dB)
5 mm	99	21,9	5 mm	99	18,8
4,5 mm	97,5	21,9	4,5 mm	94,7	18,8
4 mm	93,2	21,9	4 mm	88,1	18,8
3,5 mm	84,9	21,9	3,5 mm	82,2	18,8
3 mm	80,2	21,9	3 mm	79,5	18,8
2,5 mm	74,8	21,9	2,5 mm	74,4	18,8
2 mm	69,3	21,9	2 mm	65,4	18,8
1,5 mm	61,5	21,9	1,5 mm	54,8	18,8
1 mm	54,8	21,9	1 mm	48,1	18,8
0,8 mm	48,5	21,9	0,8 mm	35,8	18,8
0,5 mm	41,5	21,9	0,5 mm	41,1	18,8

ID	Screen height (%)	Amplitude (dB)	ID	Screen height (%)	Amplitude (dB)
5 mm	99	20,5	5 mm	99	19,2
4,5 mm	98,1	20,5	4,5 mm	95,3	19,2
4 mm	93,5	20,5	4 mm	89,2	19,2
3,5 mm	85	20,5	3,5 mm	84,2	19,2
3 mm	80,6	20,5	3 mm	79,6	19,2
2,5 mm	74,9	20,5	2,5 mm	74,9	19,2
2 mm	69,1	20,5	2 mm	65,6	19,2
1,5 mm	61,9	20,5	1,5 mm	54,9	19,2
1 mm	55,2	20,5	1 mm	48,3	19,2
0,8 mm	48,7	20,5	0,8 mm	35,4	19,2
0,5 mm	41,2	20,5	0,5 mm	41,0	19,2

Table 3.7 PA data retrieved from the flaws at different depths (specimen Type 1)

ID	Sound Path	Remaining Screen Height	ID	Sound Path	Remaining Screen Height
1	11,1	1	1	10,8	0,5
2	22,28	39	2	20,32	35,6
3	36,2	52	3	35,1	52,3
4	46,59	62,6	4	48,53	60,9
5	57,23	69,7	5	56,39	69,9
6	65,75	77	6	67,6	77,8
7	81,1	84,1	7	80,9	83,5
8	93,34	87,6	8	94,1	88
9	104,11	88,6	9	106	89,9
10	117,19	92,5	10	119,2	92,6
ID	Sound Path	Remaining Screen Height	ID	Sound Path	Remaining Screen Height
1	13	1	1	11,5	0,8
2	23,3	36,2	2	21	36,8
3	36,1	52,9	3	36,1	53,8
4	45,8	58,6	4	49,2	61,5
5	58	70	5	57,5	69,9
6	66,1	77,6	6	66,4	78
7	82,2	82,8	7	82	84,5
8	94,5	88	8	95,2	88
9	105,1	89,5	9	107,2	89,9
10	118,2	92,3	10	117,7	92,6

Table 3.8 PA data retrieved from the flaws at different sizes at the same depth (Specimen Type 2)

ID	Flaw Size(mm)	Screen Height		ID	Flaw Size(mm)	Screen Height
1	5	99		1	5	99
2	4,5	97,5		2	4,5	94,7
3	4	93,2		3	4	88,1
4	3,5	84,9		4	3,5	82,2
5	3	80,2		5	3	79,5
6	2,5	74,8		6	2,5	74,4
7	2	69,3		7	2	65,4
8	1,5	61,5		8	1,5	54,8
9	1	54,8		9	1	48,1
10	0,8	48,5		10	0,8	35,8
11	0,5	41,5		11	0,5	41,1
Focal depth 41,8				Focal Depth 38,3		

ID	Flaw Size(mm)	Screen Height		ID	Flaw Size(mm)	Screen Height
1	5	98		1	5	99,5
2	4,5	97,2		2	4,5	95,5
3	4	93		3	4	89,2
4	3,5	85,3		4	3,5	84,7
5	3	81,7		5	3	81,2
6	2,5	74,4		6	2,5	76,2
7	2	70,1		7	2	67,3
8	1,5	62,6		8	1,5	55,5
9	1	56		9	1	49,9
10	0,8	47		10	0,8	37,1
11	0,5	42,3		11	0,5	36,6
Focal depth 41,8 mm				Focal Depth 38,3 mm		

Table 3.9 Conventional ultrasonic inspection on butt welded specimen type 3

Defect No	S_p	H_a (dB)	$A^{'}$	$L_{(mm)}$	D_a
1	35,4	1,4	22 mm	43	5,3
2	38,45	4,2	26 mm	82	3,32
3	39,34	0,12	25 mm	140	3,36
4	37,66	2,2	23 mm	160	4,1
5	85,57	1,2	65 mm	194	3,8
6	35,10	2,0	19 mm	249	5

3.3 Probability of Detection (PoD) Analysis

All data retrieved from the inspection records determine the best model for the PoD analysis, model which represents the data as a straight line and approximate constant variance were selected for further analysis.

According to MIL-HDBK-1823A, the best model for assessing the data in terms of PoD is to use log(X) and Cartesian(Y) since there is a linear relationship among the collected data and constant slope.
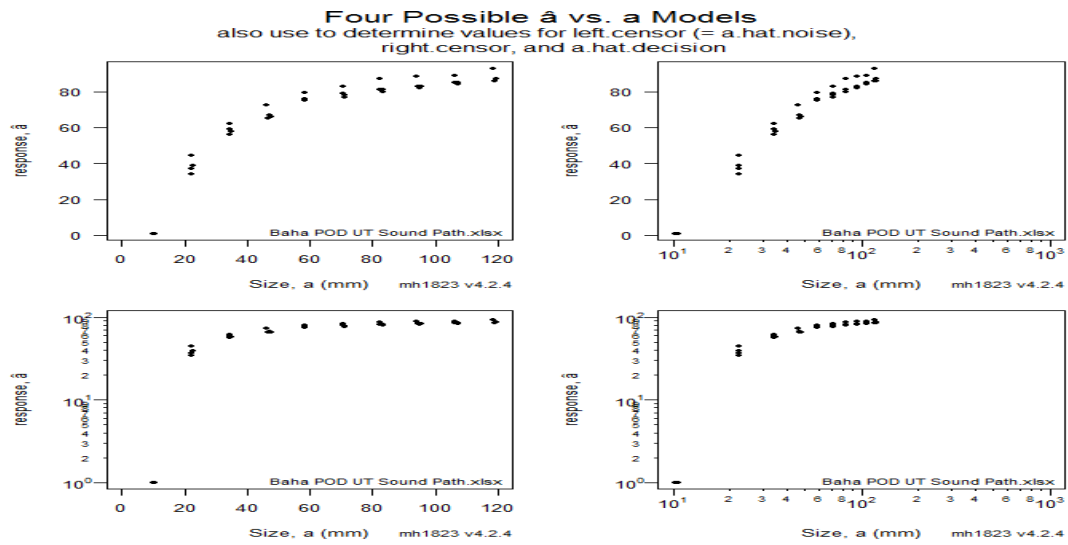
Figure 3.3 Four possible a vs â models for Type 1 specimen (UT)

3.3.1 a vs â Linear Model for PoD Analysis of Type 1 Specimen (UT)

In linear model the x- axis is represented by logarithmic values and y- axis is represented by Cartesian values, the bounding or censoring values have to be resolved. All signal response data have two censoring, first one is left censor or background noise and the second one is right censor corresponding to maximum amplitude value obtained from inspection. Since the left and right censors are the significant factors whether a data is beneficial or useless, a special attention or measure must be taken while determining the boundaries.

Inspection threshold (â_th) and decision threshold (â_dec) are indispensable which have a direct impact on PoD curves. The inspection threshold is the smallest value of $\hat{a}$ recorded by the system, $\hat{a}$ is the decision threshold any signal above it is interpreted as a hit, and below it as a miss. $\hat{a}$ value has a direct relationship with 50 % PoD. Decision threshold is always greater than or equal to inspection threshold [29].
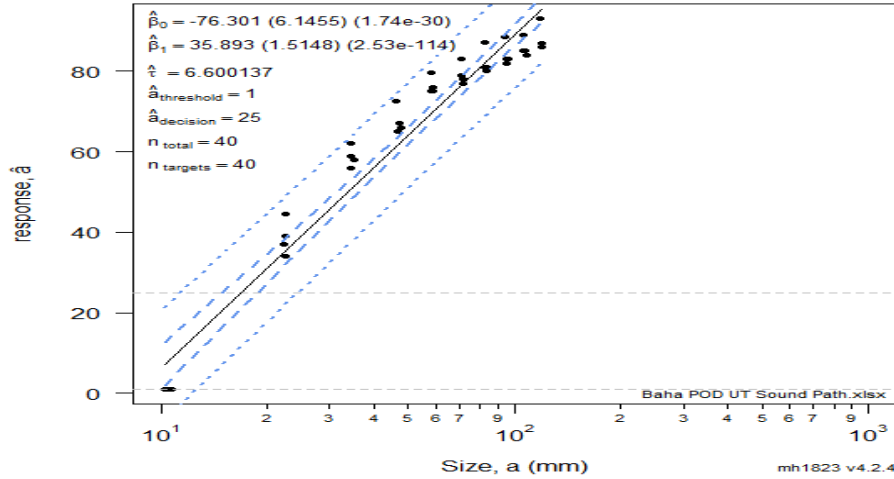
Figure 3.4 *a vs â* linear models for specimen type 1 (UT)

For PoD determination of the specimen type 1, sound path versus signal amplitude evaluation data were recorded and transferred to mh1823 statistical program. In order to generate PoD curve, the left censor is fixed on "1" and right censor is adjusted on "100" for all cases. â_decision is the crucial point in the POD analysis of signal response data. The noise level detection for decision threshold can be admitted any value above the noise level. However, determination of decision threshold affects the detectability of the smallest defect size and false-positive detections (Figure 3.4).
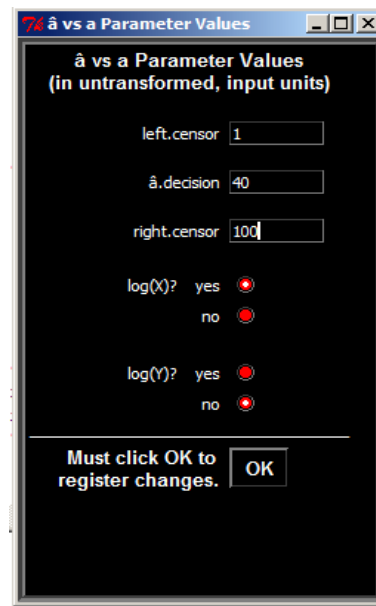
Figure 3.5 *a vs â* parameter values in UT [26]

The flaw size versus signal response parameters were used for PoD curves and analysis. The decision threshold influences directly on accuracy of testing. Also, four fundamental criteria; linearity of the parameters, uniform variance, uncorrelated responses and normal distribution of test flaw sizes have to be considered before assessing any data [17].

To fulfill the conditions of PoD status, the decision threshold (â $_{decision}$) was determined as 40 (Figure 3.5).

3.3.2   a vs â Linear Model for PoD Analysis of Specimen Type 1 (PA)

In order to acquire linear model determination of data collected by Phased Array inspections, the decision threshold (â $_{decision}$) was determined as 25 since the PA transducers having ability of focus depth adaptation and its near field zone is less than that of conventional ultrasonic transducers (Figure 3.6).
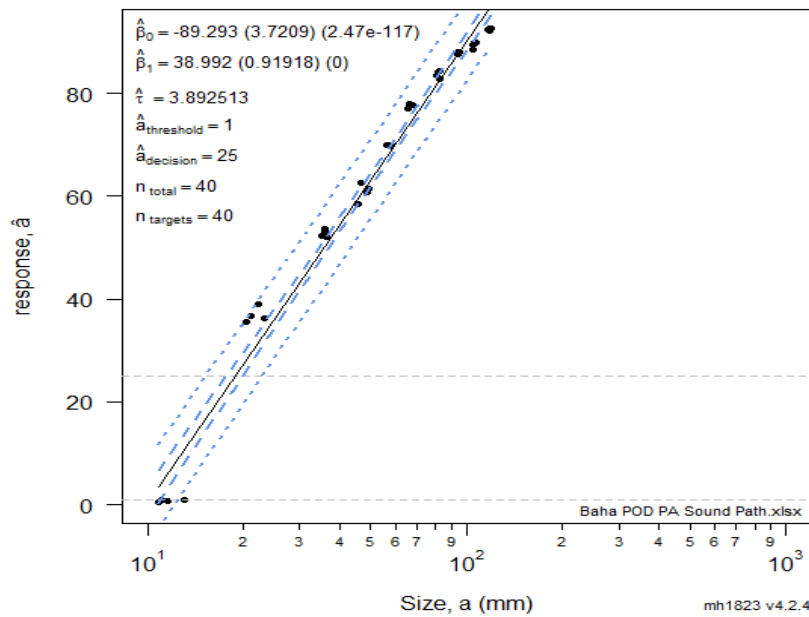
Figure 3.6 *a vs â* linear model Specimen Type 1 (PA)

3.3.3 PoD Analysis of Specimen Type 1

PoD curve of specimen type 1 data derived from artificial flaw depth (a) versus signal response (â) for ultrasonic testing and Phased Array are exhibited in Figure 3.7 and 3.8 respectively. In case for ultrasonic testing the 50 % PoD of flaw (a_{50}) is 25.54 mm in depth. In addition, 90 % PoD of flaw (a_{90}) is 32.33 mm in depth and 90 % PoD of flaw with a confidence interval of 95 % of a flaw ($a_{90/95}$) depth is 35.05 mm from surface were obtained.
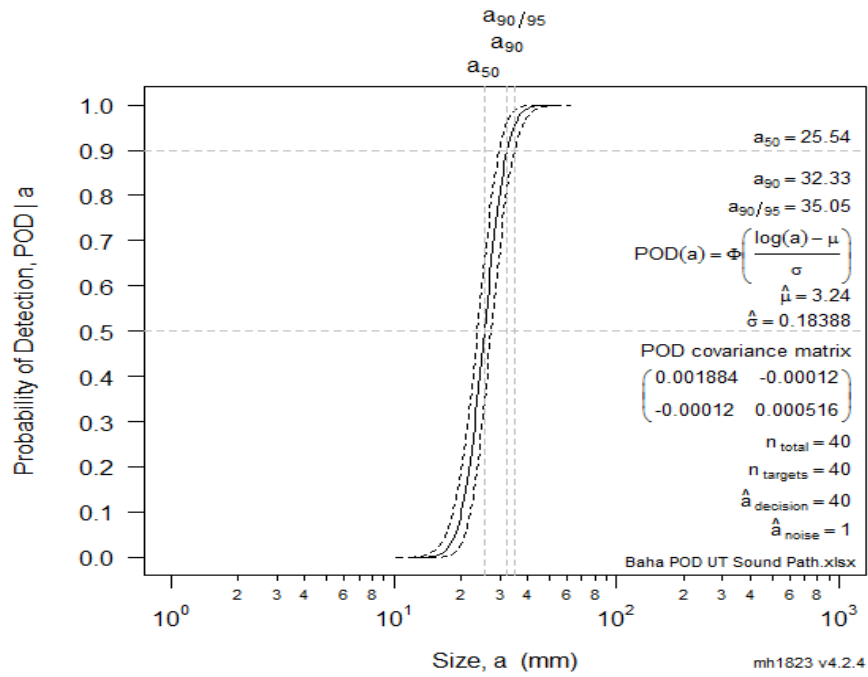
Figure 3.7 PoD curve of specimen type 1 (UT)
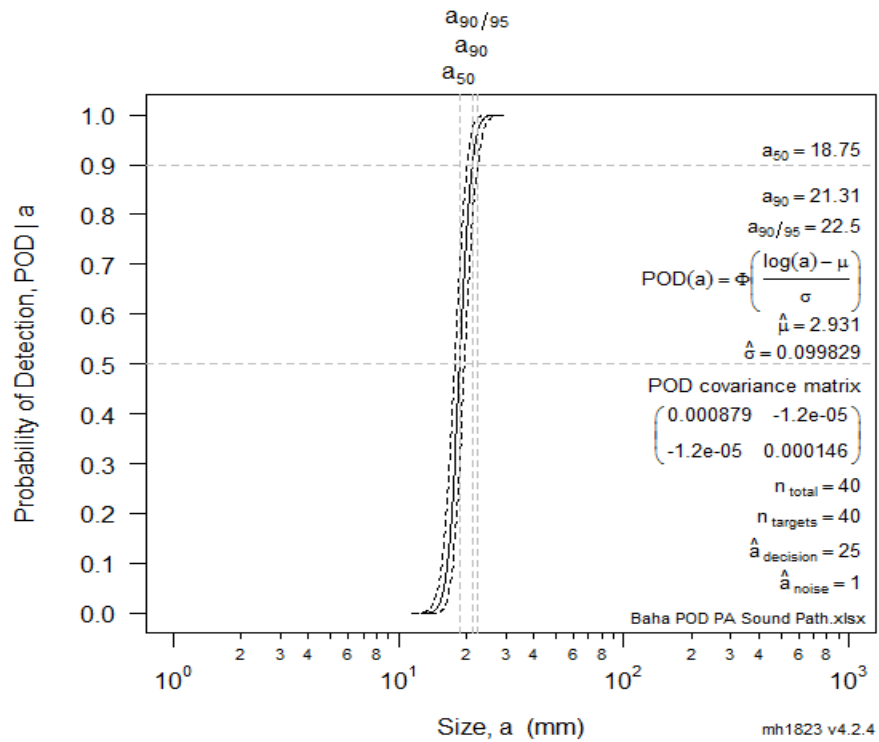
Figure 3.8 PoD curve of specimen type 1 (PA)

85

Moreover, in case of Phased Array system, the 50 % PoD of flaw (a_{50}) is 18.75 mm in depth and 90 % PoD of flaw (a_{90}) is 21.31 mm in depth. Finally, 90 % PoD of flaw with a confidence interval of 95 % of a flaw ($a_{90/95}$) depth is 22.35 mm.

According to results derived from PoD graphs, Phased Array testing gives better results than conventional ultrasonic testing since near field zone is a setback for conventional ultrasonic while the focus depth adaptation is an advantage for Phased Array. Furthermore, depth of first flaw is 5 mm which was detected by PA while conventional ultrasonic testing was not able to detect it due to near field zone effect.

3.3.4 PoD Analysis of Specimen Type 2

PoD curves for specimen type 2 given in Figure 3.09 and 3.10 show that the reliability of the Phased Array system for determining the flaw size is slightly better than that of the ultrasonic system.

Flaw sizes are representing 50 % PoD (a_{50}) values for 1.028 mm in the ultrasonic testing and 1.009 mm for the Phased array system. Projection of 90 % PoD of flaw size (a_{90}), 1.177 mm and 1.138 mm are determined for UT and PA respectively. Lastly, 90 % PoD with a confidence interval of 95 % of a flaw ($a_{90/95}$) sizes are 1.236 mm in the ultrasonic system and 1.19 mm in the Phased array system.

According to these results Phased Array inspection's advantage over the conventional ultrasonic is diminished for the specimen type 2. Since the distance of all flaw depths are same (40 mm), there is no near field zone for UT and PA. Consequently, it must be mentioned that the generated PoD curves highly depend on the data involved in calculations. The significant factor is the decision threshold which is determined by noise level for the material and linearity in terms of probability detection curving rules.
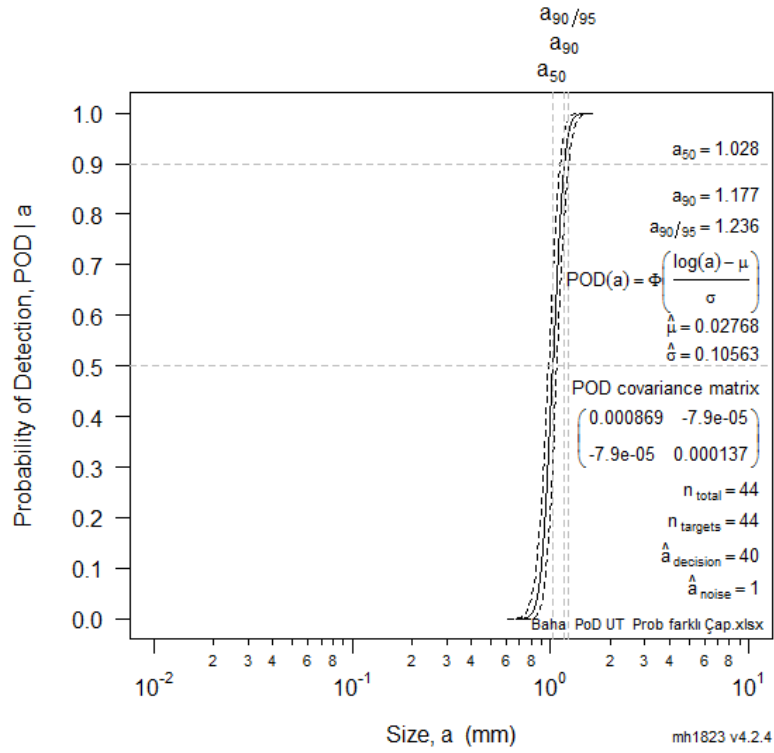
Figure 3.9 PoD curve for Type 2 specimen (UT)
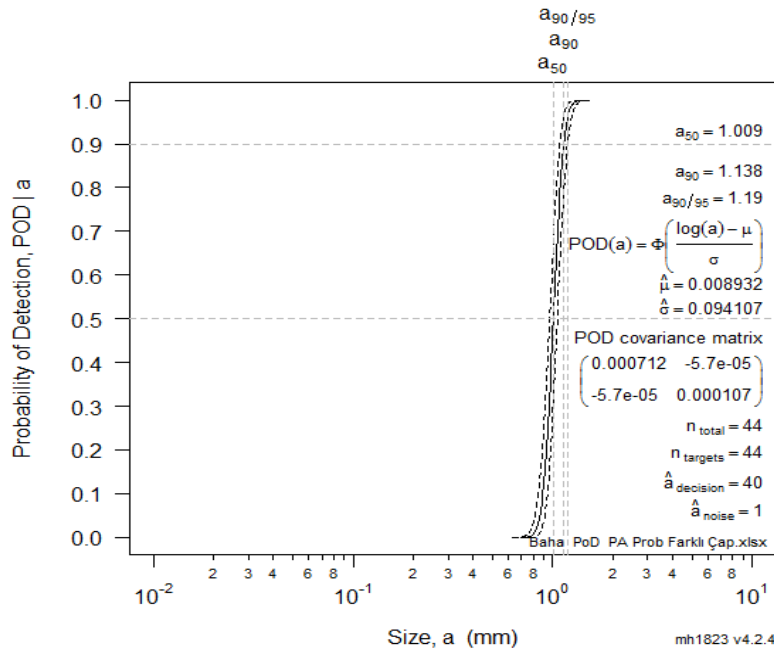
Figure 3.10 PoD curve for Type 2 specimen (PA)

Table 3.10 Reliability values of flaw sizes and depths for ultrasonic (UT), phased array (PA) systems

Reliability	Specimen Type 1		Specimen Type 2	
	UT	**PA**	**UT**	**PA**
50 % PoD	25.54 mm	18.75 mm	1.028 mm	1.009 mm
90 % PoD	32.33 mm	21.31 mm	1.177 mm	1.138 mm
90 % PoD with a confidence interval of 95 %	35.05 mm	22.5 mm	1.236 mm	1.19 mm
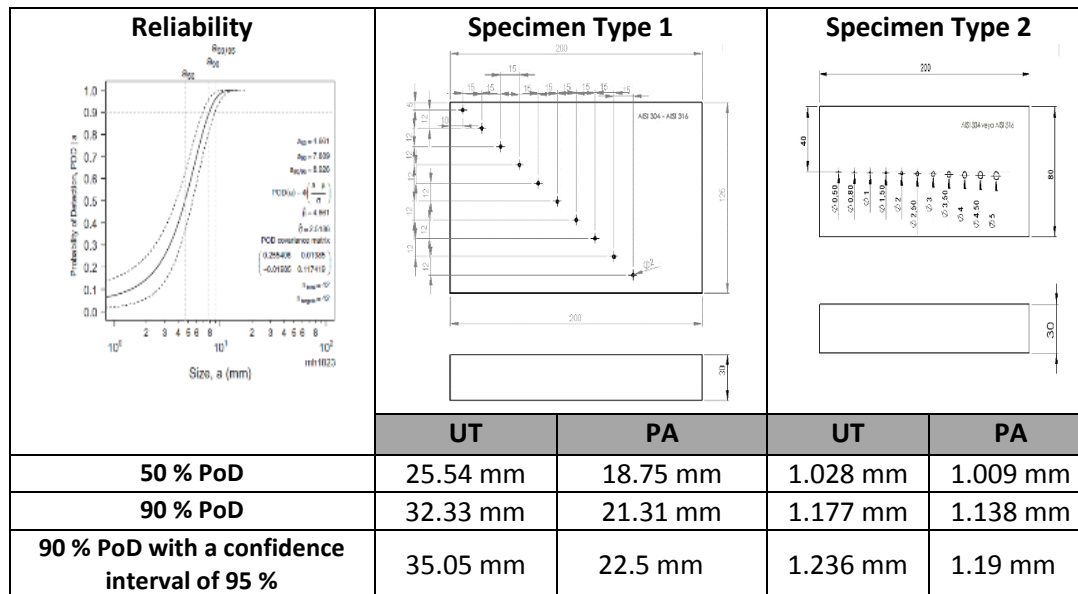
The reliability of system depends on acceptance level, in other words selection of decision threshold and in these cases, repeatability of the results by different operators. Beside human factor, some other variables exist (Table 3.11).

Table 3.11 the Essential Variables in Ultrasonic and Phased Array Testing [19]

Flaw size / flaw orientation / flaw surface texture
Beam characteristics
The Flaw position according to sound path
Potential that the flaw was off-axis
Anisotropic characteristics of the materials tested
Coupling variation due to test surface texture
Texture of the local surface conditions where a skip is required
Weld cap and weld root geometry
Mismatch conditions, etc.

3.4 Evaluation of Manual Phased Array inspections

In ideal situation, the butt welded plate should have artificial defects representing common discontinuities such as;

1. Smooth planar, to represent lack of side wall fusion.
2. Rough planar, to represent cracks.
3. Volumetric, to represent porosity or slag.

However, due to machining problems only volumetric bottom holes and one slot along the weld line were created (Figure 3.11).
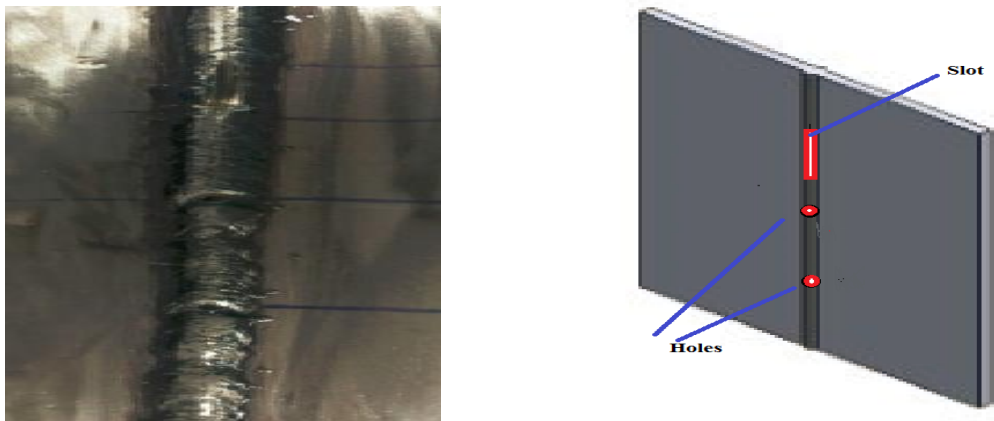
Figure 3.11 The holes and slot on the specimen type 3

During manual Phased Array inspections, by 5 MHz, 0.5 mm pitch size and 32 elements, the first angle 30° and last angle 70° of transducer, along with the delay line wedge were used. The results derived from time based inspections are demonstrated in Figure 3.12 - 3.13 subsequently.
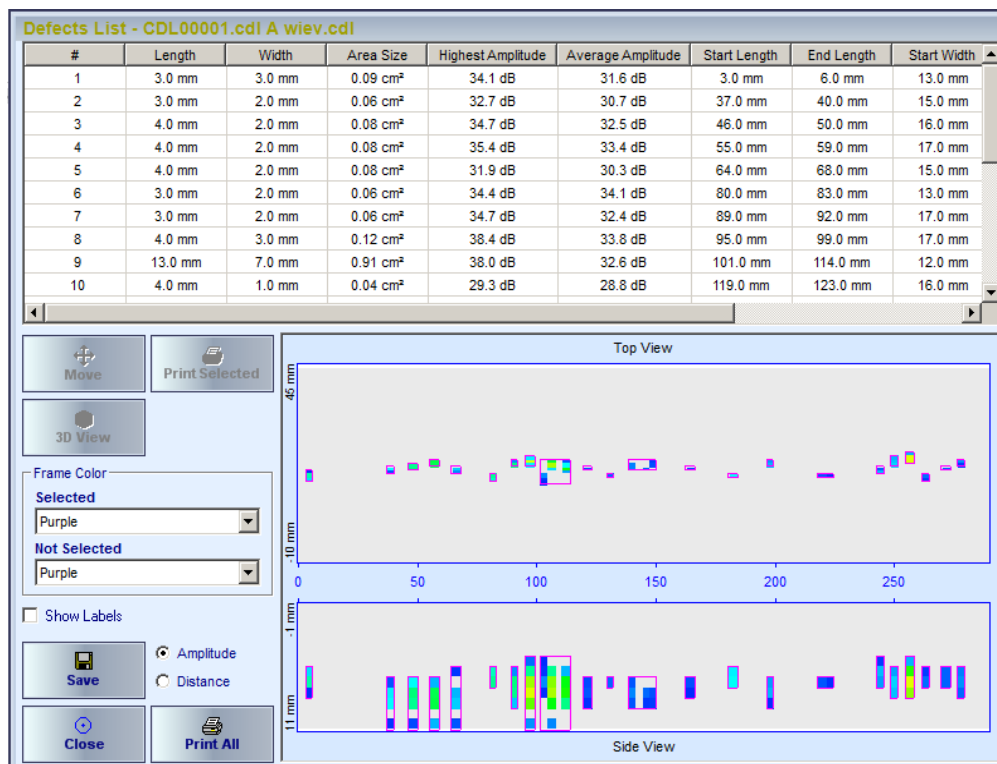
Figure 3.12 the Detected flaws list and schematic display of flaws-1 (MPA)
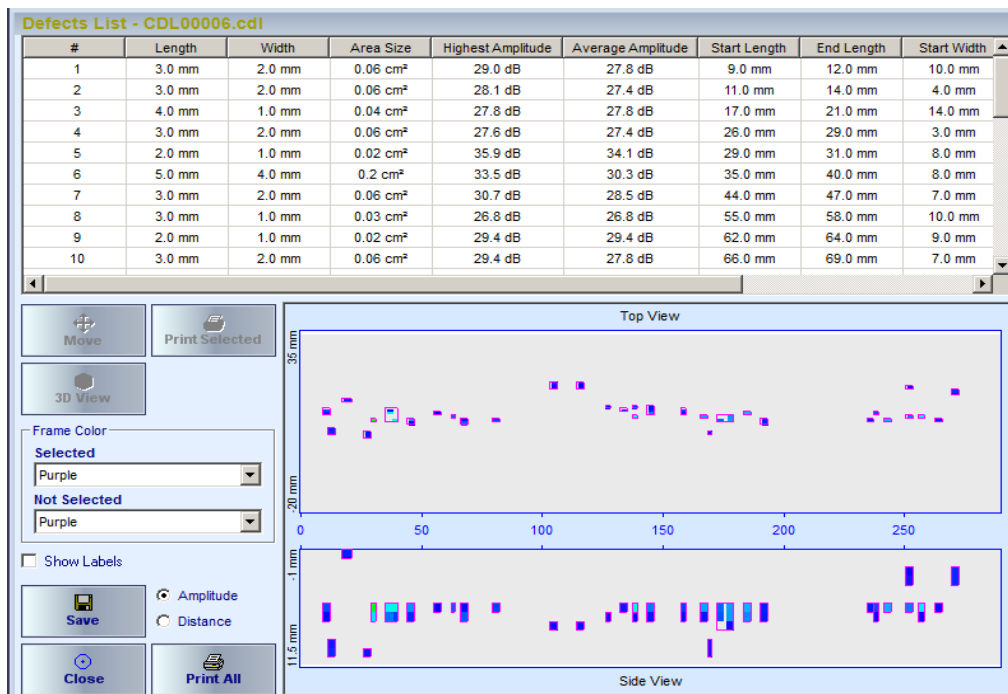
Figure 3.13 The Detected flaws list and schematic display of flaws-2 (MPA)

90

Both inspection trials were performed without encoder so that the positions of defects are not accurate but meandering scan of the weld and swiveling of the probe give some opportunities regarding detection of flaws (Figure 3.14). It is observed that manual Phased array inspections find out the bottom holes the position at 95 mm, 160 mm and slot from 205 mm to 240 mm together with some other unknown natural weld flaws.
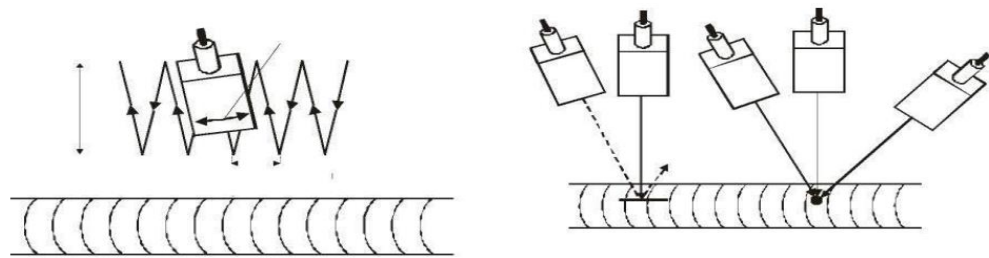
Figure 3.14 Meandering scan of the weld and swiveling of the probe [2]

Meandering and swiveling of the probe similar to conventional ultrasonic testing, increase the chance of flaw detection since the PA system has more capabilities like focal depth, sectorial scan and 32 number of elements firing instead of single element transducer in ultrasonic testing. The bottom line is that Manual Phased Array detected existing artificial holes and slot along with a lack of fusion which is a prevailing discontinuity for butt welded plate in case of both side welding. Although lack of fusion is not properly positioned by manual Phased Array system because of lack of encoder, the flaw had been detected successfully yet (Figure 3.15).
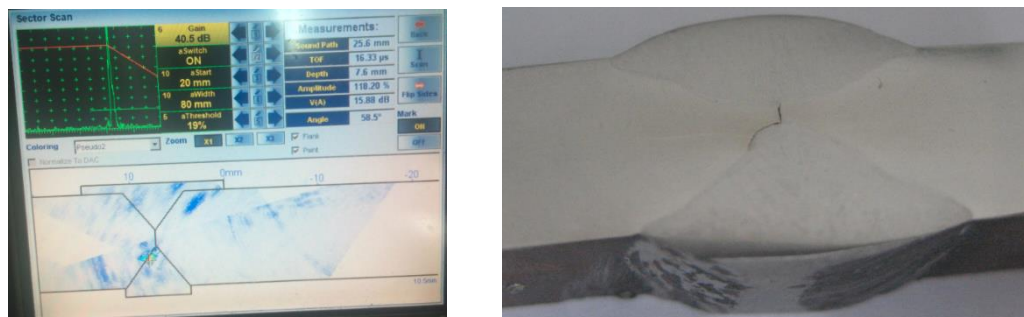
Figure 3.15 The lack of fusion on manual PA display and destructive macro test

91

3.5 Evaluation of Automated Phased Array Inspections

Automated Phased Array inspections were carried out three times for 10 mm focal depth, and two times for 25 mm focal depth. After removing the repeated detections the final defect list were prepared for one line scan with encoder type Olympus ENC 1-2.5-DE as the Table 3.12 and 3.13.

Table 3.12 Phased Array 1st Trial (10 mm focal depth)

1st Inspection Table												
Entry #	Scan (mm)	Index (mm)	Group	Channel	A% (%)	DA^ (mm)	PA^ (mm)	SA^ (mm)	A% (%)	DA^ (mm)	ViA^ (mm)	VsA^ (mm)
1 *	12.00	0.50	1	53.0º	73.2	6.06	8.98	23.16	73.2	6.06	8.98	12.00
2 *	0.00	0.50	1	51.0º	77.1	5.65	7.90	22.80	77.1	5.65	7.90	0.00
3 *	300.00	0.50	1	55.0º	2.4	---	---	---	2.4	---	---	---
4 *	180.00	0.50	1	70.0º	27.8	8.62	16.53	25.19	27.8	8.62	16.53	180.00
5 *	48.00	0.50	1	67.0º	34.4	7.45	22.03	32.11	34.4	7.45	22.03	48.00
6 *	0.00	0.50	1	57.0º	25.1	7.27	10.67	23.37	25.1	7.27	10.67	0.00
7 *	96.00	0.50	1	69.0º	30.9	6.29	9.12	17.55	30.9	6.29	9.12	96.00
8 *	72.00	0.50	1	70.0º	29.0	9.12	17.91	26.66	29.0	9.12	17.91	72.00
9 *	36.00	0.50	1	64.0º	27.8	8.51	15.63	26.21	27.8	8.51	15.63	36.00
10*	60.00	0.50	1	70.0º	29.0	9.16	22.64	31.70	29.0	9.16	22.64	60.00
11 *	24.00	0.50	1	70.0º	32.9	2.48	-0.34	7.24	32.9	2.48	-0.34	24.00
12 *	84.00	0.50	1	70.0º	27.0	8.93	23.26	32.36	27.0	8.93	23.26	84.00

Table 3.13 Phased Array 2nd Trial (25 mm focal depth)

1st Inspection												
Entry #	Scan (mm)	Index (mm)	Group	Channel	A% (%)	DA^ (mm)	PA^ (mm)	SA^ (mm)	A% (%)	DA^ (mm)	ViA^ (mm)	VsA^ (mm)
1 *	0.00	0.50	1	62.5º	55.2	7.22	16.41	27.67	55.2	7.22	16.41	0.00
2 *	144.00	0.50	1	57.5º	32.5	6.59	12.19	24.95	32.5	6.59	12.19	144.00
3 *	216.00	0.50	1	75.0º	28.6	7.04	94.32	104.47	28.6	7.04	94.32	216.00
4 *	180.00	0.50	1	75.0º	43.4	7.28	95.20	105.38	43.4	7.28	95.20	180.00
5 *	252.00	0.50	1	75.0º	41.1	7.27	95.17	105.35	41.1	7.27	95.17	252.00
6 *	96.00	0.50	1	75.0º	30.9	6.65	92.86	102.96	30.9	6.65	92.86	96.00
7 *	84.00	0.50	1	57.0º	54.4	6.23	12.28	25.28	54.4	6.23	12.28	84.00
8*	204.00	0.50	1	75.0º	66.5	7.09	94.52	104.68	66.5	7.09	94.52	204.00
9 *	48.00	0.50	1	64.5º	57.5	6.96	19.49	30.30	57.5	6.96	19.49	48.00
10*	72.00	0.50	1	70.0º	28.6	3.83	3.37	11.19	28.6	3.83	3.37	72.00
11*	24.00	0.50	1	63.5º	58.3	7.92	16.24	27.08	58.3	7.92	16.24	24.00
12 *	240.00	0.50	1	75.0º	34.0	6.40	91.95	102.02	34.0	6.40	91.95	240.00

The inspections with the focal depth of 10 mm and 25 mm showed the same detection capability. In order to evaluate the results easily, the Table 3.12 and 3.13 are combined in Table 3.14.

Table 3.12 and 3.13 were reconstructed according to scan positions for avoiding repeated measures considering easy evaluation. There are fifteen individually defect possibility based on the one line automated Phased array scan, one by one was examined in S-scan (Table 3.14).

Table 3.14 The list of flaws detected by Phased Array method

Detected Flaws Combined Table												
Entry #	Scan (mm)	Index (mm)	Gro up	Channe l	A (%)	DA^ (mm)	PA^ (mm)	SA^ (mm)	A% (%)	DA^ (mm)	ViA^ (mm)	VsA^ (mm)
1 *	0.00	0.50	1	51.0º	77.1	5.65	7.90	22.80	77.1	5.65	7.90	0.00
2*	12.00	0.50	1	53.0º	73.2	6.06	8.98	23.16	73.2	6.06	8.98	12.00
3 *	24.00	0.50	1	70.0º	32.9	2.48	-0.34	7.24	32.9	2.48	-0.34	24.00
4 *	36.00	0.50	1	64.0º	27.8	8.51	15.63	26.21	27.8	8.51	15.63	36.00
5 *	48.00	0.50	1	67.0º	34.4	7.45	22.03	32.11	34.4	7.45	22.03	48.00
6*	60.00	0.50	1	70.0º	29.0	9.16	22.64	31.70	29.0	9.16	22.64	60.00
7*	72.00	0.50	1	70.0º	29.0	9.12	17.91	26.66	29.0	9.12	17.91	72.00
8 *	84.00	0.50	1	70.0º	27.0	8.93	23.26	32.36	27.0	8.93	23.26	84.00
9 *	96.00	0.50	1	69.0º	30.9	6.29	9.12	17.55	30.9	6.29	9.12	96.00
10*	144.00	0.50	1	57.5º	32.5	6.59	12.19	24.95	32.5	6.59	12.19	144.00
11 *	180.00	0.50	1	70.0º	27.8	8.62	16.53	25.19	27.8	8.62	16.53	180.00
12*	204.00	0.50	1	75.0º	66.5	7.09	94.52	104.68	66.5	7.09	94.52	204.00
13 *	216.00	0.50	1	75.0º	28.6	7.04	94.32	104.47	28.6	7.04	94.32	216.00
14 *	240.00	0.50	1	75.0º	34.0	6.40	91.95	102.02	34.0	6.40	91.95	240.00
15 *	252.00	0.50	1	75.0º	41.1	7.27	95.17	105.35	41.1	7.27	95.17	252.00

The first indication (Figure 3.16) is at the depth of 5.65 mm, it is more likely to be lack of fusion or incomplete penetration since the position of flaw is near to beginning of the root pass.

The second indication (Figure 3.17) is more likely to be subsequent of the flaw beginning from starting point of the plate. It is well known that start – stop or finish zones are prone to be created defects particularly in gas metal arc welding procedure (GMAW), in this case it is approximately 20-25 mm. Flaw length of 3rd (Figure 3.18) indication is approximately 25 mm at the depth of 2.48 mm.
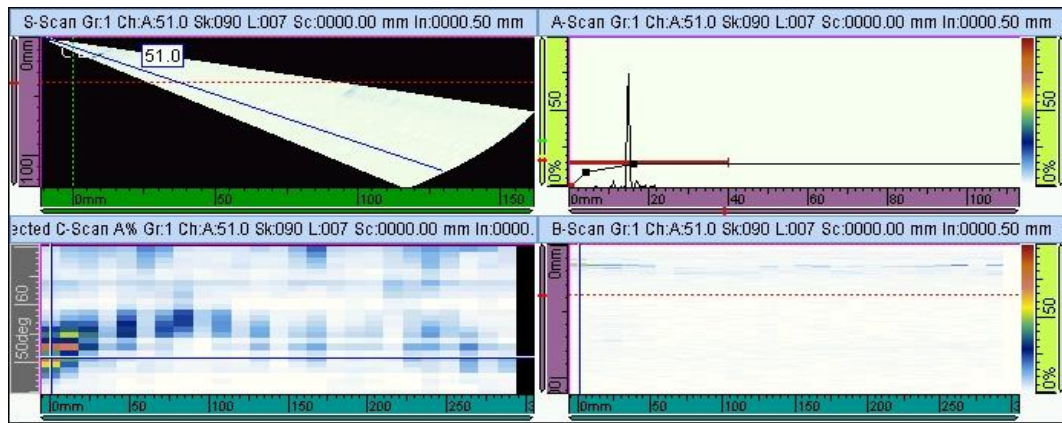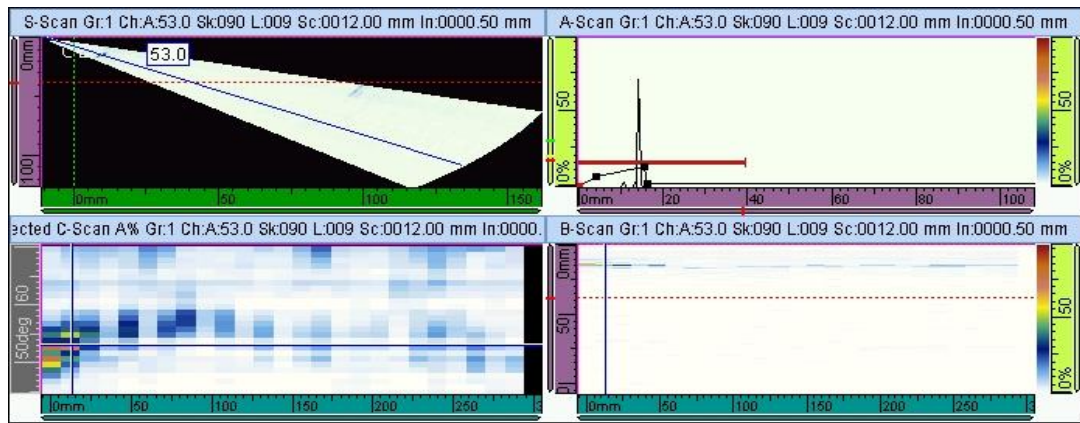
Figure 3.16 Evaluation of 1st data
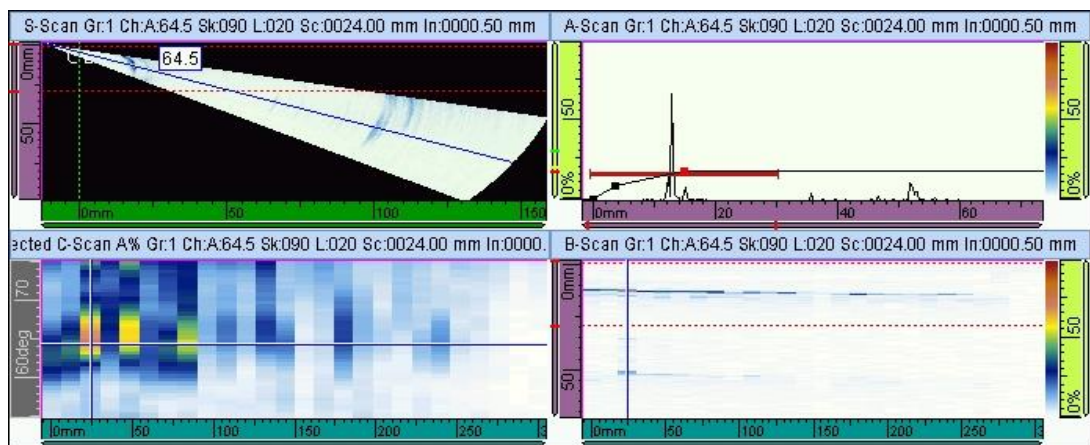

Figure 3.17 Evaluation of 2nd data

Figure 3.18 Evaluation of 3rd data

4th, 5th and 6th indications (Figure 3.19, 3.20, 3.21) resemble probably small defects at the depth of 8.51, 7.45 and 9.16 mm respectively.

7th and 8th indications (Figure 3.22 and 3.23) are very close to bottom of the plate since their depth starting point at 9.12 and 8.93 mm in the t=10 mm nominal thickness of the plate.
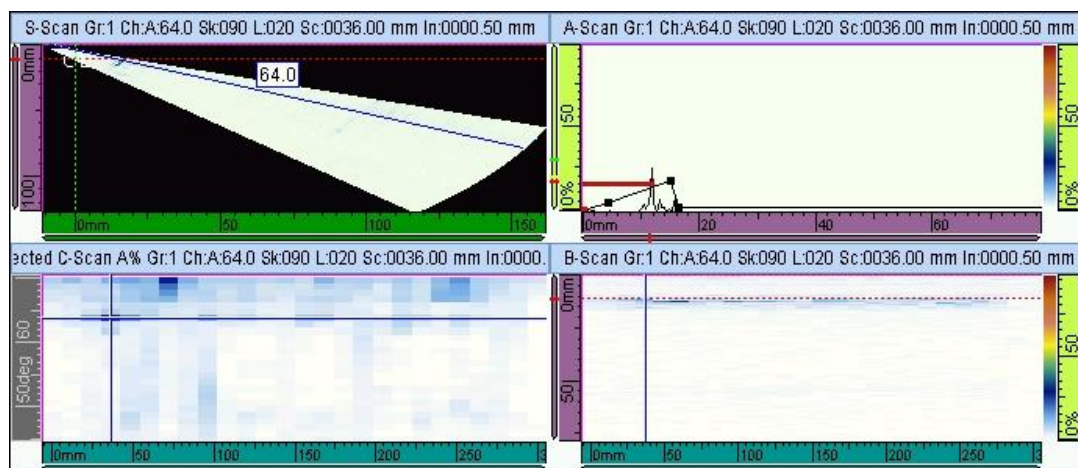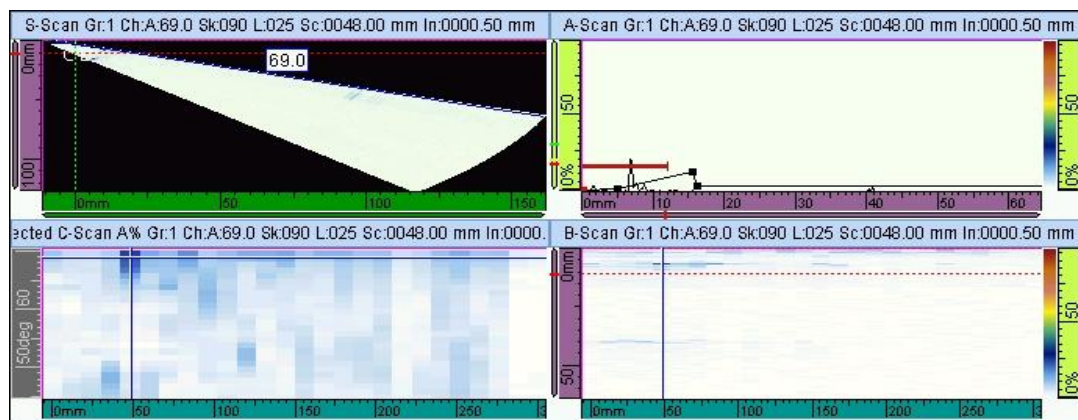

Figure 3.19 Evaluation of 4th data
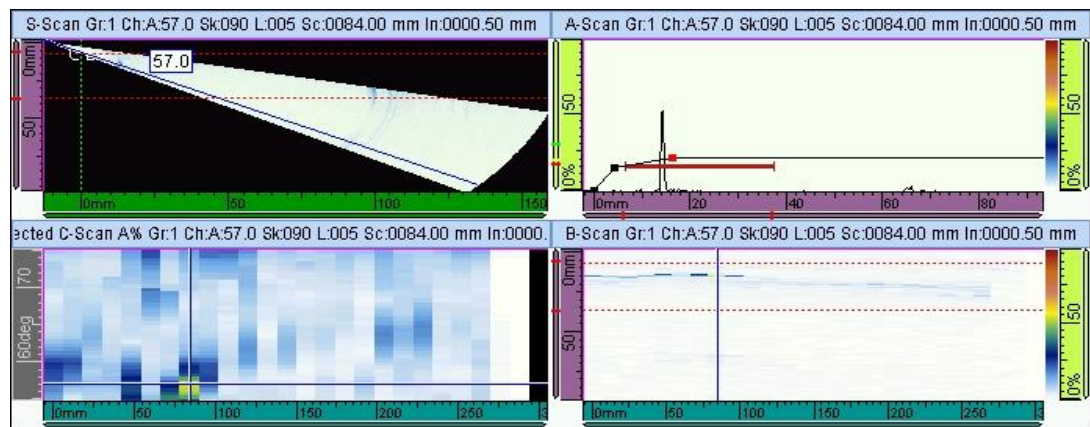

Figure 3.20 Evaluation of 5th data

Figure 3.21 Evaluation of 6th data
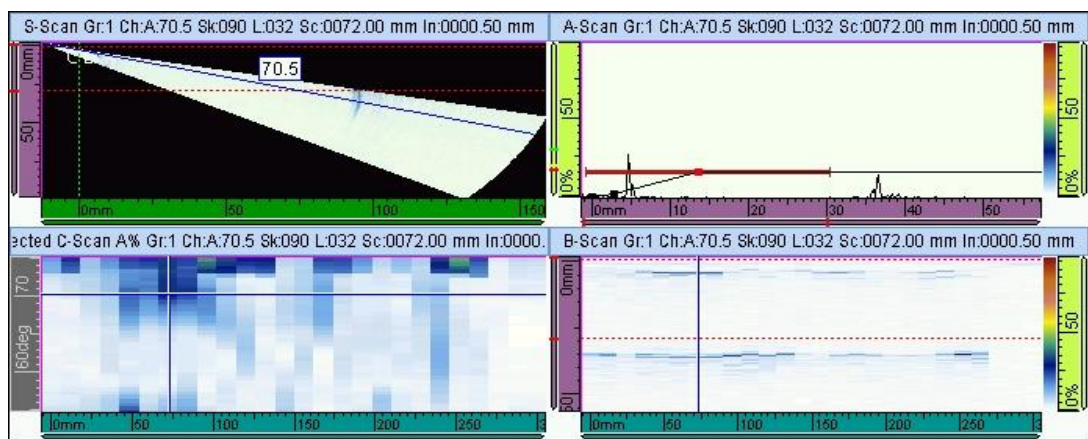
Figure 3.22 Evaluation of 7th data
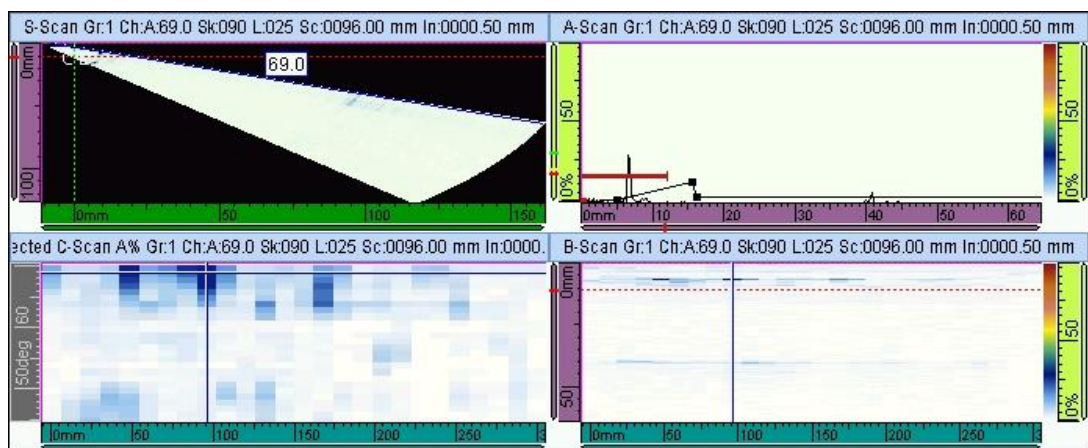
Figure 3.23 Evaluation of 8th data

9th and 10th indications (Figure 3.24) correspond to the bottom holes that were artificially created. 11th (Figure 3.25) indication possibly refers to a small defect at the depth of 8.62 mm.

Figure 3.24 Evaluation of 9th and 10th data
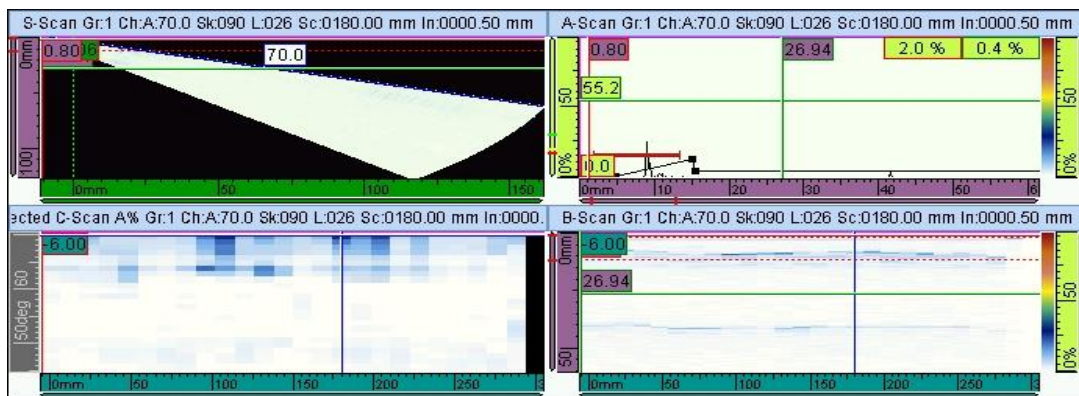
Figure 3.25 Evaluation of 11th data

12th to 15th (Figure 3.26-3.27) indications more likely correspond to the slot artificially created starting from 205 mm to ending at 245 mm. Since the slot was not created in properly, signal amplitudes diverted.
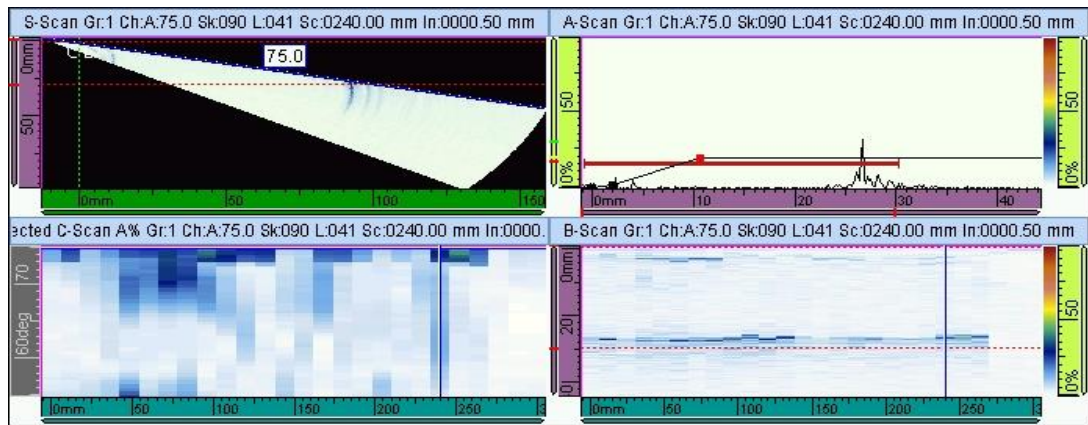
Figure 3.26 Evaluation of 12th data
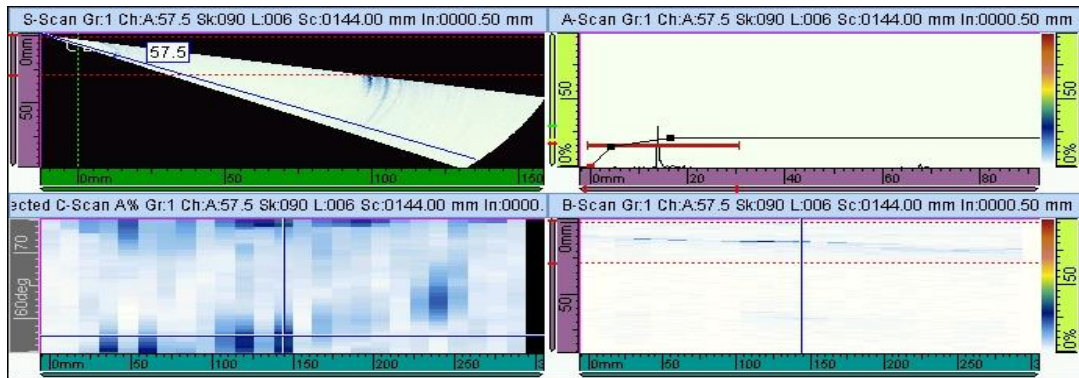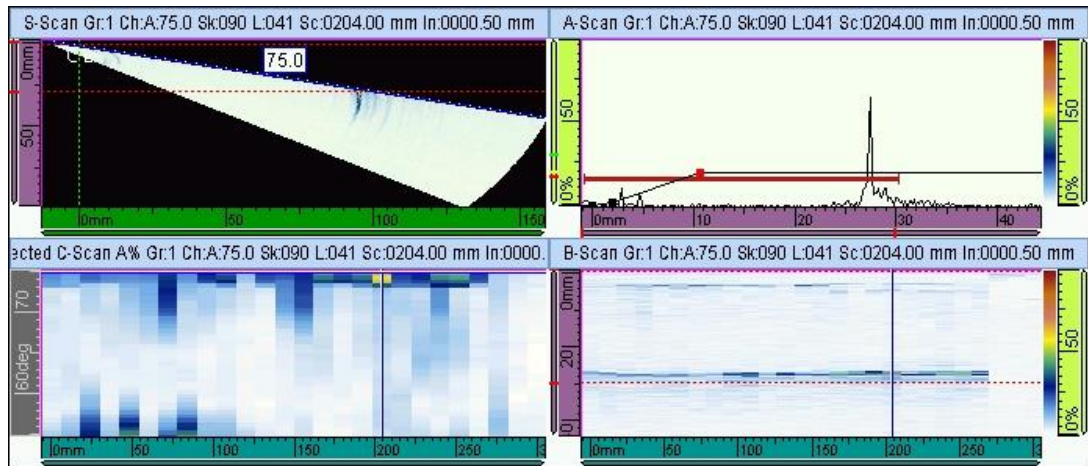

Figure 3.27 Evaluation of 13th, 14th and 15th data

To sum up, automated Phased Array system is successful to detect positions and sizes of inherent weld discontinuities including artificially flaws. Although manual Phased Array inspection has a slight advantage to detect discontinuities by meandering and swiveling of the probe, it does not give a clue about defect position and size. Manual Phased Array is still successful to detect lack of fusion in the side wall of root pass which requires some angle. Automated Phased Array provides exact position and sizes of incomplete root fusion along with lack of fusion in the side wall and moreover, it succeeded to detect artificial flaws. Therefore, automated Phased Array has superiority

99

in terms of detecting discontinuities over the manual Phased Array and conventional ultrasonic testing.

As for ultrasonic testing, detection success on artificial flaws test blocks (Specimen Type 1 and Type 2) has insignificant difference compare to manual Phased Array in the manner of PoD (Figure 3.09 – 3.10). On the other hand, conventional ultrasonic testing is not successful for detection of flaws in butt welded plate (Specimen Type 3) compare to Phased Array system. Since beam angles are refracted and speed of sound is eligible for change due to anisotropic media, Phased Array is secure the inspection with firing multiple elements, steering and focusing abilities rather than one single transducer element of conventional ultrasonic testing. It can be deduced that ultrasonic testing detection capability is less than Phased Array and artificial defect position is deviated (Table 3.9).

3.6 The radioscopy testing of the butt welded plate (specimen type 3)

The results of automated and manual Phased Array inspections were compared with radioscopic inspection (Figure 3.28) for verification purpose.

Figure 3.28 Radioscopic image of the specimen type 3 (200 kV)
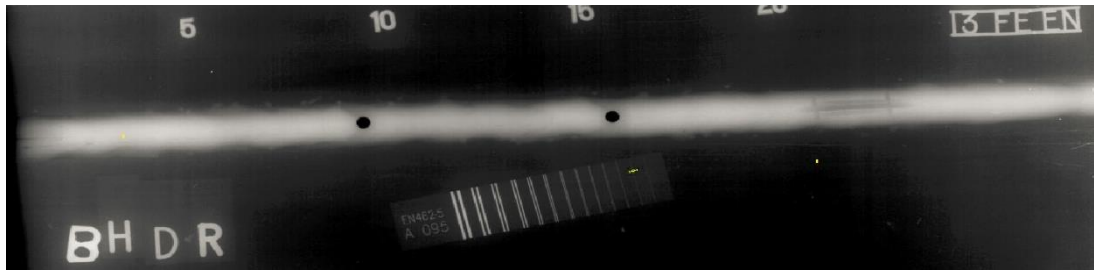
Figure 3.29 Radiographic image of the specimen type 3 (200 kV)

As seen in the Figure 3.28, there is an incomplete fusion in the root of weld between the reference point at 0 mm and lasting at 25-30 mm. The image proves that the lack of fusion in the side wall was detected clearly. Meanwhile automated and manual Phased Array inspections also detect the incomplete fusion in the root pass and lack of fusion in the side wall of the root pass.

While the real time radioscopy was able to detect volumetric incomplete and lack of fusion, it does not provide certain sizes of these discontinuities. On the other hand, indications of other flaws detected by automated Phased Array were not able to detect by real time radioscopy.

3.7 The macroscopic inspection of the butt welded plate (specimen type 3)

Prior to macroscopic examination the surface of the specimen was etched with specimen 60:40 ratio −70 wt. % HNO_3 H_2O, 10 mA / cm^2 for 4-5 seconds. Incomplete fusion in the root pass and lack of fusion in the side wall of the root pass are clearly seen in Figure 3.29.

Figure 3.30 The macroscopic image of the specimen type 3

101

CHAPTER 4

CONCLUSION

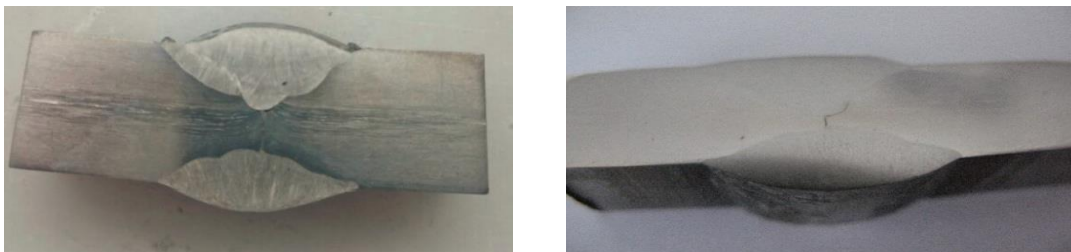The main objective of this thesis is to investigate and compare the abilities of manual and automated Phased array systems with conventional ultrasonic test system for detection of the flaws in austenitic stainless steel blocks and welds.

The results were compared with the probability of detection (PoD) concept. Three types of test blocks were prepared from AISI Type 304 steel. First specimen is the block having 2 mm Ø side drilled holes created at different depths from 5 mm to 113 mm; second specimen has various side drilled holes with diameters between 0.5 mm to 5 mm created at the 40 mm depth; third specimen is the GMAW welded 10 mm thick plate having artificial and natural defects.

Initially, conventional ultrasonic testing was compared with manual Phased Array (PA) system for detecting the artificially created flaws. Next, the manual PA system (time based inspection) was compared with the automated PA system (encoder based inspection) for detection of the artificially created defects (bottom holes and slot) in a block and natural discontinuities in the welded plate. Grain size, micro hardness, attenuation rate measurements, radioscopic and macroscopic inspections were also performed.

The following conclusions can be drawn from this study:

- Anisotropic behavior of austenitic stainless steel is a major setback in terms of detection and positioning of the defects by ultrasonic testing.

- The PoD values and curves show no significant differences between conventional ultrasonic method and manual Phased Array method in terms of detecting artificial flaws, except the flaw in 5 mm depth. While the flaw in 5 mm depth was identified easily by PA method due to its focusing ability, it was missed in conventional ultrasonic method because of the near field zone effect.

- Phased array method has a slight advantage for detection of the artificial defects in comparison to conventional ultrasonic method due to automated calibration, beam focusing and steering properties of the PA system.

- On the butt welded specimen, the manual and automated PA inspections are more successful than conventional ultrasonic testing based on counts of detected flaw possibilities as well as positions and sizes of the defects.

- While the automated PA system has superior detection and positioning abilities over the manual PA system, the manual PA system has superiority of faster scanning and swiveling of the probe. Moreover, in the manual PA the determination of size and positioning of the defects are dependent on the operator which brings the risk of human factor.

- The amplitude of ultrasonic wave is reduced as it passes through parent metal to the weld metal. The higher is the incidence angle, the greater is the amplitude of wave. Thus, to transfer more energy into the weld, higher incidence angle should be used. For that reason, it was observed that higher angles detection capability are successful than lower angles. Another reason is that 10 mm thickness plate is insufficient to approach the probe to weld line in the manner of lower angle incidences.

- The real time radioscopy and destructive macroscopic tests verified that the automated Phased Array system is accomplished for detecting, sizing and positioning incomplete root fusion and lack of fusion in the side wall of root

pass. Manual PA only gives an indication about lack of fusion on the side wall of root pass.

Recommendations for further studies:

- In order to monitor the effect of microstructure of test specimen in inspection reliability, artificially created flaws in the heat affected zone of the welded samples might be studied. Moreover, lower frequencies for avoiding of anisotropic material characteristics must be studied.

- Advanced Phased Array methods can be applied such as sampling Phased Array method, Reverse Phase Matching or Data Post-Processed Using Synthetic Aperture Focusing Technique (SAFT).

- Significant advantages of an electrodynamic probe (Eddy Current) Testing as compared to the existing techniques can be studied.

REFERENCES

[1] Introduction of Ultrasonic Technology, http://www.honda-el.co.jp/en/hb/182160_index.html, (last accessed on February 12th, 2015.)

[2] W. A. K. Deutsch, S. Kierspel, Manual Weld Inspection with Ultrasound-Conventionally or with Phased Arrays? 18th World Conference on Nondestructive Testing, Durban, South Africa 16-20 April 2012.

[3] J. R. Davis, ASM Handbook: Nondestructive evaluation and quality control, in vol. 17, ASM International, pp. 494 – 495, 1989.

[4] Introduction to Non-Destructive Testing Techniques, the NDT Center, Ultrasonic Testing Hashemite University, Jordan, 2005.

[5] Wave Propagation, http://66.80.214.36/ti/news/technical/Ultrasonic-Wave-Propagation-Review, (last accessed on February 12th, 2015.)

[6]ModeConversion,https://www.ndeed.org/EducationResources/CommunityCollege/Ultrasonics/Physics/modeconversion.htm, (last accessed on April 22th, 2015.)

[7] B. Boro Djordjevic, Remote Non-Contact Ultrasonic Testing of Composite Materials Center for Nondestructive Evaluation, 15th WCNDT, Rome, Italy, 2000.

[8] P. He, Direct Measurement of Ultrasonic Dispersion Using a Broadband Transmission Technique, Ultrasonic, pp. 67-70, 1999.

[9] Turkish Standard Institution Non Destructive Laboratory Ultrasonic Testing Education Notes, 2012.

[10] Wave interaction and Wave interference, https://www.nde-ed.org/EducationResources/CommunityCollege/Ultrasonics/Physics/WaveInterference.htm, (last accessed on March 7th, 2015.)

[11] M. Moles, Phased Arrays for General Weld Inspections, Olympus NDT, p. 1, 2012.

[12] Advances in Phased Array Ultrasonic Technology Applications, Olympus NDT, 2007.

[13] Phased Array Testing Basic Theory for Industrial Applications, Olympus NDT, pp. 22-24, 2012.

[14] Phased Array Ultrasonic Technology 2nd Edition, Eclipse Scientific, pp. 177-178, 2012.

[15] Phased Array Technical Guidelines, Useful Formulas, Graphs and Examples, RD Tech, May 2005.

[16] G. A. Matzkanin, H. T. Yolken, Probability of Detection (PoD) for Nondestructive Evaluation (NDE), Nondestructive Testing Information Analysis Center (NTIAC) August 2001.

[17] J. H. Kurz, A. Jüngert, S. Dugan, G. Dobmann, Probability of Detection (POD) determination using ultrasound phased array for considering NDT in probabilistic damage assessments, 18th World Conference on Nondestructive Testing, Durban, South Africa, 2012.

[18] J. R. Davis, ASM Handbook: Nondestructive evaluation and quality control, ASM International, vol. 17, 1989, pp. 1438-1440.

[19] E.A. Ginzel, M. Matheson, B.Feher, Probability of Rejection - In conformance with DNV OS F101, Materials Research Institute, Eclipse Scientific Products, Research In Motion, Waterloo, Ontario, Canada.

[20] R. J. Hudgell, B. S. Gray, The ultrasonic inspection of austenitic materials state of the art report, United Kingdom Atomic Energy Authority Northern Division Report CSNI Report No. 94, 1985, p. 5.

[21] S. Kou, Welding Metallurgy, Second Edition, University of Wisconsin, 2002, pp 432-433.

[22] P. Ducharname, S. Rigault, I. Strijdonk, Automated Ultrasonic Phased Array Inspection Of Fatigue Sensitive Riser Girth Welds With A Weld Overlay Layer Of Corrosive Resistant Alloy (CRA), Canada, 2009.

[23] F. Hanning, D.L. Engelberg, Metallographic screening of grain boundary engineered type 304 austenitic stainless steel, Materials Characterization, 2014, pp. 111-115.

[24] P. P. Nanekar, B. K. Shah, Characterization of material properties by ultrasonics, National Seminar on Non-Destructive Evaluation, 2003, pp. 4-5.

[25] G. Bregliozzi, A. Di Schino, J.M. Kenny, H. Haefke, The influence of atmospheric humidity and grain size on the friction and wear of AISI 304 austenitic stainless steel, April 2003.

[26] C. Annis, Statistical Best-Practices for Building Probability of Detection (POD) models, R package mh1823 statistical program software version 4.0.1, http://StatisticalEngineering.com/mh1823/, 2014.

[27] M. Moles, Manual phased arrays for weld inspections using North American codes, 17th World Conference on Nondestructive Testing, 25-28 Oct 2008, Shanghai, China.

[28] P. Ramuhalli, B. Watson, M.S. Good, T.J. Peters, A. A. Diaz, M. Dixit, M.T. Anderson, L.J. Bond, Ultrasonic Characterization of Cast Austenitic Stainless Steel Microstructure: Discrimination between Equiaxed- and Columnar-Grain Material– An Interim Study, U.S. Department of Energy, 2009, pp. 42-44.

[29] C. Annis, MIL-HDBK-1823A, Nondestructive Evaluation System Reliability Assessment, 2009.

[30] S. Pudovikov, A. Bulavinov, M. Kröning Ultrasonic inspectability of austenitic stainless steel and dissimilar metal weld joints, MPA-Seminar "Werkstoff- & Bauteilverhalten in der Energie- & Anlagentechnik" 9-10 October 2008.

[31] H. I. Aaronson, J. K. Abraham, N.R. Adsit, S. M. Allen, P. Ambalal, R.J. Barnhurst ASM Metals Handbook Volume 9 Metallography and Microstructures, 1985.

[32] ASTM E 1382, Standard Test Methods for Determining Average Grain Size Using Semiautomatic and Automatic Image Analysis, 2004.

[33] Sanjeevareddy Kolkoori, Quantitative Evaluation of Ultrasonic Wave Propagation in Inhomogeneous Anisotropic Austenitic Welds using 3D Ray Tracing Method: Numerical and Experimental Validation, BAM-Dissertationsreihe, PhD. Thesis, Berlin 2014.

[34] J.A. Ogilvy, Ultrasonic beam profiles and beam propagation in an austenitic weld using a theoretical ray tracing model, Ultrasonics, Vol. 24, pp. 337-347, 1986.

[35] Kupperman, D. S. and Reimann, K. J. Visualisation of ultrasonic beam distortion in anisotropic stainless steel. Proc. Int. Conf. on Quantitative NDE in the Nuclear Industry, San Diego, Ed. R. B. Clough, ASM published, 1983.

[36] J. Moysana, A. Apfela, G. Corneloupa, B. Chassignole, Modelling the grain orientation of austenitic stainless steel multipass welds to improve ultrasonic assessment of structural integrity, International Journal of Pressure Vessels and Piping, France, 2003.

[37] R. Ferreira, M. S. Motta, L. S. Gomes, M. Ogawa, A.R. Pimenta, Technical Evaluation of Ultrasound Phased Array Inspection in Welded Joints of AISI 304L Austenitic Stainless Steel, SENAI Welding Technology Centre, Rio de Janeiro, Brasil, 2013.

[38] C. Boveyron, D. Villard, R. Boudot, Ultrasonic Testing Of Cast Stainless Steel Components, Direction des Etudes et Recherches EDF-DBR, France, June 1992.

[39] Kaynak Tüketim Malzemeleri, Magmaweld Ürün Kataloğu, Oerlikon Kaynak Elektrodları ve Sanayi A.Ş., 04 / 2015.